5-2014

# Cascaded Inverters for Grid-Connected Photovoltaic Systems

Bailu Xiao
*University of Tennessee - Knoxville*, bxiao@utk.edu

To the Graduate Council:

I am submitting herewith a dissertation written by Bailu Xiao entitled "Cascaded Inverters for Grid-Connected Photovoltaic Systems." I have examined the final electronic copy of this dissertation for form and content and recommend that it be accepted in partial fulfillment of the requirements for the degree of Doctor of Philosophy, with a major in Electrical Engineering.

Leon M. Tolbert, Major Professor

We have read this dissertation and recommend its acceptance:

Fred Wang, Burak Ozpineci, Bin Hu

Accepted for the Council:

Carolyn R. Hodges

Vice Provost and Dean of the Graduate School

(Original signatures are on file with official student records.)

# Cascaded Inverters for Grid-Connected Photovoltaic Systems

A Dissertation Presented for the

Doctor of Philosophy

Degree

The University of Tennessee, Knoxville

Bailu Xiao

May 2014

## Dedication

This dissertation is dedicated to my husband Dr. Kai Zhu,
and our families.

# Acknowledgements

I would like to thank all the people who have encouraged, inspired, and advised me in the preparation of this dissertation.

First and foremost, I would like to express my deepest gratitude to my advisor Dr. Leon. M. Tolbert, for the opportunities offered and the guidance given throughout my PhD studies as well as my daily life. Dr. Tolbert is a very patient and knowledgeable advisor, without his persistent support this dissertation would not have been possible.

I am also deeply grateful to Dr. Fred Wang, Dr. Burak Ozpineci, and Dr. Bin Hu, for their valuable instructions. I greatly appreciate their time and input to this dissertation.

Within the Power Electronics Laboratory, I owe many thanks to my colleagues. I enjoyed the conversations and discussions that have had a great impact on my research and myself. Special thanks to Dr. Lijun Hang, Dr. Faete Filho, Dr. Jun Mei, Ke Shen, Cameron Riley, Yutian Cui and Tan Yang for their help and time on my research project.

Last but not the least, I would like to thank my parents, and my husband Dr. Kai Zhu, for their unconditional love and support.

# Abstract

With the extraordinary market growth in grid-connected PV systems, there is increasing interests in grid-connected PV inverters. Focus has been placed on inexpensive, high-efficiency, and innovative inverter solutions, leading to a high diversity within the inverters and new system configurations. This dissertation chooses cascaded multilevel inverter topologies for grid-connected PV systems to reduce the cost and improve the efficiency.

First, a single-phase cascaded H-bridge multilevel PV inverter is discussed. To maximize the solar energy extraction of each PV string, an individual maximum power point tracking (MPPT) control scheme is applied, which allows independent control of each dc-link voltage. A generalized nonactive power theory is applied to generate the reactive current reference. Within the inverter's capability, the local consumption of reactive power is provided to realize power factor correction. Then, the modular cascaded H-bridge multilevel inverter is connected to a three-phase utility system and nine PV panels. Individual MPPT control is also applied to realize better utilization of PV modules. Also, mismatches between PV panels may introduce unbalanced power supplied to the three-phase grid-connected system. Thus, a modulation compensation scheme is applied to balance the three-phase grid current by injecting a zero sequence voltage. A modular cascaded multilevel inverter prototype has been built and tested in both the single-phase and three-phase PV system. Simulation and experimental results are presented to validate the proposed control schemes.

The three-phase cascaded voltage source inverter (VSI), as another cascaded inverter topology, is also proposed for grid-connected PV applications. The equivalent model and average model of the three-phase cascaded VSI are established to realize the central control. In

addition, the control scheme applied in the traditional three-phase two-level VSI is modified for this application. Simulation and experimental results are presented as well. The targets of reducing the cost and improving the overall efficiency of the PV inverters can be achieved by applying the cascaded PV inverters and the proposed control schemes.

# TABLE OF CONTENTS

# LIST OF TABLES

# LIST OF FIGURES

# 1 Introduction

Increased demand of energy throughout the world, shortage of fossil fuels, and environmental problems caused by conventional power generation has led to an urgent search for renewable energy sources. Renewable energy is energy that comes from natural resources such as sunlight, wind, tides, and geothermal heat, which are naturally replenished at a constant rate. Renewable energy sources are clean, inexhaustible, and are thought to be "free" energy sources, such as solar and wind energies. Over the past few years, renewable energies represent a rapidly growing share of total energy supply, including heat and transportation. In 2011 (the latest year for which data are available), about 16% of global final energy consumption came from renewables, and the share of renewable energy sources (including hydro) in electricity generation is around 19% [1].

## 1.1 Solar Energy

Among various types of renewable energy sources, solar energy has become very popular and demanding. The sun delivers energy to the earth at the rate of $1.2 \times 10^5$ TW, which is about $10^4$ times of what mankind currently produces and consumes [2]. Solar energy can be collected and used in many ways.

Photovoltaic (PV) devices use semiconductor materials to convert sunlight to electricity. Thermophotovoltaics uses the energy of heat, or infrared radiation, to generate electricity. Concentrating solar power (CSP) systems use the concentrated heat of the sun as the heat source for conventional power plants. Solar heating technologies use the sun's heat to meet a variety of needs, such as heating swimming pools, and heating water or air for residential and commercial

use. Solar lighting systems collect sunlight and use optical fibers to transmit it inside the building to supplement conventional lighting.

There is extraordinary market growth in solar energy. For solar PV systems, almost 30 GW of operating capacity was added in 2012, increasing total global capacity by 42% to 100 GW. More than 900 MW of concentrating solar power systems was installed in 2012, bringing global capacity to about 2,550 MW. Solar heating capacity increased by 14% in 2012 to reach approximately 255 GW, excluding unglazed swimming pool heating [3].

## 1.2 Photovoltaic Systems

Photovoltaic systems are ideally distributed generation (DG) units, and they offer the advantages of free and unlimited energy source, being pollution free, little maintenance, and no noise. Since 2004, photovoltaic passed wind as the fastest growing energy source in % increase in the world. The average annual growth rates of renewable energy capacity from end-2007 through 2012 [3], [4] are shown in Fig. 1.1. It can be seen that solar PV grew the fastest of all renewable energy sources during last five years, with operating capacity increasing by an average of 60% annually.

The PV market was driven by many reasons, such as decreasing costs, new applications, continued strong policy support, and strong investor interest. The most important reason, decreasing prices, has been caused by the following factors: 1) an increasing efficiency of solar cells; 2) manufacturing technology improvements; and 3) economies of scale [5]. Since the first recognition in 1839 [6], solar cell technology has achieved tremendous progress. The first solar modules commercially produced at a cost of < $1/watt occurred in 2009. Conversion efficiencies of the modules reached 11.1%, and the module manufacturing cost was $0.84 per watt [7]. Sanyo

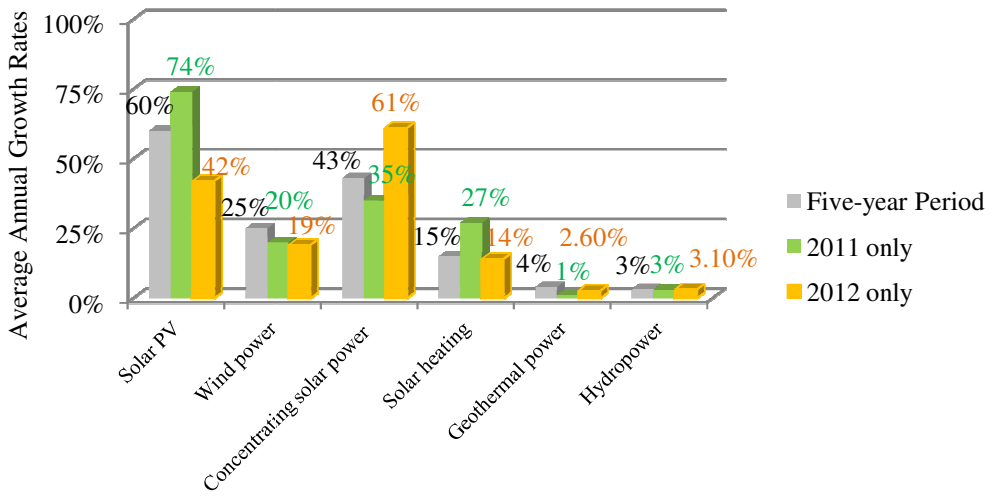


Figure 1.1. Average annual growth rates of renewable energy capacity (end-2007 to 2012).

Electric produces 200 W modules with efficiency of 17.24%. In 2012, the highest research-cell efficiencies have reached 43.5% by using multiple junction cells at high solar concentrations.

The global cumulative installed PV capacity share [3] is given in Fig. 1.2. Germany and Italy accounted for 48% of global PV capacity, and the United States stands in the 3rd place, with 7.2% of the capacity share.

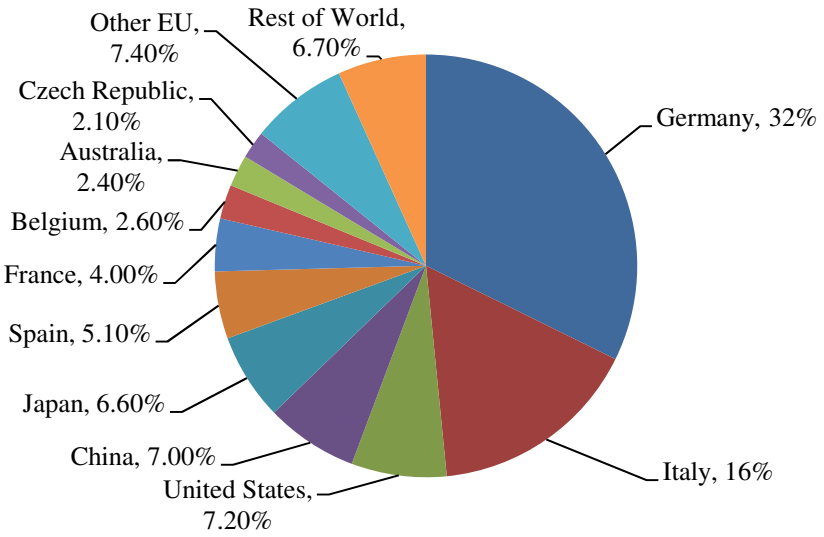


Figure 1.2. Global cumulative installed PV capacity share (until 2012).

In 2012, Europe still accounted for the predominant share of the global PV market, with 57% of all new capacity. China was the top non-European PV market in 2012, with 3.5 GW newly installed, followed by the United States with 3.3 GW.

In PV systems, the trend towards large-scale grid integration is continuing. 29.7 GW and 29.4 GW of PV systems were connected to the grid in 2011 and 2012, respectively, up from 16.8 GW in 2010 [3], [4]. Eight countries added more than 1 GW of solar PV to their grids in 2012. In the United States, utilities integrated almost 2.4 GW of solar electric capacity in 2012. The market share for large-scale solar projects was 1,106 MW or 46 percent of all annual solar capacity, a growth of almost 160% over 2011 [8].

The dramatically expanding PV market is estimated to continue. Fig. 1.3 gives the global annual PV market scenarios from 2000 to 2016 [9]. European Photovoltaic Industry Association (EPIA) expects that more than 77 GW PV systems will be newly installed in 2016, and the global cumulative installed PV capacity would be 350 GW with the right policies in place.

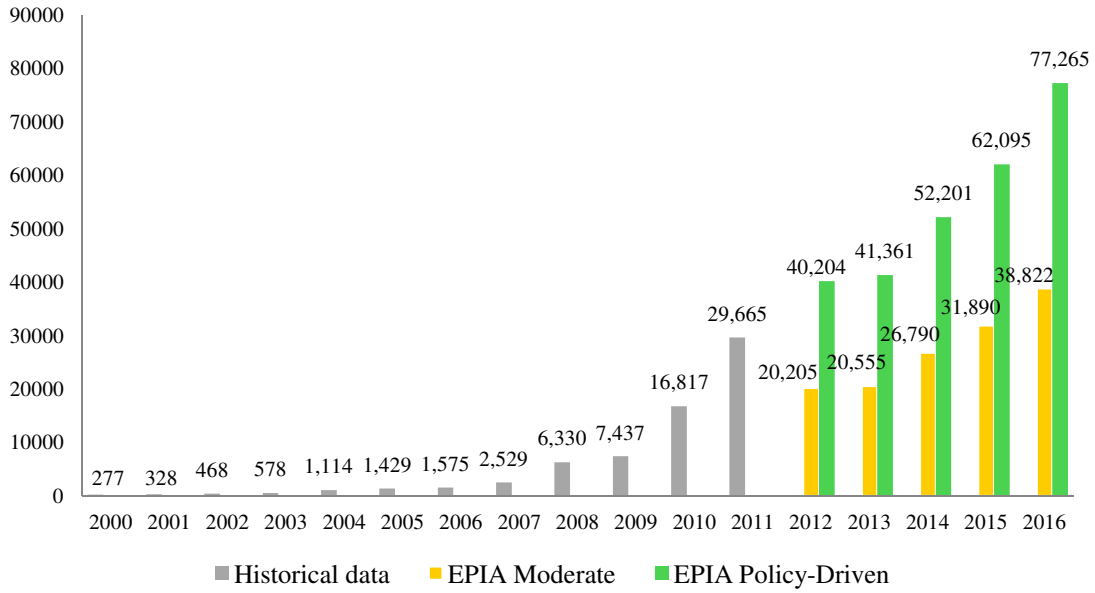


Figure 1.3. Global annual PV market scenarios (from 2000 to 2016, MW).

## 1.3 Motivation and Strategy

With the extraordinary market growth in grid-connected PV systems, there is increasing interests in grid-connected PV inverters. The main target is to reduce the cost and improve the efficiency of PV inverters.

Fig. 1.4 shows the 2010 benchmark price breakdowns by element for fixed-axis utility-scale PV systems [10]. It can be seen that after the PV module cost and installation fee, the PV inverter cost accounts for the third largest part of the cost of PV systems. As module prices continue to fall, the contribution of the PV inverter cost to the cost of solar energy will increase. Thus, to ensure that solar power is a viable and economic source for the world's power needs and to make solar energy compete better with incumbent electricity technologies, the cost of PV inverters needs to be reduced.

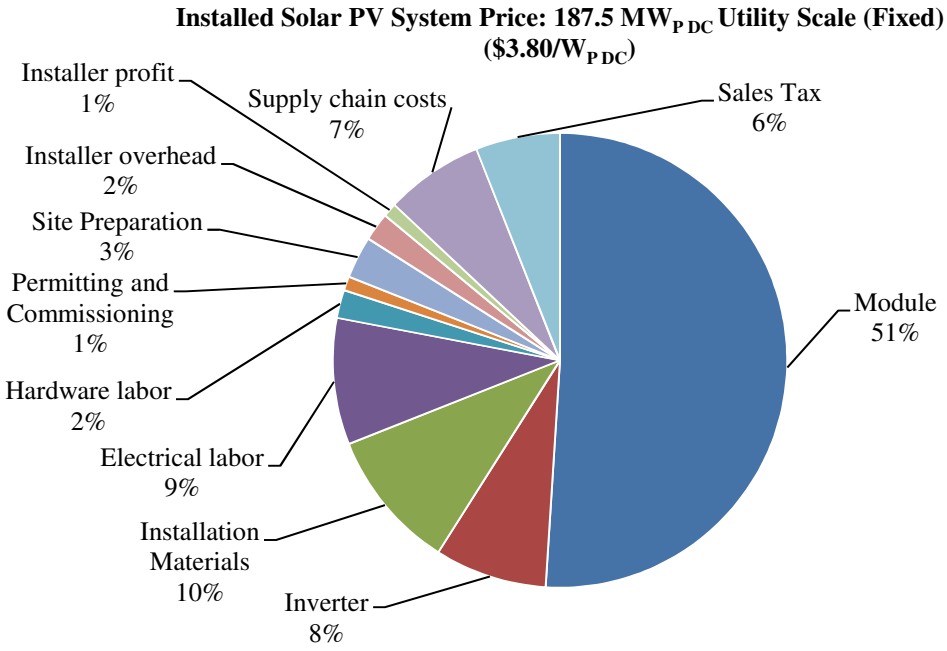


Figure 1.4. Benchmark 2010 fixed-axis utility-scale PV system price: breakdown by element.

In the United States, the PV inverter cost is currently $0.33 per watt. Department of Energy (DOE) has set a goal to achieve a total installed cost of utility-scale PV systems of $1 per watt by 2020, where only $0.10 per watt is for power electronics. To achieve this target for PV inverters, both technologies that harvest more energy from the sun and technologies that reduce PV inverters cost and overall balance of system (BOS) costs need to be developed. In this dissertation, cascaded inverter topologies are chosen for grid-connected PV systems to reduce the cost and improve the efficiency, and control schemes with individual maximum power point tracking (MPPT) control are developed to harvest more solar energy.

First, the cascaded inverter topologies use several converters connected in series to reach the high voltage/power level. The voltage stresses on the semiconductor switches in each converter will be reduced. Thus, low voltage rating MOSFETs, which cost less, can be even applied to large-scale PV systems to reduce the cost of PV inverters. Although more components are employed in this topology, the modular design and mass production will lead to low manufacturing cost. The target of $0.10 per watt for PV inverters can be reached.

On the other hand, the cascaded PV inverter can reach a high power level without having to sacrifice the utilization of PV modules, leading to a high overall efficiency of PV systems. In addition, compared to other converter topologies, the cascaded topology itself has higher efficiency due to the low switching frequency. By applying the cascaded topology, the target of high efficiency will be achieved as well.

Thus, the cascaded H-bridge multilevel inverter is applied to both single-phase and three-phase grid-connected PV systems. The control scheme with individual MPPT control will be developed to improve the overall efficiency. A modular cascaded H-bridge multilevel inverter was built in the laboratory and tested with PV panels under different conditions.

However, the cascaded H-bridge multilevel inverter topology employs a large number of electrical and mechanical components, especially in three-phase applications. Thus, a three-phase cascaded voltage source inverter (VSI), which keeps many advantages of the cascaded H-bridge multilevel inverter and has fewer components, is also proposed for grid-connected PV systems. The control scheme for the conventional three-phase two-level VSI was modified for this application. A three-phase cascaded VSI prototype was built and connected to PV panels for testing.

## 1.4 Dissertation Outline

According to the strategy discussed above, the outline of the dissertation is listed as follows.

Chapter 2 is the literature review. Various configurations of PV systems are summarized and surveyed, and grid-connected PV inverter topologies are categorized and discussed. Meanwhile, a MPPT system is also discussed.

Chapter 3 presents the single-phase cascaded H-bridge multilevel inverter for grid-connected PV systems. A control scheme with individual MPPT control and reactive power compensation is proposed. Then, simulation and experimental results are given.

Chapter 4 discusses the three-phase modular cascaded H-bridge multilevel PV inverter. In addition to the individual MPPT control, modulation compensation is also introduced to the control system. A modular cascaded H-bridge multilevel inverter prototype has been built in the laboratory, and test results are presented.

Chapter 5 proposes a three-phase cascaded VSI for grid-connected PV applications. The equivalent model and average model of the proposed system are established to achieve the central control. A control scheme with MPPT control is proposed. Both simulation and

experimental results are presented.

Chapter 6 concludes the work that has been done in this dissertation and the significance of the work. Possible future work is also described in this chapter.

# 2 Literature Review

A PV inverter, which is used to convert DC power from the solar panels into AC power to be fed into the grid, is an essential element in the grid-connected PV system. With a downward tendency in the price of the PV modules, the cost of a grid-connected PV inverter is becoming more visible in the total system price. A cost reduction per inverter watt is important to make PV-generated power more attractive. Therefore, focus has been placed on inexpensive, high-efficiency, and innovative inverter solutions, which has resulted in a high diversity within the inverters, and new system configurations.

This chapter presents a literature review of the current state of the art on grid-connected PV inverters. First, the configurations of the PV system are summarized. Then, the grid-connected PV inverter topologies are categorized and discussed. Meanwhile, a Maximum Power Point Tracking (MPPT) system, which is required in grid-connected PV inverters to ensure the maximum power extraction from the PV panels, is also discussed.

## 2.1 Configurations of PV Systems

Five inverter families can be defined, which are related to different configurations of the PV system: (1) central inverters, (2) string inverters, (3) multi-string inverters, (4) AC-module inverters, and (5) cascaded inverters [11]-[15]. The configurations of PV systems are shown in Fig. 2.1.

In the middle of the 1980's the market for grid-connected PV systems developed with central inverters of several kilowatts in size. The output voltage of a PV module is relatively low, so PV modules are connected in series, which is called a string to generate a sufficiently high

voltage and avoid further amplification. To reach a higher system power level, these strings are then connected in parallel through string diodes, as shown in Fig 2.1 (a).

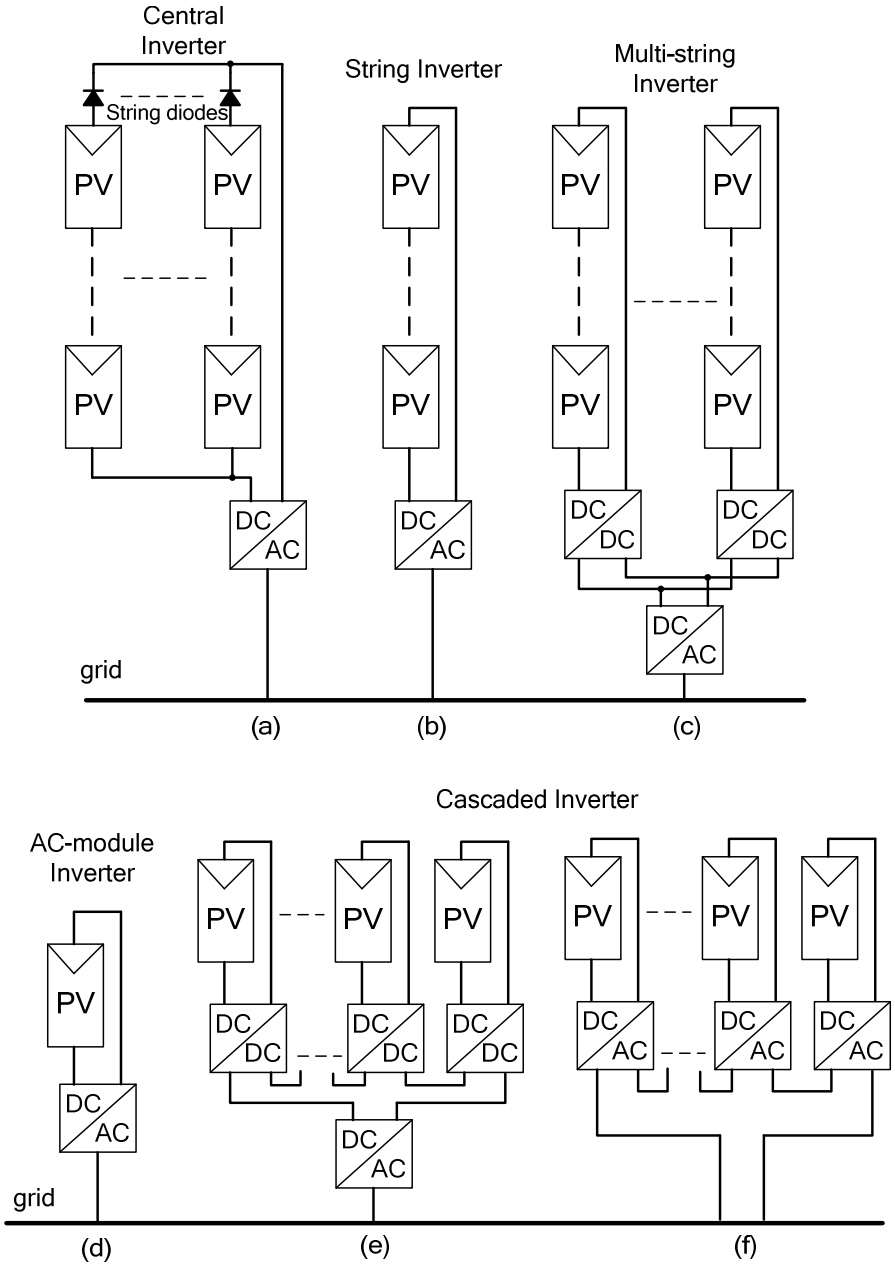


(a) Central inverter. (b) String inverter. (c) Multi-string inverter. (d) AC-module inverter. (e) Cascaded DC/DC converter. (f) Cascaded DC/AC inverter.

Figure 2.1. Configurations of PV systems.

In some papers [13], central inverters are described as the past technology of PV systems. This configuration has many drawbacks, such as mismatching losses between the PV modules due to a centralized MPPT control, losses and risk of electrical arc in DC wiring, losses in the string diodes, and poor expandability and adaptability to customers' requirements. However, the central inverter topology has advantages like simplicity, low cost, and high inverter efficiency due to the higher power rating in comparison to string inverters. Therefore, central inverters are still the first choice for medium- and large scale PV applications, where shading or different orientation of modules is avoided already at the planning stage [14], [16].

A reduced version of the central inverter, which is called a string inverter, was introduced to the market in the middle of the 1990's. String inverters are designed for a system configuration of one PV string, as shown in Fig. 2.1 (b). There are no string diodes or associated losses, and individual MPPT can be applied to each PV string. Thus, the overall efficiency is increased in comparison to the central inverter. However, a higher price per watt is also seen in the string inverter because of the rather low power level (1-5 kW). String inverters are suitable for smaller applications, especially where the modules cannot be installed with the same orientation and are subject to different shading conditions.

The multi-string inverter, as depicted in Fig. 2.1 (c), is a further development of the string inverter, where several strings are connected to a common dc–ac inverter through their own dc–dc converter [17], [18]. Multi-string inverters can reach a higher power level without having to sacrifice the advantages of the string technology. Since each PV string has a lower power DC/DC converter connected, and individual MPPT can be achieved by this DC/DC converter. Meanwhile, due to the DC/DC converter, multi-string inverters often have a very wide input voltage range, which provides freedom in the design of PV systems. In addition, further

extension can be easily realized because a new string with a DC/DC converter can be plugged into the existing system. The main drawback of multi-string inverters is that there are always two power conversion stages, which leads to a smaller peak efficiency compared to string inverters.

The AC-module inverter, which integrates the inverter and PV module into one electrical device [19]-[21], is shown in Fig. 2.1 (d). Since the AC-module inverter is attached to only one PV panel, the mismatch losses between PV modules will not exist in this configuration. Another benefit is that DC wiring is not required, and the risk of electric arc and fire in DC wiring is minimized. Also, due to the modular structure, a "Plug and Play" concept can be realized and the enlargement of PV systems can be easily achieved.

However, the AC-module inverter still has a low acceptance because of several drawbacks. First, the module-integrated inverter needs more complex circuit topologies to achieve high-voltage amplification, which results in a low converter efficiency and high cost per watt. In addition, the packaging of the inverter and PV module to one electrical device requires equal lifetimes of the inverter and PV module. However, with the current inverter technology, the lifetime of the inverter is about ten years [22], which is far less than the lifetime of PV panels, i.e., approximately 25 years. If the lifetime problem is solved, AC-module inverters will be very interesting because of their ease in use and installation [14]. Even the higher cost due to the low power level per unit might be compensated by mass production.

The cascaded inverter, which consists of several converters connected in series, can reach a high voltage level without any amplification. There are two types of the cascaded inverter. Fig. 2.1 (e) shows a cascaded DC/DC converter connection of PV modules [23], [24]. Each PV module has its own DC/DC converter, and the modules with their associated converters are still connected in series to create a high DC voltage, which is provided to a simplified DC/AC

inverter. This approach combines aspects of string inverters and AC-module inverters, and offers the advantages of individual module MPPT, cheaper but more efficient than AC-module inverters. However, there are still two power conversion stages in this configuration. Another cascaded inverter is shown in Fig. 2.1 (f), where each PV panel is connected to its own DC/AC inverter, and those inverters are then placed in series to reach a high voltage level. This cascaded inverter would maintain benefits of "converter per panel" [23], like better utilization per PV module, capability of mixing different sources, and redundancy of the system. In addition, this DC/AC cascaded inverter removes the need for the per-string DC bus and DC/AC inverter, which further improve the overall efficiency. Due to the single stage structure, this DC/AC cascaded inverter must handle all tasks, i.e., MPPT, grid current control and perhaps, reactive power compensation. Thus, further consideration and research are needed for this promising structure, which is the main focus of this dissertation.

## 2.2 Topologies of Grid-Connected PV Inverters

Grid-connected PV inverter topologies can be categorized as follows: 1) the number of power conversion stages; 2) with or without a transformer; 3) the use of decoupling capacitors and their locations [13], [25]. In this section, the inverter topologies are categorized according to the number of power processing stages.

There are three cases of single and multiple stage inverters, as shown in Fig. 2.2. Note that the symbol for the PV module shall be interpreted as either a single PV panel, or multiple PV panels in series/parallel connections.

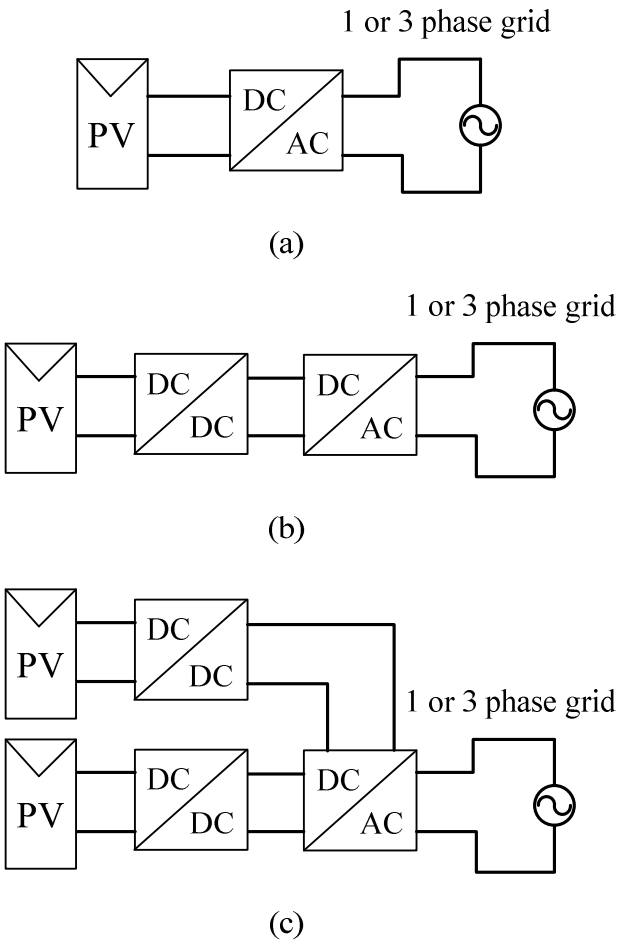


(a) Single stage inverter. (b) Dual stage inverter with single DC/DC converter. (c) Dual stage inverter with multiple DC/DC converters.

Figure 2.2. Three cases of single and multiple stage inverters.

### 2.2.1 Single Stage Inverter

The single stage inverter, as shown in Fig. 2.2 (a), is the typical configuration for central inverters, string inverters, AC-module inverters, and DC/AC cascaded inverters. It has the advantages of high efficiency and reliability, but must handle all tasks itself.

In the single-phase system, the full-bridge inverter is commonly used, as shown in Fig. 2.3. Most of the bridges use IGBTs or a combination of IGBTs and MOSFETs [12], which are

switching at high frequency to invert the input current into an AC current and reduce harmonics.

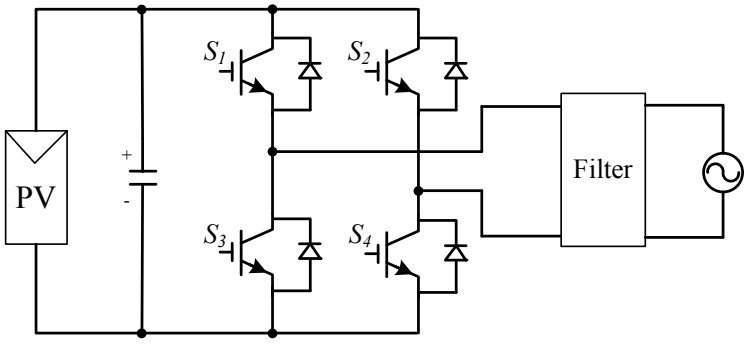


Figure 2.3. Topology of the full-bridge inverter.

Many new topologies have been proposed for single stage inverters with MPPT capability. A full-bridge configuration based on the buck-boost principle proposed by [26] is shown in Fig. 2.4. During the positive half cycle of the grid voltage, $S_1$ is kept continuously ON, and $S_3$ operates at high frequency. The path during $S_3$ turn OFF is completed through $S_1$ and $D_2$. During the negative half cycle of the grid voltage, $S_2$ is kept continuously ON, and $S_4$ operates at high frequency. The path during $S_4$ turn OFF is completed through $S_2$ and $D_1$. The output voltage of the buck-boost inverter can be larger or lower than the DC input voltage, depending on the instantaneous duty cycle. The main drawback of this topology is the high conduction loss.

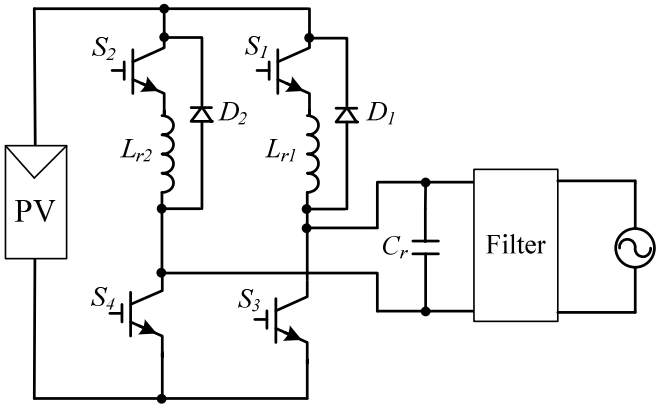


Figure 2.4. Topology of the full-bridge series-resonant buck-boost inverter.

Based on the buck-boost principle, many other single stage grid-connected PV inverters have also been proposed [27]-[29]. However, the buck-boost inverter configurations suffer from high peak inductor current stress due to the fact that the entire energy that is transferred to the grid in a switching cycle is stored in the inductor during the ON time of the switching cycle. In addition, only this stored energy is supplied to the grid, which restricts its use to low power applications.

To realize electrical isolation and overcome drawbacks of line frequency transformers, flyback topologies with a high-frequency transformer have been proposed [30]-[33]. Reference [30] has presented an isolated, flyback configuration, which consists of two sets of flyback type chopper circuit, as shown in Fig. 2.5. The main circuit is simple, using only three power devices and a high-frequency transformer. But this topology is only applicable to low power level systems due to the limitation on the value of primary inductance of the flyback transformer. Thus, this inverter topology is suitable for the AC-module inverter when its lifetime is taken into account. A power decoupling circuit is added [32] to enable use of film capacitors with small capacitance for the DC input bus, and hence the additional circuit is expected to extend the lifetime of the inverter.

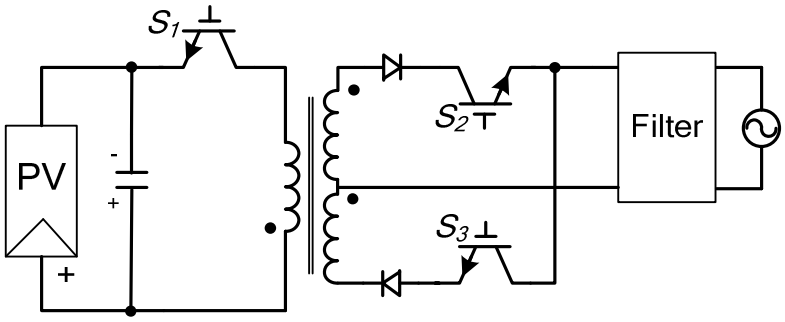


Figure 2.5. Topology of the flyback-type inverter.

In some countries, galvanic isolation is not a requirement in the low-voltage grid or power levels below 20 kW. This leads to the development of single stage transformer-less inverter topologies [14], [34]-[39]. For the transformer-less inverter topologies, if the input DC source, PV modules, and the grid do not share the same ground, the PV modules may have large leakage current, which will cause safety and electromagnetic interference problems [34]. To solve this problem, either extra switches have to be added to the existing topology or doubly grounded topologies have to be used.

HERIC (Highly Efficient and Reliable Inverter Concept) [35] is one of topologies where extra switches are added. The HERIC topology, as shown in Fig 2.6, introduces a combination of two switches and diodes in parallel to the grid. During the freewheeling periods of the inverter, the switches of the full-bridge can be open, thus the PV modules are decoupled from the grid. The H5 topology shown in Fig. 2.7 [36] also uses the idea that disconnecting the DC side from the AC side during the freewheeling to prevent a fluctuating potential of the PV generator. In the H5 topology, one switch is added to the conventional full-bridge inverter. The main drawback of these topologies is that added switches will increase the cost and system complexity.

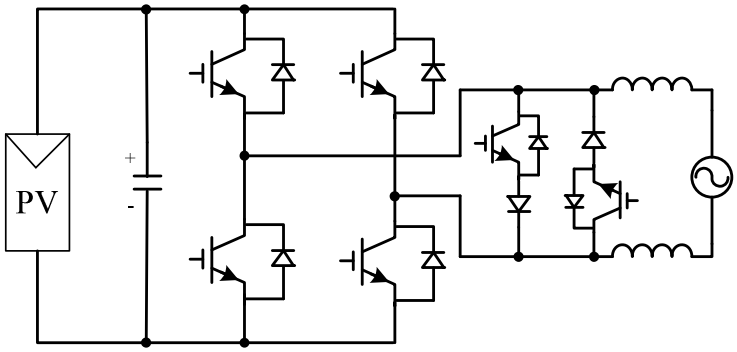


Figure 2.6. HERIC topology.

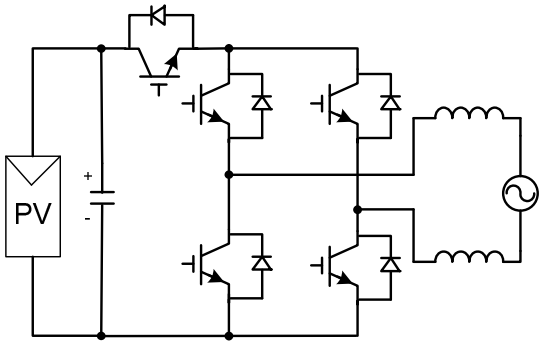


Figure 2.7. H5 topology.

Another approach to single stage transformer-less inverters is to use the doubly grounded topologies. Reference [37] has proposed the so-called “flying inductor inverter” Karschny topology, where the negative terminal of the PV generator is grounded, as shown in Fig. 2.8. The basic inverter topology is composed of a buck-boost converter that can be shifted according to the positive and negative output of the grid. This topology still employs a large amount of semiconductors, and the necessity of storing the whole energy in the inductor leads to higher losses and higher cost and size. Semi-Z-source inverters can also be used as the doubly grounded topologies [39], as depicted in Fig. 2.9. The circuit can achieve the same output voltage as the conventional full-bridge inverter does, with only two active switches, but additional passive components are required.

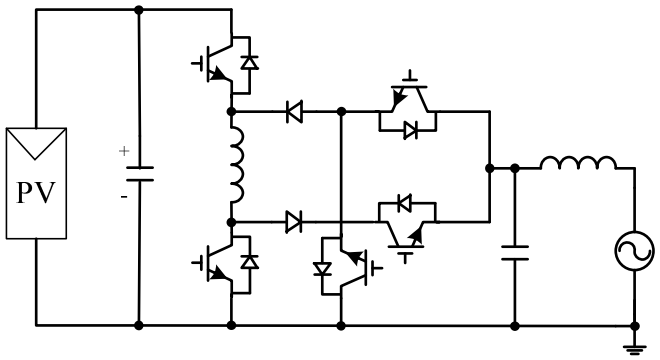


Figure 2.8. Karschny topology.

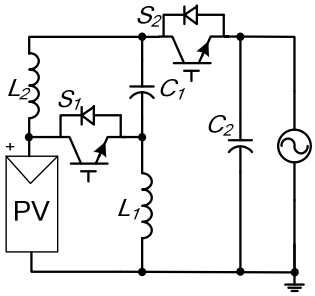


Figure 2.9. Semi-Z-source inverter.

The aforementioned topologies can only be used for central inverters, string inverters, and AC-module inverters. For DC/AC cascaded inverters, the cascaded H-bridge multilevel inverter has been proposed [40], as shown in Fig. 2.10. As a single stage inverter, the cascaded H-bridge multilevel inverter provides the advantages of low cost and high inverter efficiency. In addition, unlike other single stage inverters, this topology can be used in medium and large grid-connected PV systems without having to sacrifice the utilization of each PV module. More details of this topology are discussed in Chapter 3.

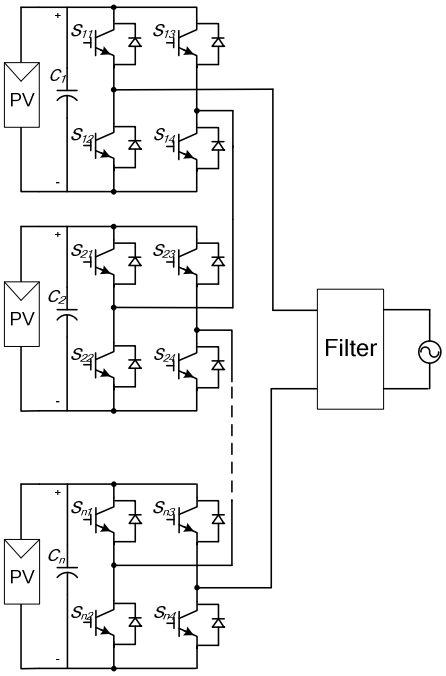


Figure 2.10. Topology of the cascaded H-bridge multilevel inverter.

In the three-phase grid-connected PV system, the typical three-phase voltage source inverter (VSI) is widely used, as shown in Fig. 2.11. Due to the buck characteristic of the VSI, it would require a high input voltage for a proper sinusoidal current feed-in. Thus, a PV string of large number of PV modules would be required, which is more likely to get affected by partial shading. Current source inverters (CSIs) can also be used as three-phase single stage PV inverters [41], [42]. Fig. 2.12 shows a MOS-equipped CSI for a PV system. The main advantage of the CSI is its inherent voltage-boost characteristic, so a high input voltage may not be necessary. The Z-source inverter proposed by [43] can boost voltage by using the shoot through states. It is another topology for three-phase single stage PV inverters [44], [45], as shown in Fig. 2.13.

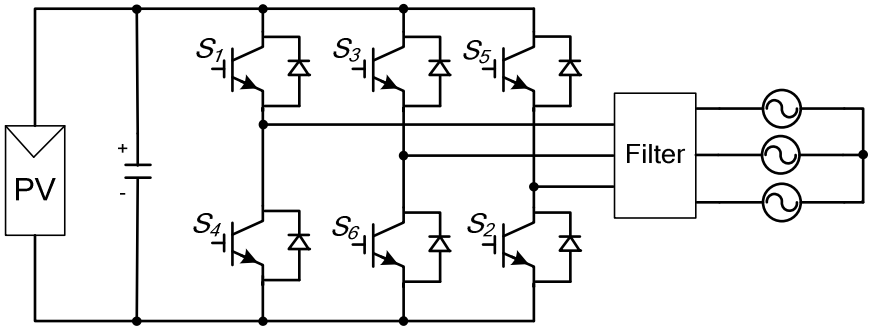


Figure 2.11. Topology of the three-phase voltage source inverter.

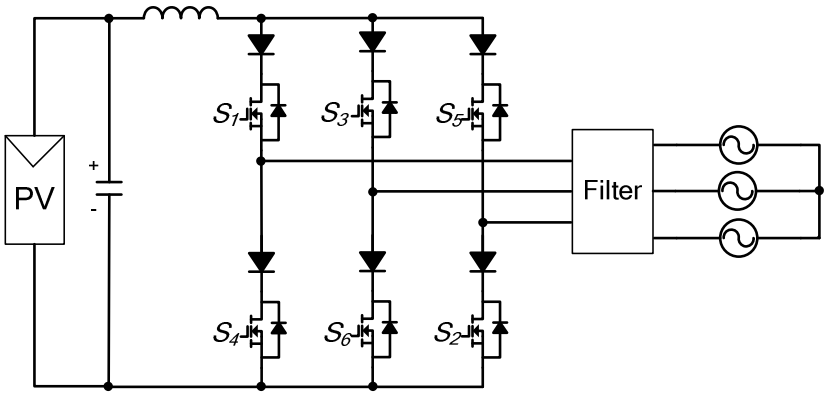


Figure 2.12. Topology of the three-phase current source inverter.

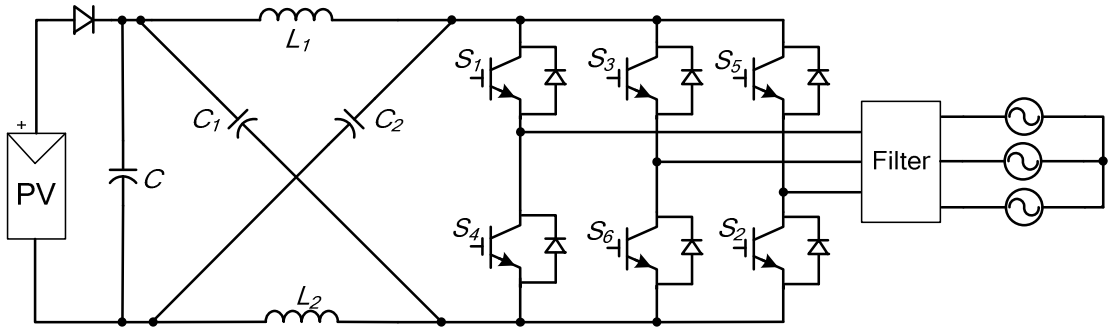


Figure 2.13. Topology of the three-phase Z-source inverter.

If galvanic isolation is not required, the three-phase VSI with split capacitor, presented in Fig. 2.14, can be used as the single stage transformer-less PV inverter. Due to the connection of the capacitor middle point to the neutral line, the voltage fluctuations present at DC+ and DC- are much smaller than in the case of the three-phase VSI [46]. Thus, the ground leakage current can be greatly reduced. The three-phase Neutral Point Clamped (NPC) inverter is another topology that is suitable to be used in a three-phase transformer-less PV system [47]. As shown in Fig. 2.15, the middle point of the PV array is also connected to the neutral line, helping to reduce the leakage current to ground. This topology, compared to the three-phase VSI with split capacitor, needs twice the switching devices and six extra diodes. However, the voltage stress on those switching devices is halved.

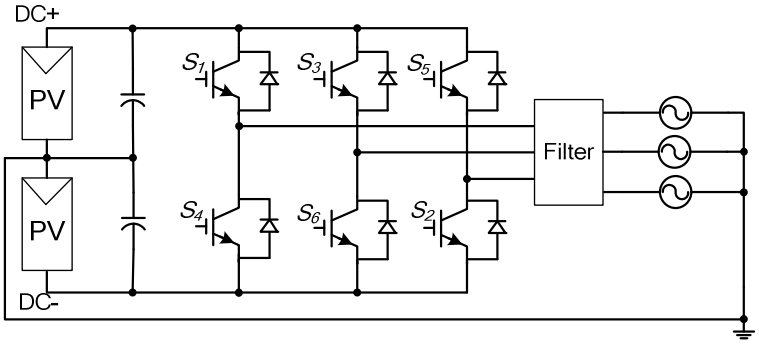


Figure 2.14. Topology of the three-phase VSI with split capacitor.

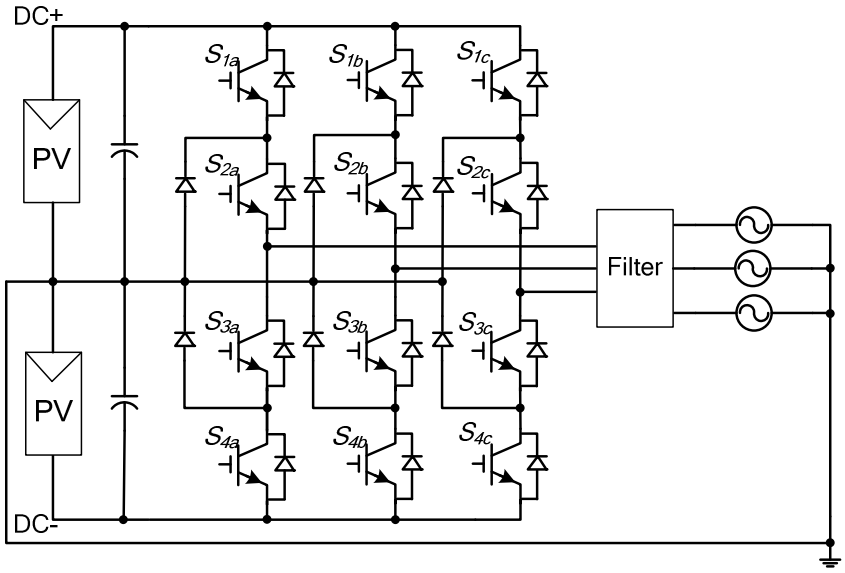


Figure 2.15. Topology of the three-phase Neutral Point Clamped inverter.

The three-phase inverter topologies presented above can only be used for the central configuration, which introduces mismatching losses between PV modules. In order to harvest more solar energy and improve the overall efficiency, three-phase cascaded inverters, such as the DC/AC cascaded configuration, can also be used in three-phase grid-connected PV applications. Two three-phase cascaded topologies have been applied as a single stage PV inverter in this dissertation. The topologies and control methods will be discussed in detail in Chapters 4 and 5.

### 2.2.2 Dual Stage Inverter with Single DC/DC Converter

Fig. 2.2 (b) shows the dual stage inverter with a single DC/DC converter. Unlike the single stage inverter, which must handle all tasks itself, the DC/DC converter is now performing the MPPT and perhaps voltage amplification, and the DC/AC inverter is taking care of the grid current control. So the boost converter is usually chosen as the first stage to provide a fixed DC voltage, and the full-bridge VSI is widely used as the second stage in the single/three-phase PV system.

High-efficiency high-voltage gain DC/DC converters have been designed for the first stage. A ZVT interleaved high step-up converter with built-in transformer has been proposed by [48]. The built-in transformer can provide high voltage conversion ratio and increase the system efficiency without an extreme duty cycle compared with the conventional boost converter.

For the dual stage PV inverter, transformer-less topologies can be designed in two ways. One is designing the transformer-less inverter topology. As shown in Fig 2.16, for example, a neutral point diode clamped inverter is applied in the second stage instead of the conventional full-bridge inverter. Since each DC link capacitor voltage needs to be higher than the grid voltage amplitude, a boost converter is used in the first stage to provide a high DC voltage.

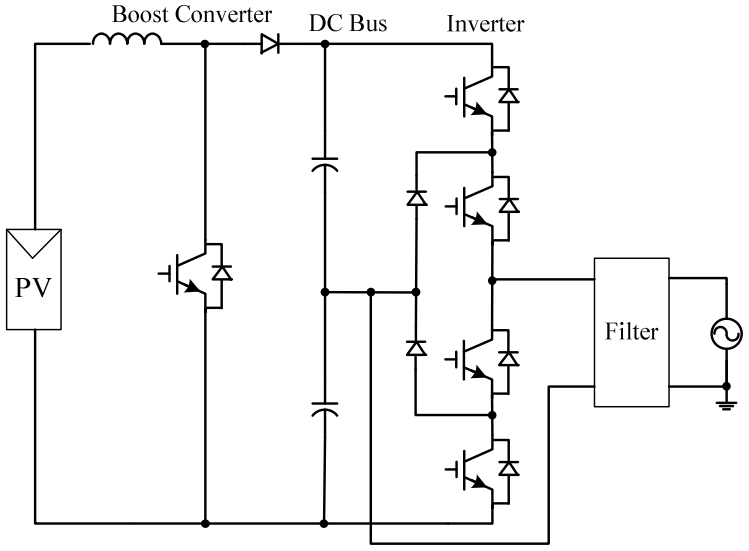


Figure 2.16. A Neutral Point Clamped inverter with a boost converter.

The other way is using a specially designed DC/DC converter in the first stage, which allows simultaneous grounding of source and load. At the same time, a bipolar output is provided to the inverter, and half-bridge topologies can be used as the second stage. A common approach to designing the first stage is to connect two basic DC/DC converter topologies in anti-parallel

[49], [50]. One example is the hybrid circuit composed of a buck-boost and zeta converters proposed in [49] and illustrated in Fig. 2.17. The advantage of these circuits is the use of a single active switch, however, the main drawbacks are the limited power level and the large amount of passive components. Another approach is to develop circuits where the energy transfer from source to load is electrically decoupled by a magnetic structure. Reference [51] has proposed a dual stage transformer-less PV inverter, where a DC/DC converter with coupled inductors is employed to realize doubly grounded and a half-bridge inverter is used as the second stage, as shown in Fig. 2.18. However, the power level is still limited by the energy storage requirements.

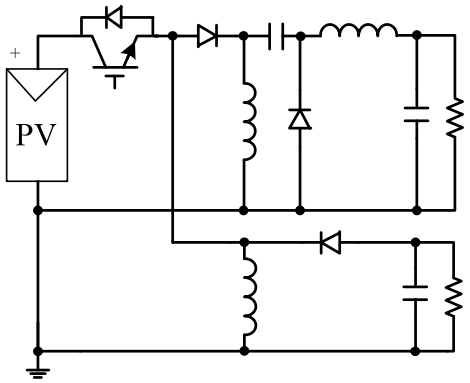


Figure 2.17. Non-isolated DC/DC converter with grounded source and bipolar output.

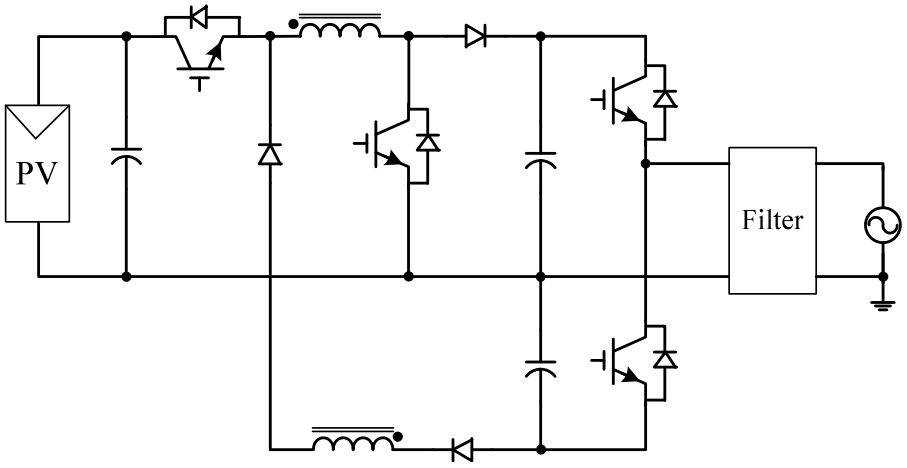


Figure 2.18. Topology of a dual stage transformer-less PV inverter.

The dual stage inverter with a single DC/DC converter can only be used in central, string or AC-module configurations, where a high power level and better utilization of PV modules cannot be achieved at the same time. To solve this issue, the dual stage inverter with multiple DC/DC converters is introduced to the multi-string and cascaded configurations.

### 2.2.3 Dual Stage Inverter with Multiple DC/DC Converters

The topology of the dual stage inverter with multiple DC/DC converters is shown in Fig. 2.2 (c). It will be the solution for the multi-string configuration if the DC/DC converters are connected in parallel. If the DC/DC converters are connected in series to create a high DC voltage, it will be the cascaded inverter.

As discussed above, in dual stage PV inverters, the only task for each DC/DC converter is MPPT and perhaps voltage amplification. The common DC/AC inverter will take care of the grid current control. The DC/AC inverter and DC/DC converter topologies have been discussed in the last two subsections and will not be repeated here. A commercially available multi-string inverter topology [52] is presented in Fig. 2.19 as an example. The circuits interfacing the PV strings are standard boost converters, and the grid-connected DC/AC inverter is a two-level VSI.

Due to the dual stage structure, the controller for each stage can be designed independently, leading to simpler controllers for dual stage PV inverters. However, compared to single stage PV inverters, dual stage inverters increase the system complexity, increase the cost, and reduce the overall efficiency as well.

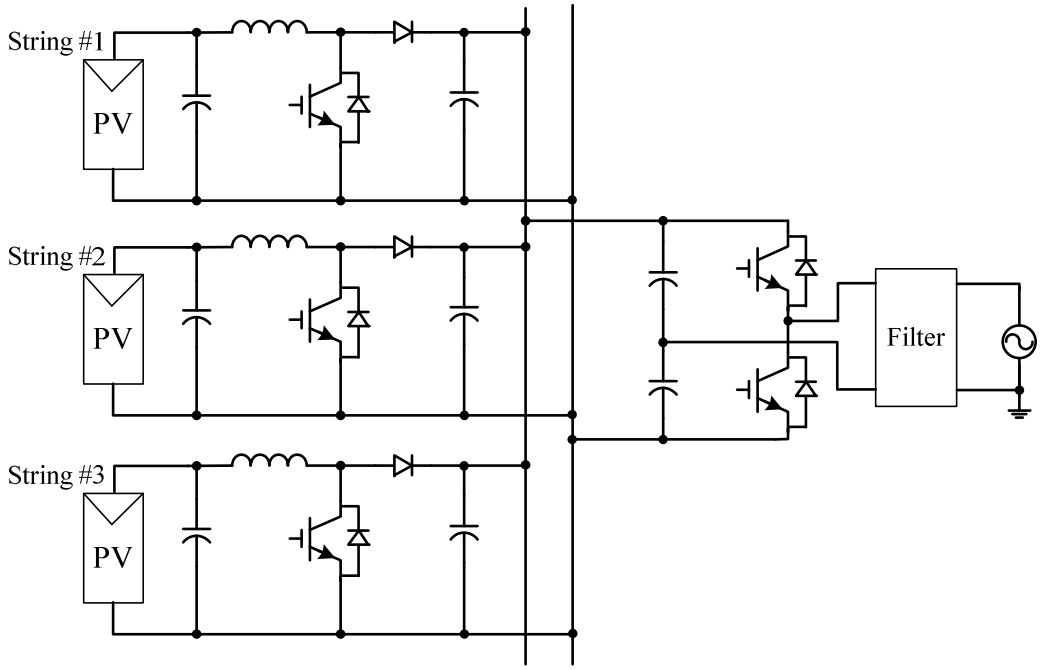


Figure 2.19. Topology of the multi-string inverter: Sunny Boy 5000TL.

## 2.3 Maximum Power Point Tracking System

To ensure the maximum power extraction from the PV array at any given time is one main objective of the grid-connected PV inverter. Therefore, the MPPT system is an essential part of grid-connected PV inverters. The PV power characteristic is nonlinear, varying with the level of solar irradiance and temperature, which makes the extraction of maximum power a complex task. In order to solve this issue, many methods for extracting the maximum power have been developed and implemented [53]-[57]. Comparisons of MPPT algorithms can be found in the literature [58]-[60].

Among those methods, Perturb and Observe (P&O) and Incremental Conductance (INC) methods are widely used in commercial products. Both use perturbative approaches for tracking the MPP, determining the voltage value at which the PV array delivers its maximum power.

P&O method involves a perturbation in the operating voltage of the PV array. As shown in

Fig. 2.20, if the operating voltage of the PV array is perturbed in a given direction and $dP/dV > 0$, it is known that the perturbation moved the array's operating point toward the MPP. The P&O algorithm would then continue to change the PV array voltage in the same direction. If $dP/dV < 0$, then the operating point was moved away from the MPP, and the P&O algorithm would change the PV array voltage in the opposite direction. The P&O method is easy to implement, but it has some drawbacks, like oscillations around the MPP in steady state operation, slow response speed, and may even fail under rapidly changing conditions [61].

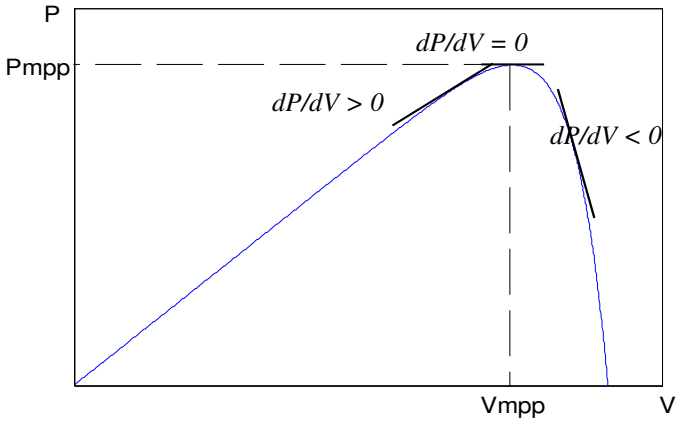


Figure 2.20. Sign of the dP/dV at different positions on the power characteristic curve.

The incremental conductance method is also based on the fact that the slope of the PV panel power curve is zero at the MPP, but it uses the PV array's incremental conductance $dI/dV$ to compute the sign of $dP/dV$. According to $d(VI)/dV = 0$, we could get that

$$\begin{cases} \Delta I / \Delta V = -I / V, & \text{at MPP} \\ \Delta I / \Delta V > -I / V, & \text{left of MPP} \\ \Delta I / \Delta V < -I / V, & \text{right of MPP} \end{cases} \tag{1}$$

Thus, the MPP can be tracked by comparing the instantaneous conductance to the incremental

conductance as shown in Fig. 2.21, where $V_{ref}$ is the reference voltage at which the PV panel is forced to operate.

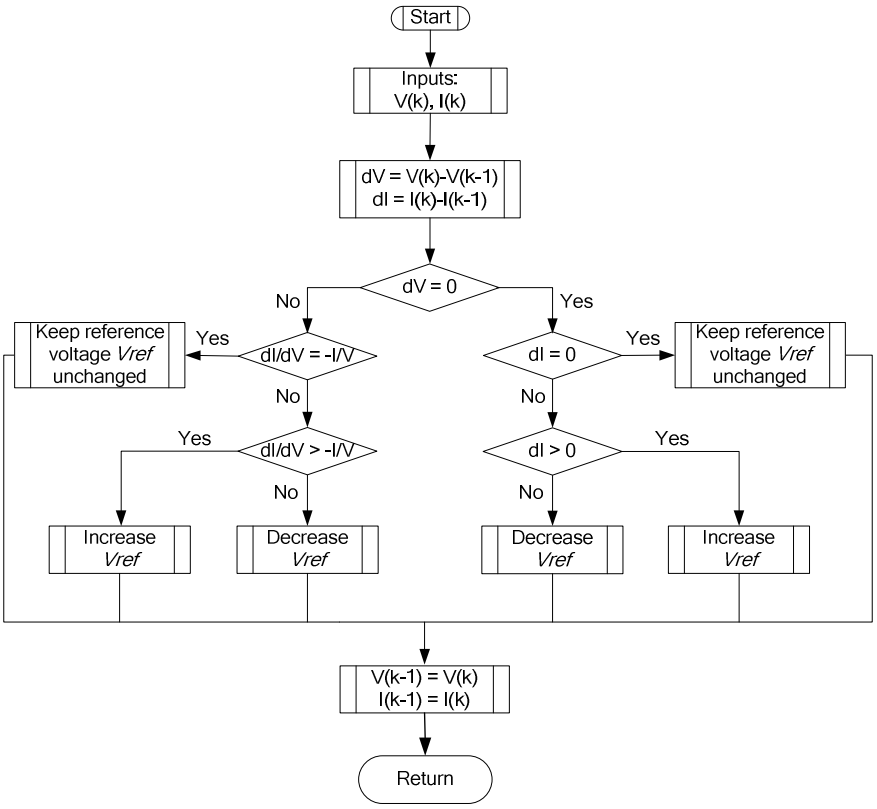


Figure 2.21. Flowchart of the incremental conductance method.

The increment size determines how fast the MPP is tracked. With bigger increments, fast tracking can be achieved. However, the system might not operate exactly at the MPP but oscillate around it. An improved incremental conductance method could solve this issue [56]. Let the increment size equal to $C \cdot \left| dP / dV \right|$ (coefficient $C$ is the scaling factor which is tuned at the design time to adjust the step size), then the step size is relatively large when the operating point is far away from the MPP, and the step size is small when the operating point is close to the MPP. Thus, both fast tracking and accurate operating can be achieved.

The efficiency maximization of the grid-connected PV inverter is useless if the maximum power extraction from the PV array is not ensured both at the steady state and under varying climatic conditions. Many MPPT algorithms are proposed and optimized to harvest more solar power from the PV array. However, the maximum power extraction is hardly achieved due to the mismatched operation of the PV array, especially in the medium- and large scale PV system, where the long PV strings are very sensitive to the partial shading caused by the nearby obstacles and even the passing of clouds.

To reduce partial shading effects, the PV modules are usually equipped with bypass diodes [62]. When bypass diodes are on, partially shaded modules can be bypassed, and the overall power generation from the PV array under partial shading conditions can be increased. However, the bypassed PV modules may still be able to generate power. Thus, this method does not allow the array to produce the maximum possible power under partial shading. In addition, turning these bypass diodes on creates losses due to their ON-state resistances. Other solutions are needed to increase the power production in presence of mismatching effects, like the dynamic reconfiguration of the PV arrays and distributed MPPT control.

The dynamic electrical array reconfiguration (EAR) strategy is carried out by inserting a controllable switching matrix between the PV modules and the central inverter, which allows the reconnection of the available PV modules. As a result, the PV system exhibits a self-capacity for real-time adaptation to the external operating conditions and improves the power production of the system [63]. However, this technique introduces a controllable switching matrix to the PV system, which increases the system cost. Moreover, for large PV arrays, there will be lots of possible configurations. It will be very difficult to find the optimal configuration in a timely manner, and real-time adaptation may not be reached.

For the distributed MPPT control, each module or group of modules has its own MPPT, thus avoiding mismatching losses caused by the partial shading or different temperatures between the modules. According to the configurations of PV systems, the distributed MPPT control can only be applied to multi-string and cascaded inverters. The distributed MPP tracking can be implemented either by connecting the output terminals of the DC/DC converters in parallel or in series [64], as shown in Fig. 2.22. With DC/DC converters, individual MPPT is performed by each DC/DC converter, and can be easily realized.

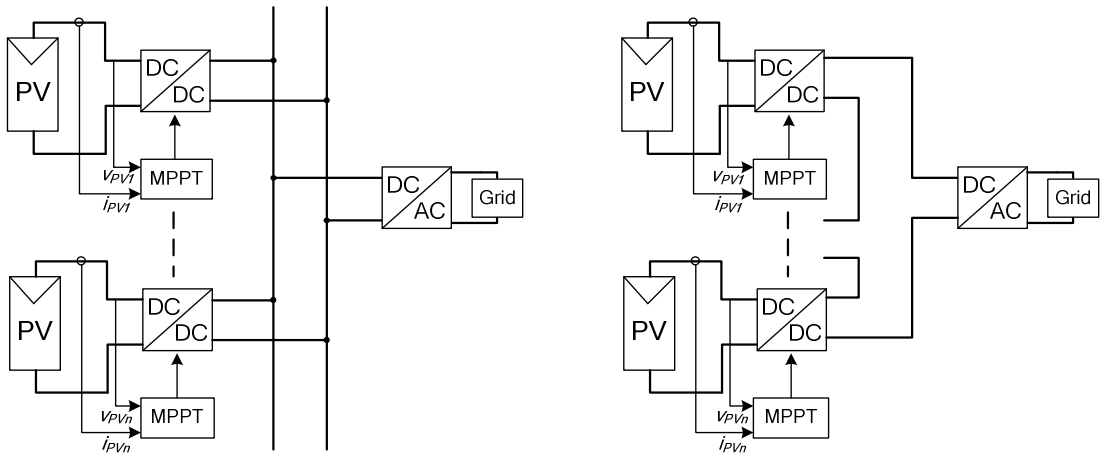


Figure 2.22. Distributed MPPT using parallel-connected and series-connected DC/DC converters.

However, as discussed above, dual stage inverters increase the system complexity, increase the cost, and reduce the overall efficiency as well. Thus, a question has been raised, can distributed MPPT control be implemented without the DC/DC converter. The answer is yes. As a single stage inverter, the cascaded H-bridge multilevel inverter has separate DC links, which make independent voltage control possible. But few papers have studied on the distributed MPPT control of cascaded H-bridge multilevel inverters, and no experimental results are given, especially for three-phase systems. There are still challenges for applying distributed MPPT

control to the cascaded H-bridge multilevel inverter. Without the DC/DC converter, individual MPPT control of each module must be realized in a central controller, which requires a complicated control algorithm. Also, in the three-phase system, unbalanced power could be supplied to the grid if distributed MPPT is achieved. The grid current must be balanced to meet PV interconnection standards. In the next two chapters, these issues are discussed in detail.

## 2.4 Summary

A literature review on grid-connected PV inverters has been provided. According to the different configurations of the PV system, five inverter families can be defined: (1) central inverters, (2) string inverters, (3) multi-string inverters, (4) AC-module inverters, and (5) cascaded inverters. The advantages and disadvantages of these inverters are discussed. Among these configurations, the DC/AC cascaded inverter can be used in medium- and large scale PV applications without sacrificing the benefits of "converter per panel". Unlike multi-string inverters or cascaded DC/DC converters, the DC/AC cascaded inverter can employ the single stage inverter, which further improves the overall efficiency and reduces the cost.

The grid-connected PV inverter topologies are also discussed. According to the number of power processing stages, the inverter topologies can be categorized as single stage inverters and dual stage inverters. Many single and dual stage inverter topologies have been reviewed. The single stage inverter has the benefits of low cost, high efficiency and reliability, but it must handle all tasks itself.

MPPT systems are discussed as well in this chapter. Many MPPT algorithms have been reviewed, and P&O and Incremental Conductance methods are introduced as examples. Solutions for increasing the power production in the presence of mismatching effects are

discussed.

# 3 Control of Single-Phase Cascaded H-Bridge Multilevel Inverter for Grid-Connected Photovoltaic Systems

Many different types of PV inverters have been discussed in the previous chapter. The cascaded H-bridge multilevel inverter requires an isolated DC source for each H-bridge; thus, the high power and/or high voltage from the combination of the multiple modules would favor this topology in medium and large grid-connected PV systems [65]-[67]. In addition, the separate DC links in the multilevel inverter make independent voltage control possible. As a result, individual maximum power point tracking (MPPT) control in each string can be achieved, and the energy harvested from PV panels can be maximized. Meanwhile, the modularity and low cost of multilevel converters would position them as a prime candidate for the next generation of efficient, robust, and reliable grid-connected solar power electronics.

A single-phase cascaded H-bridge multilevel inverter topology for a grid-connected PV system is presented in this chapter. The panel mismatch issues are addressed to show the necessity of individual MPPT control, and a control scheme with independent MPPT control and reactive power compensation is then proposed. Simulation and experimental results are provided to demonstrate the developed control scheme.

## 3.1 System Description

The cascaded multilevel inverter topology consists of $n$ H-bridge converters connected in series and is shown in Fig. 3.1. Each DC link is fed by a PV panel or a short string of PV panels to increase the power level. By different combinations of the four switches in each H-bridge, three output voltage levels can be generated, $-v_{dc}$, 0, or $+v_{dc}$. A cascaded multilevel inverter with $n$ input

sources will provide $2n+1$ levels to synthesize the AC output waveform. This $(2n+1)$-level voltage waveform enables the reduction of harmonics in the synthesized current, reducing the size of the needed output filters. Multilevel inverters also have other advantages such as reduced voltage stresses on the semiconductor switches, as well as having higher efficiency when compared to other converter topologies [40].

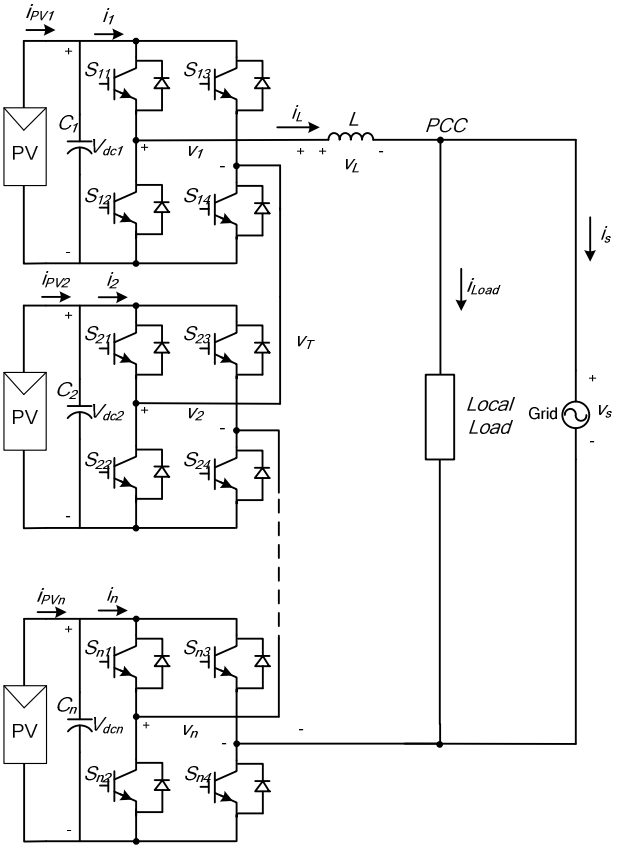


Figure 3.1. Topology of single-phase grid-connected PV system.

As shown in Fig. 3.1, the cascaded multilevel inverter is connected to the grid through an $L$ filter, which is used to reduce the switching harmonics in the current. There is also a local load connected in parallel. PV power is delivered to the load/grid according to the system operation conditions.

The output voltage of each H-bridge inverter can be described as

$$v_j = (S_{j1} - S_{j3})v_{dcj} = P_j v_{dcj} \tag{2}$$

where $v_{dcj}$ is the dc-link voltage of the $j^{th}$ ($j$ = 1, 2, … $n$) H-bridge inverter, $S_{j1(3)}$ represents the state of switch $S_{j1(3)}$ according to Fig. 3.1, and $P_j$ is the discrete switching function, which has the values -1, 0, or +1.

In order to have a linear model, the discrete switching function $P_j$ can be replaced by the continuous switching function $S_j$ in (2). During the steady-state operation, these continuous switching functions are sinusoidal and bounded in the interval [-1, 1]. Thus, the dynamic behavior of the single-phase grid-connected PV system can be described by the following equations:

$$\frac{di_L}{dt} = \frac{1}{L}(\sum_{j=1}^{n} S_j v_{dcj} - v_s - Ri_L) \tag{3}$$

$$\frac{dv_{dcj}}{dt} = \frac{1}{C_j}(i_{PVj} - S_j i_L) \tag{4}$$

$$i_L = i_{Load} + i_s \tag{5}$$

where $i_L$ is the output current of the cascaded H-bridge multilevel inverter, $L$ and $R$ are the decoupling inductance and its resistance respectively, $i_{Load}$ is the local load current, and $i_s$ is the grid current.

According to (3), the inductor ripple current $\Delta i_L$ needs to be analyzed to select inductor $L$. Assume the dc-link voltage of each H-bridge module is equal, and we have $v_{dcj} = v_{dc}$. The cascaded H-bridge multilevel inverter will switch such that

$$kv_{dc} \le v_s(\omega t) \le (k+1)v_{dc} \tag{6}$$

Without loss of generality, let $k$ = 0. The unipolar double-frequency sinusoidal pulse width modulation (SPWM) is applied, and if the fundamental current of the inductor $L$ is zero, the ripple current $\Delta i_L$ can be shown as Fig. 3.2.

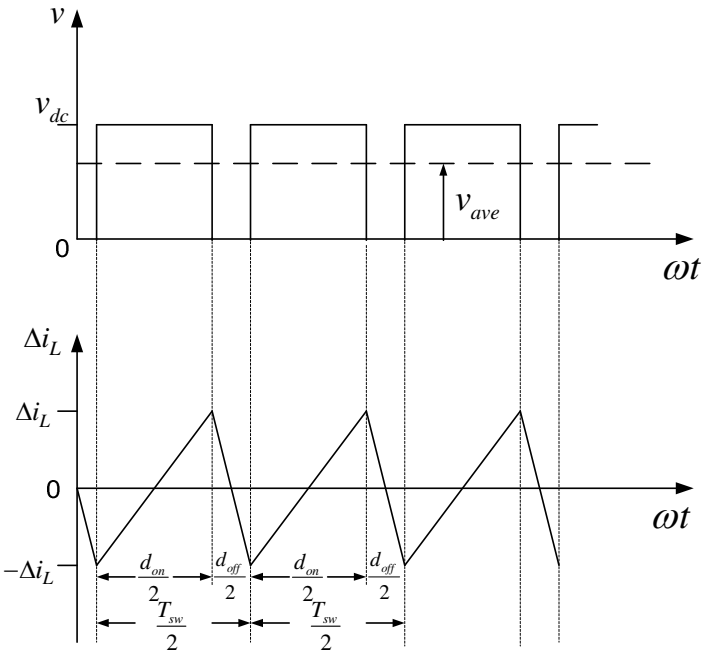


Figure 3.2. Inverter voltage and inductor ripple current $\Delta i_L$ waveforms.

From Fig. 3.2, we have

$$2\Delta i_L = \frac{v_{dc} - v_{ave}}{L} \cdot \frac{d_{on}}{2} \cdot \frac{1}{f_{sw}} \tag{7}$$

where $v_{ave}$ is the average value of the fundamental component of the inverter voltage in a switching period, $d_{on}$ is the duty ratio during this switching period, and $f_{sw}$ is the switching frequency.

During $0 < \omega t < \pi$, we have

$$v_{ave}(\omega t) = m v_{dc} \sin \omega t \tag{8}$$

$$d_{on}(\omega t) = m \sin \omega t \tag{9}$$

where $m$ is the modulation index.

From (7) – (9), the ripple current through the inductor $L$ can be expressed as

$$\Delta i_L = \frac{v_{dc}}{4 f_{sw} L}(1 - m \sin \omega t) m \sin \omega t \tag{10}$$

Thus, the relationship of the ripple current and the modulation index is obtained, as shown in Fig. 3.3. And we have

$$\Delta i_{L\max} = \frac{v_{dc}}{16 f_{sw} L} \tag{11}$$

which can be used to select the inductor $L$.

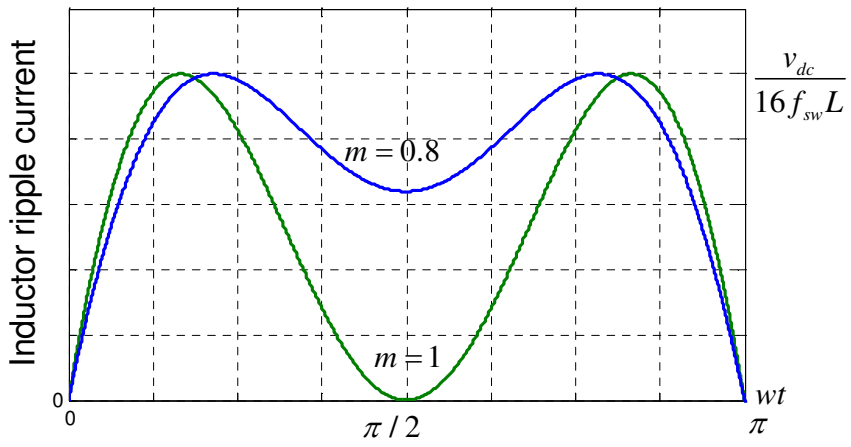


Figure 3.3. Relationship of the ripple current and the modulation index.

In this dissertation, the modular design is considered to reduce the manufacturing cost. So the dc-link capacitor of each H-bridge module would be the same capacitor $C$, and we have

$$C = \frac{P_{total}}{2n\omega_{grid}V_{dc}v_{ripple}} \tag{12}$$

where $P_{total}$ is the rated power of the cascaded multilevel inverter, $V_{dc}$ is the mean voltage across the capacitor, and $v_{ripple}$ is the amplitude of the voltage ripple.

For the PV application, $P_{total}$ is the total maximum power of all the connected PV panels, and $V_{dc}$ is the MPP voltage of the connected PV panel of one H-bridge module. To make PV panels operated around the MPPs without too much fluctuation, the ripple at the terminals of the PV modules should be sufficiently small. Calculations in [68] show that the amplitude of the voltage ripple should be below 6% of the MPP voltage in order to reach a utilization ratio of 99%. Here, the utilization ratio is given as the average generated power divided by the theoretical MPP power.

## 3.2 PV Panel Mismatches

Due to the unequal received irradiance, different temperature, and aging of the PV panels, the maximum power points (MPPs) of each PV string may be different. When there is mismatch between the PV strings, the efficiency of the overall PV system will be decreased if the MPP of each string is not tracked individually. Simulations in MATLAB/SIMULINK are carried out to show the necessity of individual MPPT control in the single-phase cascaded PV system.

### 3.2.1 Modeling of PV Module

The accurate and reliable modeling of the PV module is important to the PV system analysis and design. Some researchers have studied the model of PV modules by using 2-diode or 3-diode

model [69], [70]. However, those models can be further simplified to a single diode model, which has moderate complexity and acceptable accuracy. Fig. 3.4 shows the single diode model of a PV module, while the associated relation between PV current and voltage is shown in (13) [71].

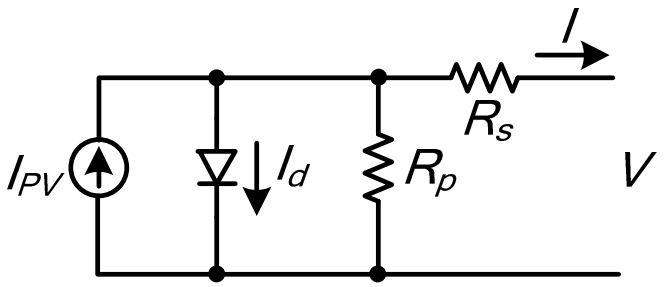


Figure 3.4. Single diode model of a PV module.

$$I = I_{PV} - I_0 \left[ e^{\left( \frac{V + R_s I}{V_t a} \right)} - 1 \right] - \frac{V + R_s I}{R_p} \tag{13}$$

where $I$ is the output current of a PV module, $I_{PV}$ is the photovoltaic current, $I_0$ is the diode reversed saturation current, $V$ is the output voltage, $V_t = N_s kT/q$ is the thermal voltage of a module with $N_s$ cells connected in series, $R_s$ is the equivalent series resistance, $R_p$ is the equivalent parallel resistance, and $a$ is the diode ideality constant.

In this dissertation, the PV module model in MATLAB/SIMULINK is built based on the single diode equation. The datasheets from PV manufacturers provide the parameters to solve for the unknowns.

Commercial PV panels, HIP-195BA19, from Sanyo, are used in the simulation and experimental tests. The specifications are shown in Table 3.1. According to the parameters, the

PV module is modeled and the *I-V* characteristics of the panel obtained by simulation are shown in Fig. 3.5.

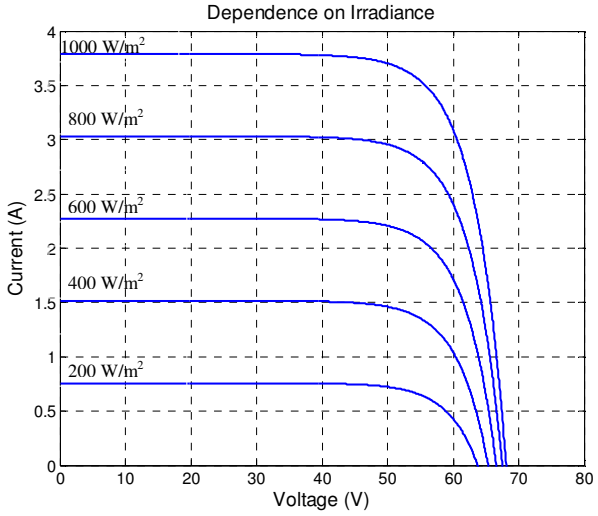


(a) Dependence on irradiance (T = 25 ˚C)

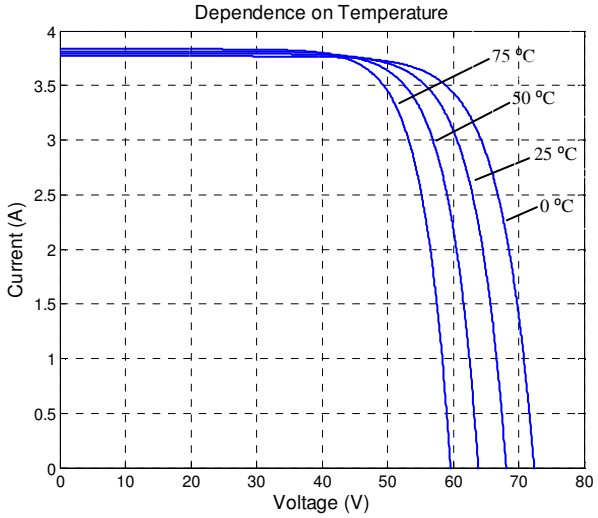


(b) Dependence on temperature (S = 1000 W/m$^2$)

Figure 3.5. Simulated *I-V* characteristics of PV module Sanyo, HIP-195BA19.

Table 3.1. Specifications of PV module Sanyo, HIP-195BA19

| | |
|---|---|
| Rated Power ($P_{max}$) | 195 W |
| Maximum Power Voltage ($V_{pm}$) | 55.3 V |
| Maximum Power Current ($I_{pm}$) | 3.53 A |
| Open Circuit Voltage ($V_{oc}$) | 68.1 V |
| Short Circuit Current ($I_{sc}$) | 3.79 A |
| Temperature Coefficient $V_{oc}$ | -0.189 V/°C |
| Temperature Coefficient $I_{sc}$ | 1.98 mA/°C |

### 3.2.2 Simulation Results

To show the necessity of individual MPPT control in the single-phase cascaded PV system, a 5-level two H-bridges inverter is simulated in MATLAB/SIMULINK. Each H-bridge has its own 195 W PV panel (Sanyo, HIP-195BA19) connected as an isolated DC source. The established PV module model is implemented to run the inverter simulations.

Consider an operating condition where each panel has a different irradiation: panel 1 has irradiance S = 1000 W/m$^2$, and panel 2 has S = 600 W/m$^2$. If only panel 1 is tracked and its MPPT controller determines the average voltage of the two panels, the power extracted from panel 1 would be around 147 W, and the power from panel 2 would be 60 W, as seen in Fig. 3.6. Without individual MPPT control, the total power harvested from the PV system is 207 W.

However, Fig. 3.7 shows the MPPs of the PV panels under the different irradiance. The maximum output power will be 195 W and 114.6 W respectively when S = 1000 W/m$^2$ and 600 W/m$^2$, which means the total power harvested from the PV system would be 309.6 W if individual MPPT can be achieved. This higher value is about 1.5 times of the one before. Thus, the individual MPPT control in each string is required to reduce the adverse effect of the

mismatches and increase the efficiency of the PV system.

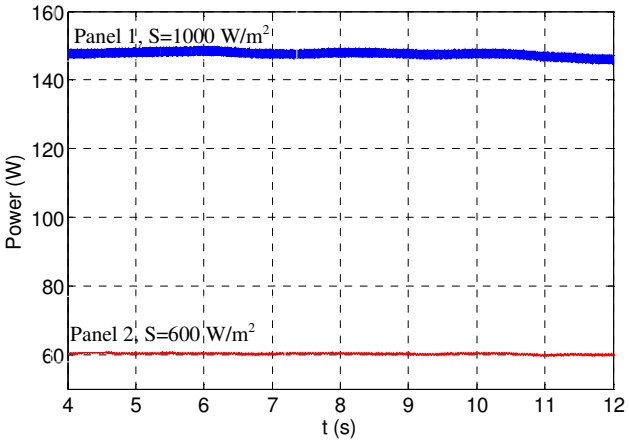


Figure 3.6. Power extracted from two PV panels.

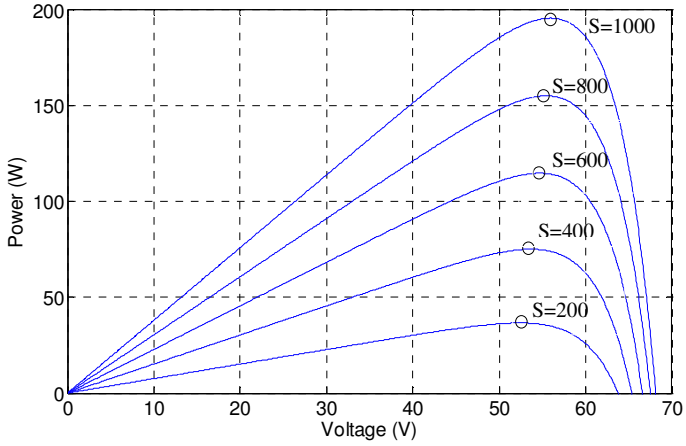


Figure 3.7. *P-V* characteristics under the different irradiance.

## 3.3 Control Scheme

The cascaded H-bridge multilevel inverters can be used in medium and large grid-connected PV systems without having to sacrifice the utilization of PV modules. However, as discussed above, this benefit can be realized only if each PV string is individually MPP tracked. Meanwhile, at higher penetrations, the impact of PV systems may accumulate and affect power

quality. The reactive power control of PV inverters provides an opportunity to maintain good power quality in the grid and optimize the performance of distribution circuits. Thus, a control scheme with individual MPPT control and reactive power compensation is proposed, as shown in Fig. 3.8. The details of the control scheme will be discussed in the next subsections.

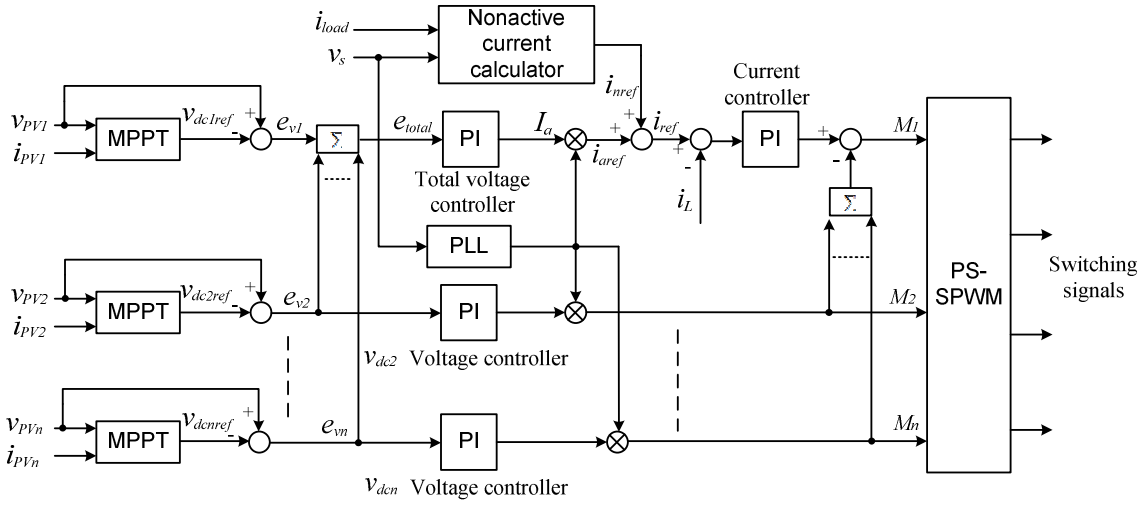


Figure 3.8. Control scheme.

### 3.3.1 Individual MPPT Control

In order to eliminate the adverse effect of the mismatches and increase the efficiency of the PV system, the PV strings need to operate at different voltages to maximize the energy harvested from each string. The separate DC links in the cascaded H-bridge multilevel inverter make independent voltage control possible.

As shown in Fig. 3.8, an MPPT controller is added to generate the dc-link voltage reference of each H-bridge. To manage distinct power transfers and different voltage levels on the *n* H-bridges, *n* voltage loops are necessary [72]. First, each dc-link voltage $v_{dcj}$ is compared to the corresponding voltage reference $v_{dcjref}$, and the sum of all the errors is controlled through a PI

controller that determines the active current reference. Reactive current reference $i_{nref}$ is obtained by using a generalized nonactive power theory, which will be discussed in the next subsection. The current controller then gives the sum of the modulation index of each H-bridge inverter.

The voltages $v_{dc2}$ to $v_{dcn}$ are controlled individually through the last $n$-1 loops. Each voltage controller gives the modulation index of one H-bridge module. The modulation index for the first H-bridge can be obtained by subtracting the remaining modulation index. After obtaining $n$ modulation indices, phase-shifted SPWM (PS-SPWM) switching scheme is applied to control the switching devices of each H-bridge.

In order to design the voltage controllers, suitable transfer functions are obtained by the linearization of (4) around the nominal operating point. For the total voltage controller, the following equation can be obtained according to (4)

$$\sum_{j=1}^{n} S_j \cdot i_L = \sum_{j=1}^{n} i_{PVj} - \sum_{j=1}^{n} C_j \frac{dv_{dcj}}{dt} \tag{14}$$

where $C_j = C$, $j = 1, 2, \ldots n$, and $C$ is the capacitance.

Considering only the dc component of $S_j \cdot i_L$ yields the following:

$$\frac{1}{2}\sum_{j=1}^{n} S_{j,\max} \cdot i_{L,\max} = \sum_{j=1}^{n} i_{PVj} - C\sum_{j=1}^{n} \frac{dv_{dcj}}{dt} \tag{15}$$

To simplify the transfer function, considering the output currents of PV panels $i_{PVj}$ as disturbances. Thus, (15) can be expressed in the Laplace domain as

$$\frac{\sum_{j=1}^{n} V_{dcj}(s)}{I_{L,\max}(s)} = -\frac{\sum_{j=1}^{n} S_{j,\max}}{2Cs} \tag{16}$$

Similarly, the design of the other $n$-1 voltage controllers can be based on the following equation

$$\frac{V_{dck}(s)}{S_{k,\max}} = -\frac{I_{L,\max}(s)}{2Cs} \tag{17}$$

where $k = 2, \ldots n$.

### 3.3.2 Reactive Power Compensation

High-penetration levels of PV generation present challenges to distribution utilities. Despite the challenges, there is also an opportunity for the utility to enhance its performance with the grid-connected PV inverters [73]-[75]. For example, the reactive power control of PV inverters provides an opportunity to improve power quality and reduce distribution losses in the grid. However, (18) and (19) provide an excellent expression for gaining intuition about the competing nature of minimizing the voltage variation and reducing distribution circuit losses [75].

The rate of energy dissipation $E_j$ and the change in voltage $\Delta V_j$ between nodes $j$ and $j$+1 of the distribution circuit are given by

$$E_j = r_j \frac{P_j^2 + Q_j^2}{V_0^2} \tag{18}$$

$$\Delta V_j = -\frac{r_j P_j + x_j Q_j}{V_0} \tag{19}$$

where $P_j$ and $Q_j$ represent active and reactive power flowing down the circuit from node $j$, $V_j$ is the voltage at node $j$, $r_j$+$ix_j$ is the complex impedance of the link between node $j$ and $j$+1, as shown in Fig. 3.9.

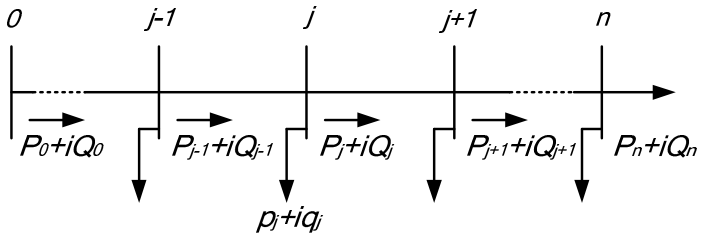


Figure 3.9. Diagram for the radial network.

Equation (18) shows that losses in any circuit segment $j$ are minimized when $Q_j = 0$, which means the consumption and generation of reactive power at the node should be equal. However, (19) shows that $Q_j = -r_j P_j / x_j$ is needed to minimize the voltage variation, which is in clear competition with loss reduction. Therefore, reactive power compensation that provides optimal voltage regulation and minimizes losses simultaneously should not be expected.

Due to the competition between optimal voltage regulation and minimization of losses, there are three reactive power control options: (1) control on local voltage only, (2) control on local flow only, and (3) hybrid control, which considers both local voltage and power flow. The control algorithm based on local voltage only is proposed in other papers. In this dissertation, the control scheme is based on local flow such that losses are minimized when reactive power flows $Q_j$ are zero. The local consumption of reactive power is supplied by the PV inverter up to the limits imposed by its capacity and generation, and power factor correction at the point of common coupling (PCC) is achieved.

To provide the local consumption of reactive power, generalized nonactive power theory [76] is applied to calculate the reactive current reference. Consistent with the standard steady-state power definitions, this theory is an extension of the standard definitions and other instantaneous power theories. The defined instantaneous active and reactive power and/or current are valid in

various power systems, whether single-phase or multi-phase, sinusoidal or non-sinusoidal, periodic or non-periodic, balanced or unbalanced.

Considering the single-phase PV system, the average power of the local load is denoted as *P(t)*:

$$P(t) = \frac{2}{T}\int_{t-\frac{T}{2}}^{t} v_{Load}(\tau) i_{Load}(\tau) d\tau \tag{20}$$

The instantaneous active current of the local load $i_a(t)$ is defined by

$$i_a(t) = \frac{P(t)}{V_p^2(t)} v_p(t) \tag{21}$$

where $v_p(t)$ is the reference voltage, and $V_p(t)$ is the rms value of $v_p(t)$. In this system, the grid voltage is chosen as the reference voltage.

Then, the instantaneous reactive current of the local load $i_n(t)$ is defined by

$$i_n(t) = i_{Load}(t) - i_a(t) \tag{22}$$

Assuming the instantaneous local load current could be measured by a local smart meter, the instantaneous reactive current is calculated as the reactive current reference of the multilevel inverter. Thus, the reactive current in the local load will be supplied by the cascaded H-bridge multilevel inverter, and the point of common coupling will be operated at unity power factor.

The reactive generation is limited by the inverter capacity, and the reactive current reference is also limited. However, the reactive power of the local load will be compensated to the greatest degree possible by the multilevel inverter, which helps to reduce the distribution circuit losses.

## 3.4 Results

Simulation and experimental tests are carried out to validate the proposed ideas. A single-phase modular cascaded multilevel inverter prototype has been built. Each H-bridge has its own 195 W PV panel (Sanyo HIP-195BA19) connected as an independent source. For simplicity and to easily appreciate the control principle, only two H-bridge modules will be considered in the simulation and experimental tests. The system parameters are shown in Table 3.2.

Table 3.2. System parameters

| Parameters | Value |
|---|---|
| DC-link capacitor | 3.6 mF |
| Connection inductor *L* | 3 mH |
| Load inductor | 20 mH |
| Load resistor | 20 ohm |
| Grid rated RMS voltage | 48 V |
| Switching frequency | 1.8 kHz |

Equation (11) is used to select the connection inductor *L*. Considering that the PV inverter cannot be operated at the rated power all the time, the current ripple is chosen as the 10% of the rated inverter current, which is calculated as

$$\Delta i_{L\max} \le 10\% \cdot \frac{nP_{PV}}{v_s} = 0.1 \times \frac{2 \times 195}{48} = 0.8125A \tag{23}$$

Thus, the connection inductor *L* is calculated as

$$L = \frac{v_{dc}}{16 f_{sw} \Delta i_{L\max}} \ge \frac{55.3}{16 \times 1800 \times 0.8125} = 2.36mH \tag{24}$$

Here, the connection inductor is selected as $L$ = 3 mH.

To verify the individual MPPT control scheme, the 5-level inverter is simulated in two different conditions. First, two PV panels are operated under the same irradiance S = 1000 W/m$^2$ and temperature T = 25 ˚C. At t = 2s, the solar irradiance on the first panel stays the same, and that for the second panel decreases to 600 W/m$^2$. The dc-link voltage waveforms of two modules are shown in Fig. 3.10. As the irradiance changes, the second dc-link voltage decreases and tracks the new MPP voltage of the second PV panel.

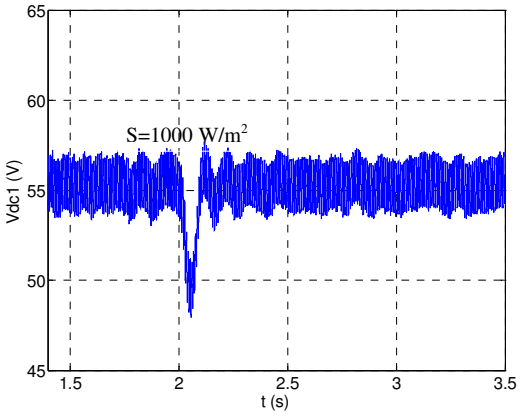


(a) DC-link voltage of module 1

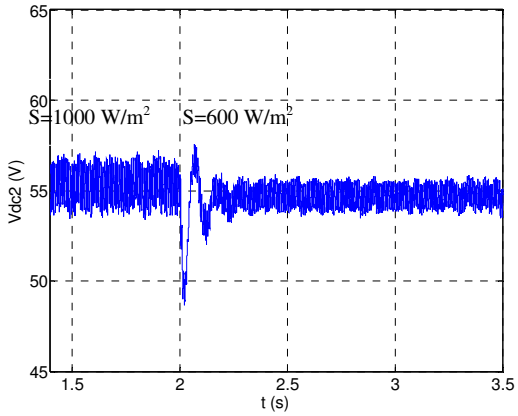


(b) DC-link voltage of module 2

Figure 3.10. Simulated dc-link voltage of two modules with individual MPPT(T=25 ˚C).

The PV current waveforms are shown in Fig. 3.11. It can be seen that the lower irradiation affects the current in the second PV panel, so the lower ripple of the dc-link voltage can be found in Fig. 3.10(b).

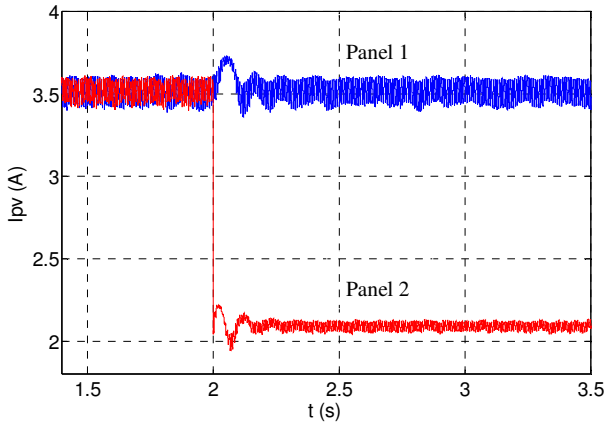


Figure 3.11. Simulated PV current of two modules with individual MPPT(T=25 ˚C).

Fig. 3.12 shows the power extracted from the two panels. At the beginning, both panels are operated under irradiance S = 1000 W/m$^2$ and generating maximum power 195 W. After t = 2s, when the solar irradiance over the second panel decreases to 600 W/m$^2$, the power extracted from panel 1 is still 195 W, and the power from panel 2 is 114.5 W. According to the *P-V* characteristics shown in Fig. 3.7, each PV panel is operating at its own maximum power point. Thus, individual MPPT has been achieved, and the efficiency of the PV system is improved.

The voltage and current waveforms of the grid and load are shown in Fig. 3.13. It can be seen that the load current is lagging the grid voltage, however, the grid current has the same phase as the voltage, which means the grid has unity displacement power factor. The output voltage of the multilevel inverter is shown in Fig. 3.14. The 5-level voltage helps to reduce the output filters.

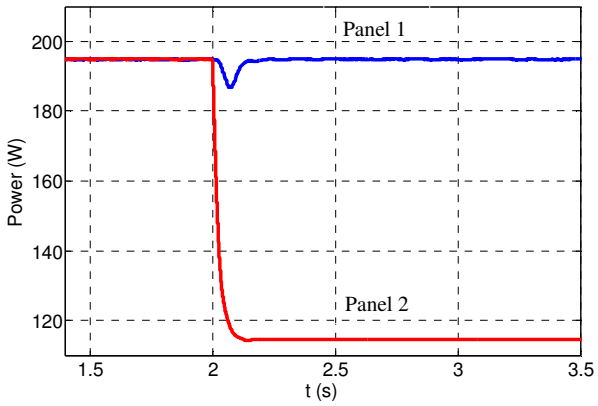


Figure 3.12. Simulated power extracted from two PV panels with individual MPPT.

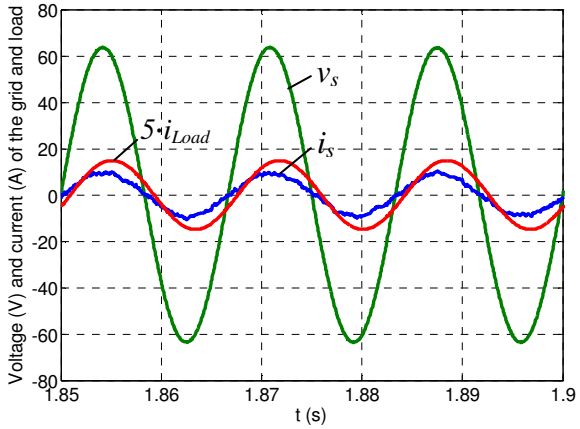


Figure 3.13. Simulated voltage and current waveforms of grid and load.

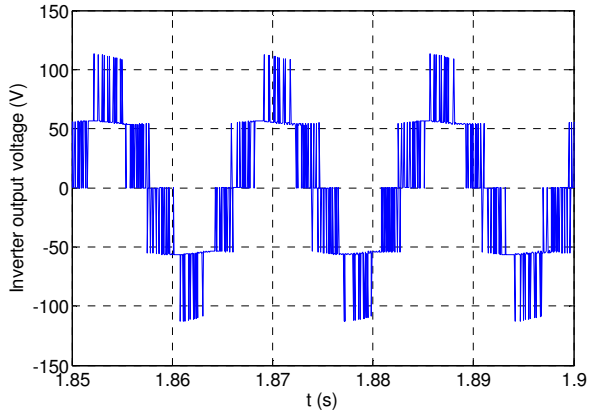


Figure 3.14. Simulated inverter output voltage.

A modular cascaded multilevel inverter prototype has been built in the laboratory. The modular design will increase the flexibility of the system, and reduce the cost as well. MOSFET IRFSL4127 is selected as inverter switches operating at 1.8 kHz. The control signals to the H-bridge inverters are sent by a dSPACE ds1103 controller. Fig. 3.15 shows the experimental solar panels and the 5-level cascaded multilevel inverter.

(a) Solar panels Sanyo HIP-195BA19

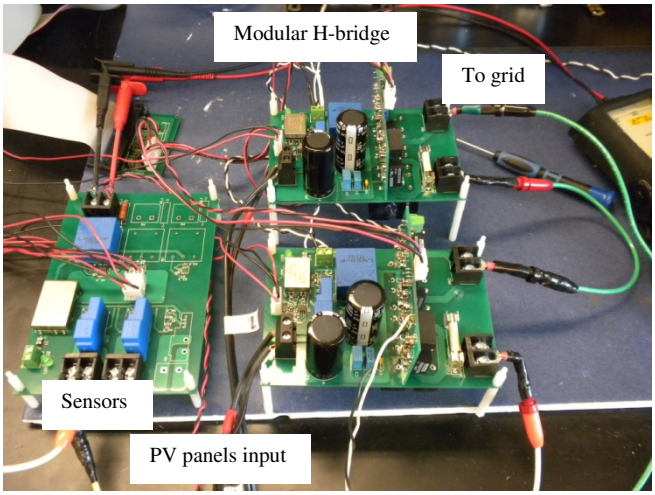


(b) Modular 5-level cascaded multilevel inverter

Figure 3.15. Experimental prototype.

The experimental results are presented in Fig. 3.16 and Fig. 3.17. Fig. 3.16 shows the grid voltage, current and the dc-link voltage of two H-bridge modules. It can be seen that the two dc-link voltages are controlled independently, which means individual MPPT can be achieved. Fig. 3.17 shows the grid voltage and current, the load current and the inverter output voltage. The experimental results also show that the grid current has the same phase as the grid voltage and has unity displacement power factor.

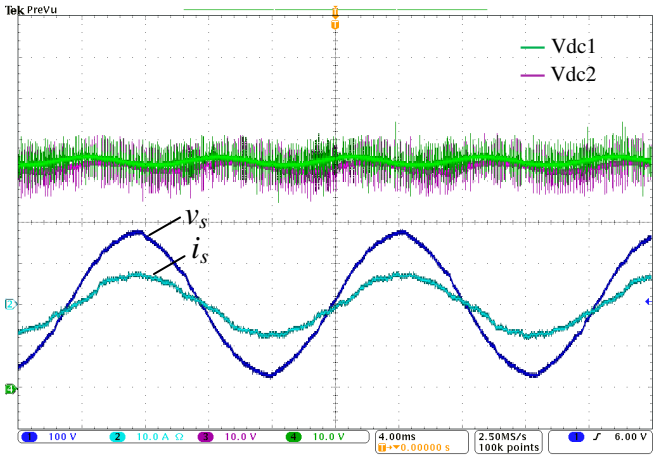


Figure 3.16. Experimental grid voltage, current and two dc-link voltages with individual MPPT.

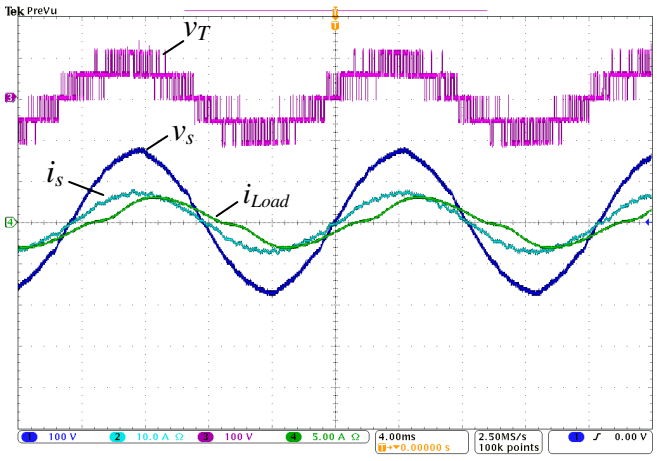


Figure 3.17. Experimental grid voltage and current, load current and inverter output voltage.

The THD of the grid current is 4.7% and the rms value is 5.0 A, as shown in Fig. 3.18. In IEEE 1547 [77], the maximum harmonic current distortion is set as 5% total demand distortion (TDD). Thus, based on the rated current 8.125 A, the TDD of the grid current is calculated as 2.9%, which is less than 5% and meets the power quality standards.

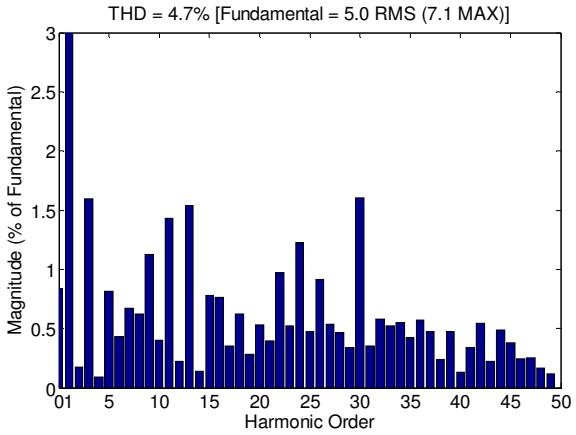


Figure 3.18. THD of the grid current $i_s$ shown in Fig. 3.15.

## 3.5 Summary

In this chapter, a single-phase modular cascaded H-bridge multilevel inverter for grid-connected PV system with reactive power compensation has been presented. Due to the cascaded configuration, the inverter has the possibility to reduce the adverse effect of PV mismatches even in medium and large grid-connected PV systems. Individual MPPT control is necessary to realize this benefit. A control scheme with independent MPPT control and reactive power compensation has been proposed. Simulation and experimental results show that individual MPPT control is achieved to maximize the solar energy extraction of each PV string, and the reactive power required by the local load is provided by the proposed system to realize the power factor correction and reduce distribution losses.

# 4 Control of Three-Phase Modular Cascaded H-Bridge Multilevel Inverter for Grid-Connected Photovoltaic Systems

The trend towards large-scale grid integration is continuing in PV systems, and three-phase inverters are more widely used in medium and large grid-connected PV systems. The cascaded H-bridge multilevel inverter topology is also a good choice for the three-phase large-scale PV system. By individual MPPT control in each string, the energy harvested from PV panels can be maximized. Meanwhile, the topology itself has higher efficiency when compared to other converter topologies, and the modular design can increase the flexibility of the system, and reduce the cost as well.

## 4.1 System Description

The three-phase modular cascaded H-bridge multilevel inverter for grid-connected PV system is shown in Fig. 4.1. Each phase consists of $n$ H-bridge converters connected in series, and the DC link of each H-bridge is fed by a short string of PV panels. The cascaded multilevel inverter is connected to the grid through $L$ filters, which are used to reduce the switching harmonics in the current.

The behavior of the cascaded H-bridge multilevel inverter has been discussed in the last chapter and will not be repeated here.

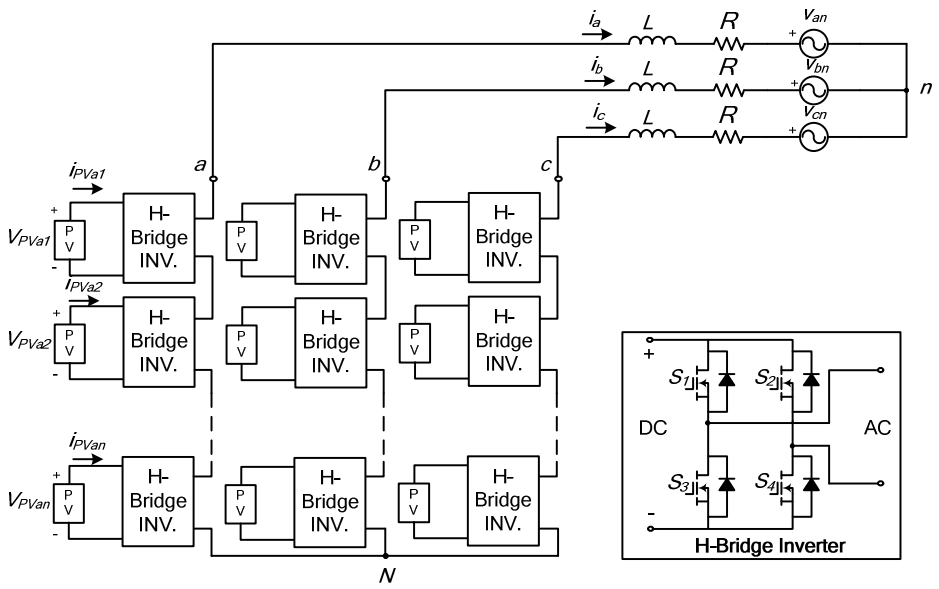


Figure 4.1. Topology for the three-phase grid-connected system.

## 4.2 Control Scheme

As discussed in the single-phase system, the individual MPPT control in each string is required to reduce the adverse effect of PV mismatches and increase the overall efficiency. In a three-phase grid-connected PV system, PV mismatches may cause more problems. Besides decreasing the overall efficiency, this could even introduce unbalanced power supplied to the three-phase grid-connected system. If there are PV mismatches between phases, the input power of each phase would be different. Since the grid voltage is balanced, the different input power will cause unbalanced current to the grid, which is harmful to the grid and not allowed by utility standards. For example, to unbalance the current per phase more than 10% is not allowed by Xcel Energy, where the percentage unbalance is calculated by taking the maximum deviation from average current and dividing it by the average current [78].

To solve the PV mismatch issue, a control scheme with individual MPPT control and modulation compensation is proposed, as shown in Fig. 4.2. The details of the control scheme

will be discussed in next three subsections.

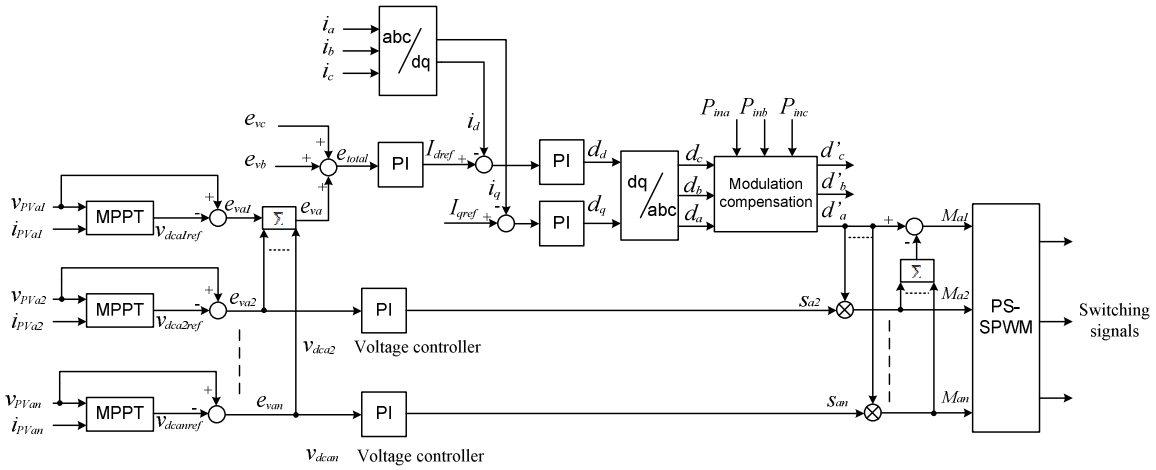


Figure 4.2. Control scheme for three-phase modular cascaded H-bridge multilevel PV inverter.

### 4.2.1 Individual MPPT Control

The individual MPPT control scheme applied in the single-phase system can be extended to the three-phase system. Fig. 4.2 shows the individual MPPT control of the cascaded H-bridge inverter in phase *a*. In each H-bridge module, an MPPT controller is added to generate the dc-link voltage reference. Each dc-link voltage is compared to the corresponding voltage reference, and the sum of all the errors is controlled through a PI controller that determines the current reference $I_{dref}$. The reactive current reference $I_{qref}$ can be set to zero. If reactive power compensation is required, $I_{qref}$ can also be given by a reactive current calculator. As the classic control scheme for three-phase systems, the grid currents in *abc* coordinates are converted to *dq* coordinates, and regulated through PI controllers to generate the modulation index in *dq* coordinates, which is then converted back to three-phase.

The voltages $v_{dca2}$ to $v_{dcan}$ are controlled individually through *n*-1 loops. Each voltage

controller gives the modulation index proportion of one H-bridge module in phase *a*. After multiplied by the modulation index of phase *a*, *n*-1 modulation indices can be obtained. Also, the modulation index for the first H-bridge can be obtained by subtracting the remaining modulation index. The control schemes in phase *b* and *c* are almost the same. The only difference is that all the dc-link voltages are regulated through PI controllers, and *n* modulation index proportions are obtained for each phase. Phase-shifted SPWM (PS-SPWM) switching scheme is then applied to control the switching devices of each H-bridge.

It can be seen that for one H-bridge module out of the 3*n* modules, its modulation index is obtained by subtraction. The reason is that 3*n* voltage loops are necessary to manage different voltage levels on 3*n* H-bridges, and one is the total voltage loop, which gives the current reference $I_{dref}$. So only 3*n*-1 modulation indices can be determined by the last 3*n*-1 voltage loops, and one modulation index has to be obtained by subtraction.

### 4.2.2 Modulation Compensation

With the individual MPPT control in each H-bridge, the input power of each phase would be different, which introduces unbalanced current to the grid. To solve the problem, a zero sequence voltage can be imposed upon the phase legs in order to affect the current flowing into each phase [79], [80]. The idea can be explained by the following equations

$$\begin{cases} v_{aN} = v_{an} + L\dfrac{di_a}{dt} + Ri_a - v_{Nn} \\ v_{bN} = v_{bn} + L\dfrac{di_b}{dt} + Ri_b - v_{Nn} \\ v_{cN} = v_{cn} + L\dfrac{di_c}{dt} + Ri_c - v_{Nn} \end{cases} \tag{25}$$

where $v_{iN}$ ($i$=*a, b, c*) is the output phase voltage of the three-phase inverter as shown in Fig. 4.1,

$v_{in}$ is the phase voltage of the grid, $L$ and $R$ are the decoupling inductance and its resistance respectively. By injecting the zero sequence voltage $v_{Nn}$, the output phase voltage of the inverter will be unbalanced. If the unbalanced voltage is proportional to the unbalanced power, the grid current will be balanced.

Therefore, a modulation compensation scheme is applied, as shown in Fig. 4.3. First, the unbalanced power is weighted by ratio $r_i$, which is calculated as

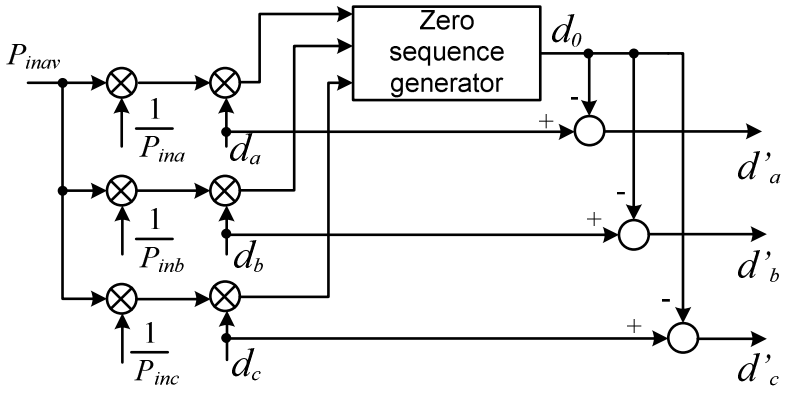


Figure 4.3. Modulation compensation scheme.

$$r_i = \frac{P_{inav}}{P_{ini}} \tag{26}$$

where $P_{ini}$ is the input power of phase $i$ ($i$=$a$, $b$, $c$), and $P_{inav}$ is the average input power.

The injected zero sequence modulation index can be generated as

$$d_0 = \frac{1}{2}[\min(r_a \cdot d_a, \quad r_b \cdot d_b, \quad r_c \cdot d_c) + \max(r_a \cdot d_a, \quad r_b \cdot d_b, \quad r_c \cdot d_c)] \tag{27}$$

where $d_i$ is the modulation index of phase $i$ and is determined by the current loop controller.

Then, the modulation index of each phase is updated by

$$d'_i = d_i - d_0 \tag{28}$$

A simple example is presented to show the modulation compensation scheme more clearly. Assume the input power of each phase is unequal,

$$P_{ina} = 0.8, \quad P_{inb} = 1, \quad P_{inc} = 1 \tag{29}$$

By injecting a zero sequence modulation index at t = 1s, the balanced modulation index will be updated, as shown in Fig. 4.4. It can be seen that with the compensation, the updated modulation index is unbalanced proportional to the power, which means the output voltage ($v_{iN}$) of the three-phase inverter is unbalanced and finally results in a balanced grid current.

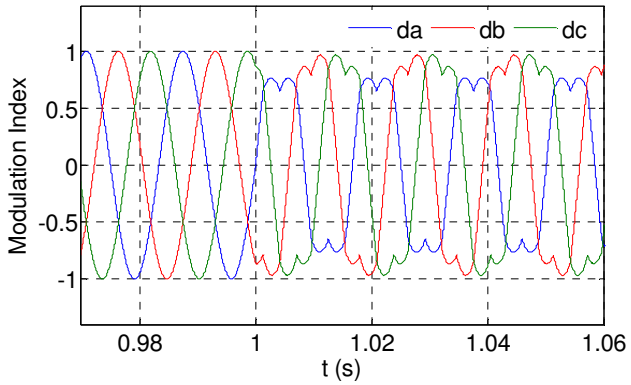


Figure 4.4. Modulation index before and after modulation compensation.

### 4.2.3 Discussion of Proposed Control Scheme

The aim of the proposed control scheme is to make each PV module operate at its own MPP, so that maximum solar power can be extracted even if there are PV mismatches. As shown in Fig. 4.2, the dc-link voltage of each H-bridge inverter, or in the other word, the output voltage of each PV module, is controlled individually to track its own MPP voltage. However, it is possible that the dc-link voltage of the H-bridge inverter cannot reach the reference, and the connected PV

module is not operated at the MPP. The possibility will be analyzed as follows.

According to (3), for each phase, we have

$$\dot{V}_s + (Ls + R)\dot{I}_s = \sum_{j=1}^{n} m_j \dot{V}_{dcj} \tag{30}$$

where $\dot{V}_s$ and $\dot{I}_s$ are the fundamental phasors of the grid voltage and current, $m_j$ is the modulation index of the H-bridge module $j$ ($j$ = 1, 2, … $n$), and $\dot{V_{dcj}}$ is defined as the phasor that is in the direction of $\dot{V}_s + (Ls + R)\dot{I}_s$ with the size of $V_{dcj}$.

With the proposed control scheme, the modulation index of each H-bridge module is determined by an individual voltage loop. If PV mismatches happen, for example, there are shadings on the connected PV panels of the H-bridge modules 1 to $k$, the extracted solar power from these modules will decrease, and the modulation indices $m_1$ to $m_k$ will be small. Meanwhile, the dc-link voltages $V_{dc1}$ to $V_{dck}$ will also drop due to the shadings. To provide the desired output voltage, the term $\sum_{j=k+1}^{n} m_j \dot{V}_{dcj}$ must increase. Since PV modules should be operated at their own MPPs, the dc-link voltages $V_{dc(k+1)}$ to $V_{dcn}$ will not change, and the modulation indices $m_{k+1}$ to $m_n$ will increase. If the inverter can generate the desired voltage without overmodulation, the control scheme will work successfully. However, there is possibility that the dc-link voltages $V_{dc(k+1)}$ to $V_{dcn}$ must increase to generate the desired output voltage, and the connected PV panels of the H-bridge modules $k$+1 to $n$ cannot be operated at MPPs. This can only happen under extreme conditions, like the PV currents of the shaded panels are almost zero and the other panels are still operated at the rated power, leading to very low modulation indices of the H-bridges connected to shaded PV panels. Considering the redundancy of the cascaded H-bridge multilevel inverter, the individual MPPT control scheme should work well in most cases.

For the three-phase PV system, the modulation compensation scheme is proposed to balance the grid current under the unbalanced supplied solar power. However, there is also limitation for the compensation scheme. If the supplied power is very unbalanced, like the power of one phase is much lower than that of the other two phases, the power ratio of that phase will be far larger than 1. According to the principle of the compensation scheme, this may result in overmodulation in the phases with high power. In order to prevent the overmodulation, the power ratio $r_i$ ($i$=$a$, $b$, $c$) should be limited to a certain value $r_{max}$, which is related to the modulation index of the inverter operated under the balanced power. When the calculated power ratio $r_i$ is larger than $r_{max}$, the updated modulation index cannot be unbalanced proportional to the power, which means the output voltage ($v_{iN}$) of the three-phase inverter is not proportional to the power, and the current cannot be balanced.

On the other hand, by injecting a zero sequence modulation index, the compensation scheme improves the utilization of dc-link voltages. More importantly, the compensation scheme reduces the possibility that the PV panels have to be operated at voltages higher than the MPP voltages. As discussed above, if some H-bridge modules in one phase have low extracted solar power and have small modulation index proportions, other modules in the same phase will have larger modulation index proportions to provide the desired output phase voltage, which may cause overmodulation, or the connected PV panels of these modules have to be operated at voltages higher than the MPP voltages. However, by applying the modulation compensation, the modulation index of the phase with less input PV power will be smaller, which helps to prevent overmodulation of those modules with larger modulation index proportions and reduce the possibility of the fail of the individual MPPT control.

## 4.3 Results

To validate the proposed control scheme, simulation and experimental tests are carried out. A modular cascaded multilevel inverter prototype has been built in the laboratory, as shown in Fig. 4.5. The modular design will increase the flexibility of the system, and reduce the cost as well. MOSFETs IRFSL4127 are selected for the inverter switches and operate at 1.5 kHz. The control signals to the H-bridge inverters are sent by a dSPACE ds1103 controller.

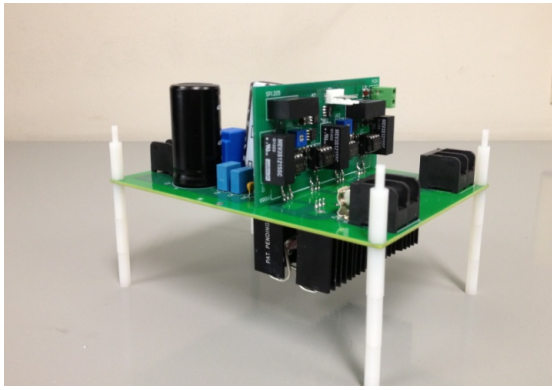

Figure 4.5. H-bridge module prototype.

A three-phase 7-level cascaded H-bridge inverter is simulated and tested experimentally. Each H-bridge has its own 185 W PV panel (Astronergy CHSM-5612M) connected as an independent source. The specifications of PV panel Astronergy CHSM-5612M are shown in Table 4.1. The inverter is connected to the grid through a transformer, and the phase voltage of the secondary side is 60 Vrms.

From (11), the inductor $L$ can be calculated as

$$L = \frac{v_{dc}}{16 f_{sw} \Delta i_{L\max}} \geq \frac{36.38}{16 \times 1500 \times 10\% \times 9.25} = 1.64mH \tag{31}$$

To reach a utilization ratio of 99% of PV modules, the amplitude of the voltage ripple should be below 6% of the MPP voltage. From (12), the dc-link capacitor can be calculated as

$$C \geq \frac{nP_{PV}}{2n\omega_{grid}V_{mpp} \cdot 6\%V_{mpp}} = \frac{3\times185}{2\times3\times2\pi\times60\times36.38\times6\%\times36.38} = 3.09mF \qquad (32)$$

In this dissertation, the dc-link capacitor is selected as $C$ = 3.6 mF, and the inductor is selected as $L$ = 2.5 mH. The system parameters are shown in Table 4.2.

Table 4.1. Specifications of PV module Astronergy, CHSM-5612M

| | |
|---|---|
| Rated Power ($P_{max}$) | 185 W |
| Maximum Power Voltage ($V_{pm}$) | 36.38 V |
| Maximum Power Current ($I_{pm}$) | 5.09 A |
| Open Circuit Voltage ($V_{oc}$) | 45.12 V |
| Short Circuit Current ($I_{sc}$) | 5.39 A |
| Temperature Coefficient $V_{oc}$ | -0.355%/°C |
| Temperature Coefficient $I_{sc}$ | 0.062%/°C |

Table 4.2. System parameters

| Parameters | Value |
|---|---|
| DC-link capacitor | 3.6 mF |
| Connection inductor $L$ | 2.5 mH |
| Grid resistor $R$ | 0.1 ohm |
| Grid rated phase voltage | 60 Vrms |
| Switching frequency | 1.5 kHz |

To verify the proposed control scheme, the three-phase grid-connected PV inverter is simulated in two different conditions. First, all PV panels are operated under the same irradiance

S = 1000 W/m$^2$ and temperature T = 25 ˚C. At $t$ = 0.8s, the solar irradiance on the first and second panels of phase $a$ decreases to 600 W/m$^2$, and that for the other panels stays the same. The dc-link voltages of phase $a$ are shown in Fig. 4.6. At the beginning, all PV panels are operated at the MPP voltage 36.4 V. As the irradiance changes, the first and second dc-link voltages decrease and track the new MPP voltage of 36 V, while the third panel is still operated at 36.4 V. The PV current waveforms of phase $a$ are shown in Fig. 4.7. It can be seen that the lower irradiation affects the current in the first and second PV panels, so the lower ripple of the dc-link voltage can be found in Fig. 4.6(a).

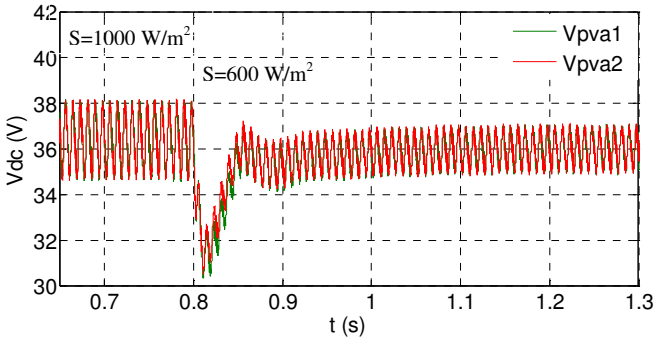


(a) DC-link voltage of module 1, 2

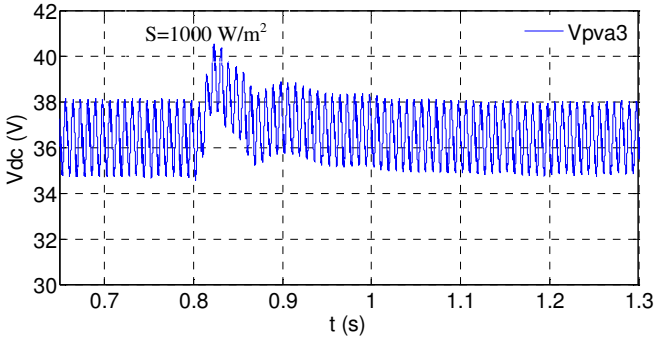


(b) DC-link voltage of module 3

Figure 4.6. Simulated dc-link voltages of phase $a$ with individual MPPT(T=25 ˚C).

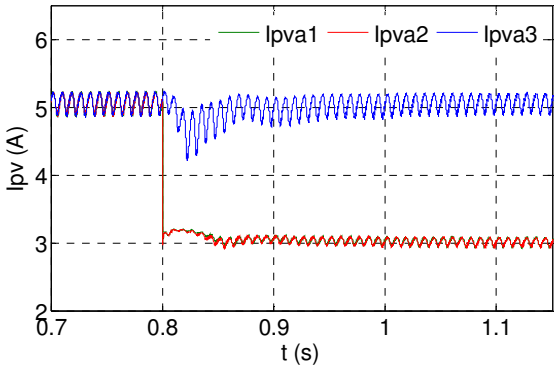


Figure 4.7. Simulated PV currents of phase *a* with individual MPPT(T=25 ˚C).

The dc-link voltages of phase *b* are shown in Fig. 4.8. All phase *b* panels track the MPP voltage 36.4 V, which shows that they are not influenced by other phases. With the individual MPPT control, the dc-link voltage of each H-bridge can be controlled independently. In the other words, the connected PV panels of each H-bridge can be operated at its own MPP voltage and will not be influenced by the panels connected to other H-bridges. Thus, more solar energy can be extracted, and the efficiency of the overall PV system will be increased.

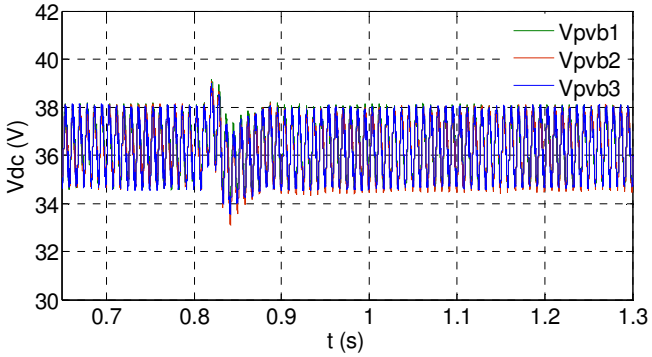


Figure 4.8. Simulated dc-link voltages of phase *b* with individual MPPT(T=25 ˚C).

Fig. 4.9 shows the power extracted from each phase. At the beginning, all panels are operated under irradiance S = 1000 W/m$^2$, and every phase is generating maximum power 555 W.

After $t$ = 0.8 s, the power harvested from phase $a$ decreases to 400 W, and the power from the other two phases stays the same. Obviously, the power supplied to the three-phase grid-connected inverter is unbalanced. However, by applying the modulation compensation scheme, the power injected to the grid is still balanced, as shown in Fig. 4.10. In addition, comparing the total power extracted from PV panels with the total power injected to the grid, it can be seen that there is no extra power loss caused by the modulation compensation scheme.

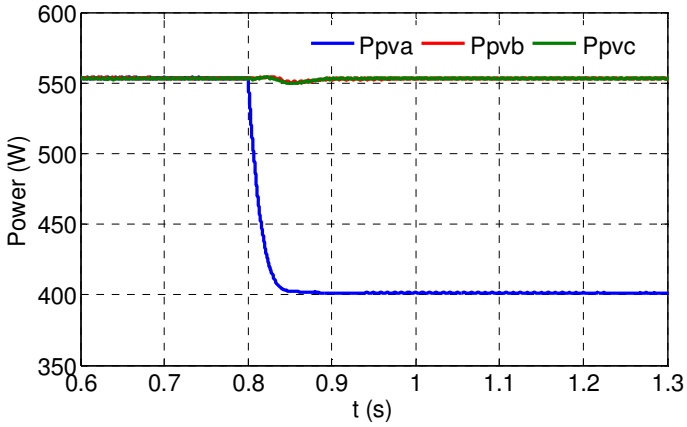


Figure 4.9. Simulated power extracted from PV panels with individual MPPT.

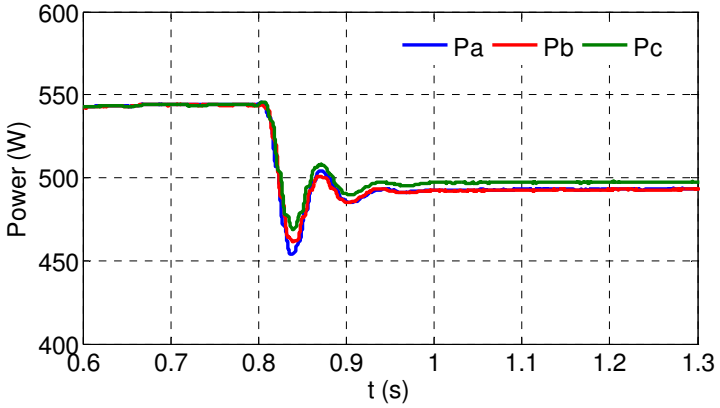


Figure 4.10. Simulated power injected to the grid with modulation compensation.

Fig. 4.11 shows the output voltages ($v_{iN}$) of the three-phase inverter. Due to the injected zero

sequence component, they are unbalanced after $t$ = 0.8s, which help to balance the grid current shown in Fig. 4.12.

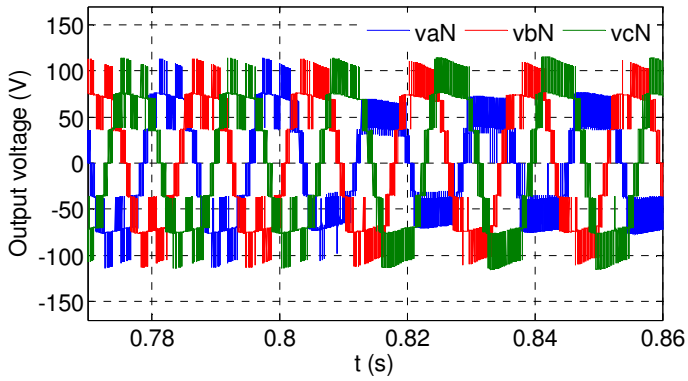


Figure 4.11. Simulated three-phase inverter output voltage waveforms with modulation compensation.

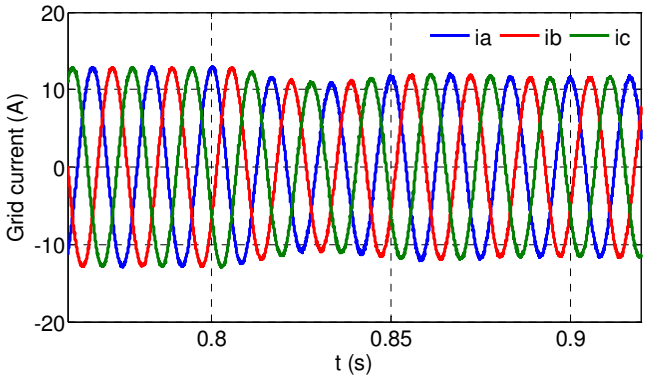


Figure 4.12. Simulated three-phase grid current waveforms with modulation compensation.

If the solar power supplied to the three-phase grid-connected PV inverter is very unbalanced, due to the limited power ratio, the modulation compensation scheme may fail to make the injected grid current exactly balanced. However, the compensation scheme still works in making the grid current more balanced.

To show this, the three-phase grid-connected PV inverter is operated in the following

condition: the solar irradiance on the first and second panels of phase *a* is 150 W/m$^2$, that for the other panels is 1000 W/m$^2$, and temperature T = 25 ˚C. First, the modulation compensation scheme is applied to the control system. At $t$ = 1 s, the modulation compensation block is switched off.

With the individual MPPT control, the solar power extracted from each phase is shown in Fig. 4.13. The power extracted from phase *a* is 236 W, and the power from phase *b* and *c* are both 555 W. Compared to the *P-V* characteristics of the PV module Astronergy CHSM-5612M, each PV module is operated at its own MPP voltage and generates the possible maximum power.

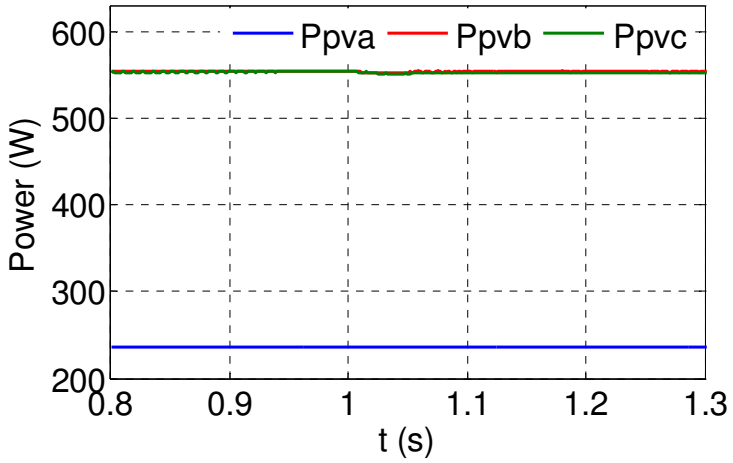


Figure 4.13. Simulated power extracted from PV panels with individual MPPT.

According to (26), the power ratio $r_a$ is calculated as 1.9, which is larger than the power ratio limit $r_{max}$ = 1.35. Thus, the updated modulation index cannot be unbalanced proportional to the power, and the grid current cannot be exactly balanced. As shown in Fig. 4.14, before $t$ = 1 s, even with the modulation compensation scheme, the percentage unbalance of the grid current is calculated as 5.0%. However, without the modulation compensation, the RMS values of the injected grid currents $i_a$, $i_b$, and $i_c$ are 5.98 A, 7.96 A and 8.24 A, respectively. The percentage

unbalance is 19.1%, which is much higher than the utility standard 10%. Though the compensation scheme has the limitation in balancing the injected grid current, it still helps to reduce the percentage unbalance of the grid current.

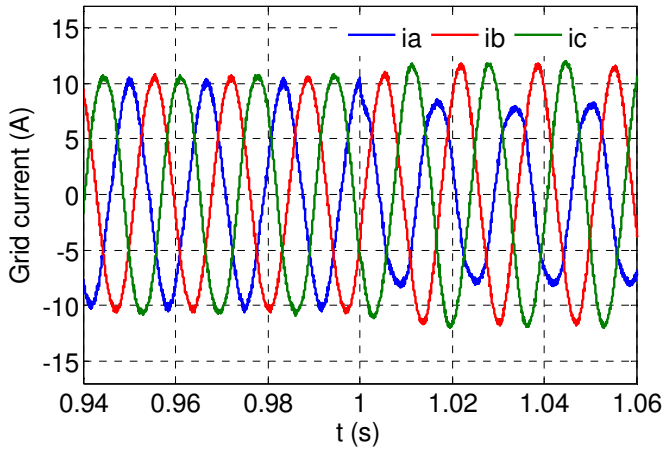


Figure 4.14. Simulated three-phase grid current waveforms.

Meanwhile, the modulation compensation scheme helps to prevent overmodulation of the third module in phase *a*. Fig. 4.15 shows the modulation index of each H-bridge module in phase *a*. Without the modulation compensation, the third module will be over-modulated. Since the connected PV panel of the first and second modules has lower irradiance and generates less power, the modulation index proportion of these two modules is smaller. To maintain the desired output voltage, the third module has much larger modulation index proportion, leading to overmodulation. As shown in Fig. 4.14, the THD of current $i_a$ is 7.0% after $t$ = 1 s, which becomes higher due to the overmodulation in phase *a*. However, by applying the modulation compensation scheme, the modulation index of phase *a* is reduced and helps to prevent overmodulation. It can be seen from Fig. 4.15 that the overmodulation in the third module of phase *a* is prevented when the modulation compensation scheme is applied.

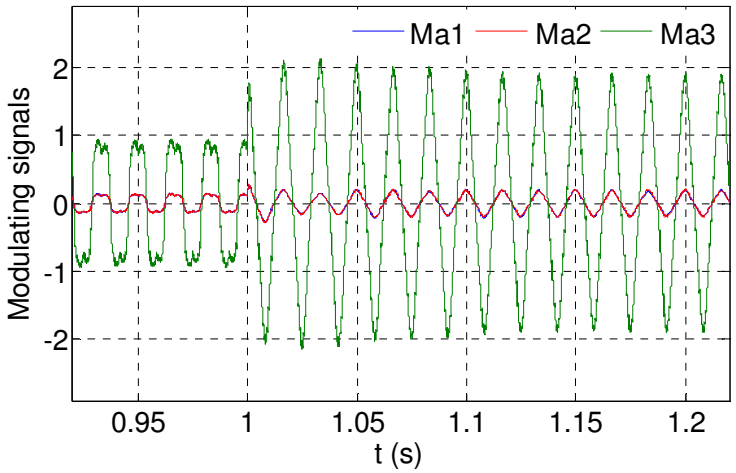


Figure 4.15. Simulated modulation index of each H-bridge module in phase *a*.

As discussed above, the cascaded H-bridge multilevel inverter provides advantage of high inverter efficiency. An efficiency model has been developed for a three-phase cascaded H-bridges converter based on the prototype developed for this dissertation. A 30 kW three-phase 11-level cascaded H-bridge inverter, which utilizes 15 H-bridge modules (5 modules per phase), is considered. The inverter is connected to grid (480 V), and the switching frequency is also 1.5 kHz.

The efficiency of the multilevel inverter at different power levels is shown in Fig. 4.16. It can be seen that the modular 11-level cascaded H-bridge inverter has highest efficiency of 98.0% when it is operated at 9 kW. The total power loss includes the switching and conduction loss of MOSFET devices, the conduction loss of diodes, the inductors' loss, the power loss of gate drivers and the power loss of DC and AC sensors. With the inverter operated at 9 kW as an example, the power loss distribution chart is shown in Fig. 4.17. Since one DC voltage sensor LV 20-P and one DC current sensor HY 5-P are employed in each H-bridge module to realize the MPPT, the power supplied to DC sensors (total of 23.9 W) accounts for a large share of

power loss. If resistors are used for sampling instead of those DC sensors, the auxiliary power will be much lower, and the efficiency of the multilevel inverter can be further increased. Meanwhile, due to the low switching frequency of the cascaded multilevel inverter, the switching loss is a small amount compared to the conduction loss of devices.

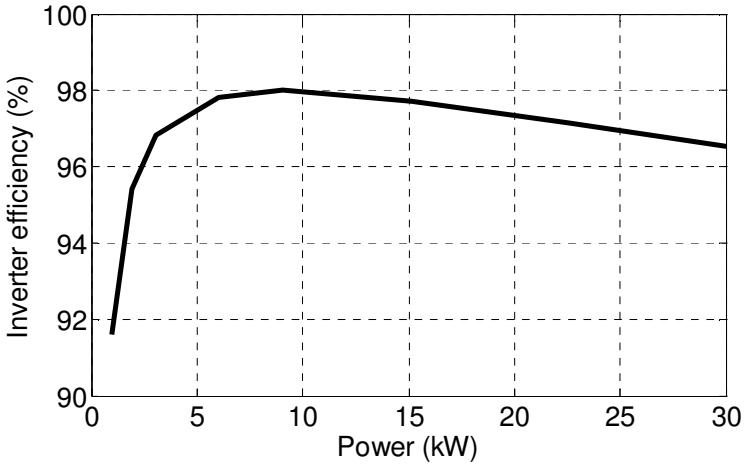


Figure 4.16. Simulated efficiency of the 30 kW multilevel inverter prototype for different input power.

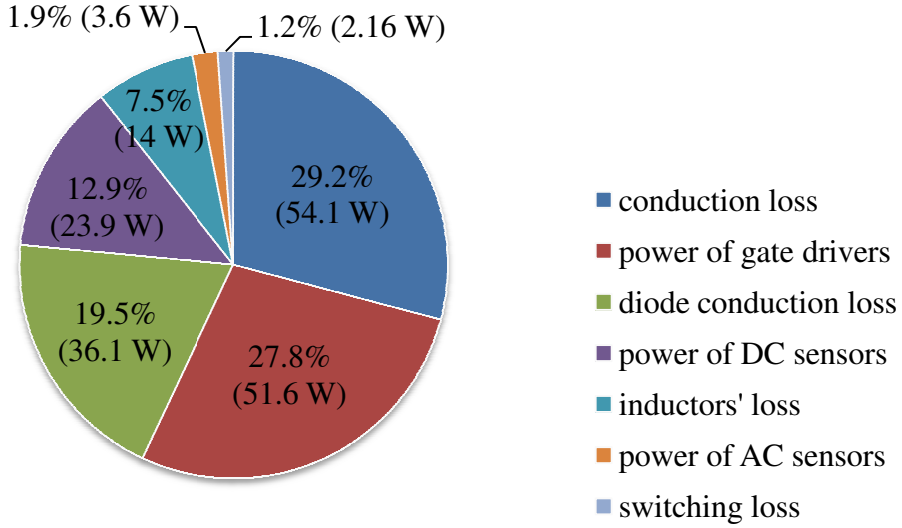


Figure 4.17. Power loss distribution chart at 9 kW input power.

A three-phase 7-level cascaded H-bridge inverter has been built by 9 H-bridge modules (3 modules per phase) in the laboratory. Fig. 4.18 shows the experimental solar panels and the three-phase cascaded multilevel inverter. As mentioned above, the dc link of each H-bridge module is fed by one PV panel Astronergy CHSM-5612M.

(a) Solar panels Astronergy CHSM-5612M

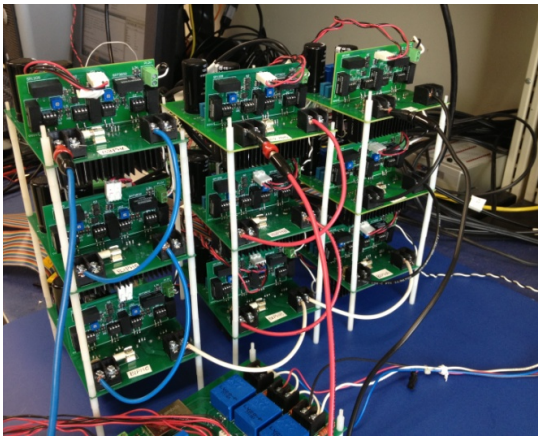

(b) Modular three-phase 7-level cascaded H-bridge inverter

Figure 4.18. Experimental prototype.

First, the function of the MPPT system is tested. All MPPT controllers are switched off and the dc-link voltage reference of all H-bridge modules is set to 35 V at the beginning. Then, for

each H-bridge module, its own MPPT controller is switched on and generates the dc-link voltage reference. The extracted solar power is shown in Fig. 4.19. After MPPT applied, the output voltages of all PV panels are tracking their own MPP voltage, and the harvested solar power is increasing to the possible maximum power. Fig. 4.20 shows the three-phase grid current waveforms. The injected grid current is increasing after MPPT controllers are switched on. The MPPT system ensures the maximum power extraction from the PV panels at any given time and improves the efficiency of the PV system.

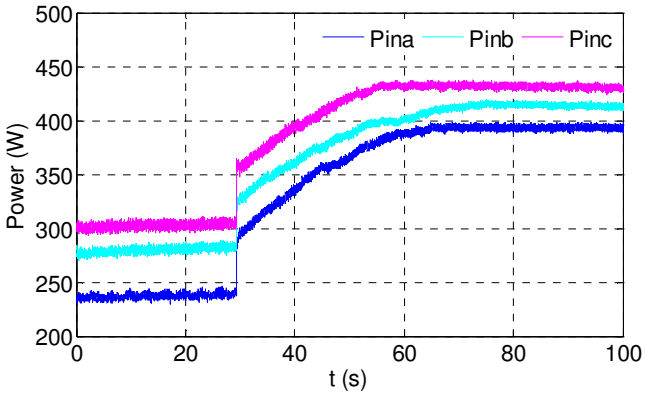


Figure 4.19. Power extracted from PV panels without and with MPPT.

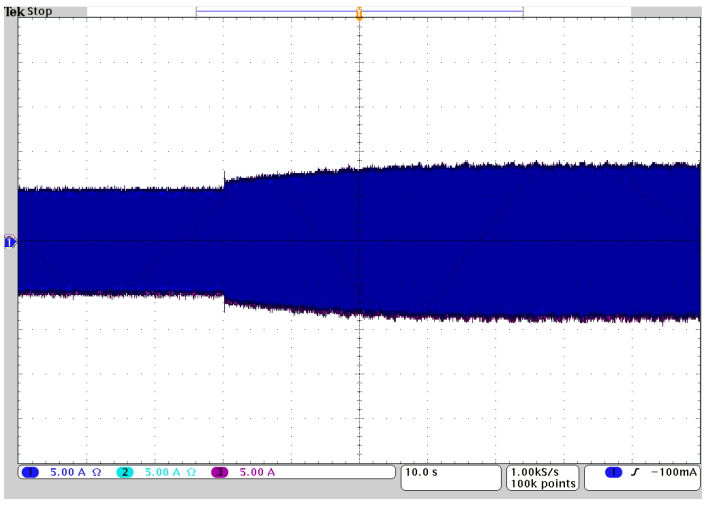


Figure 4.20. Experimental three-phase grid current waveforms without and with MPPT.

To validate the proposed control scheme, the three-phase grid-connected PV inverter has been tested under different conditions. In the tests, cards with different sizes are placed on top of PV panels to provide partial shading effectively changing the solar irradiance.

Test 1: one panel of one phase is partly covered.

Test 1.1: a small blue card (9 cm × 7 cm) is placed on the third panel of phase *a*, and one cell of the panel is partly covered, as shown in Fig. 4.21.

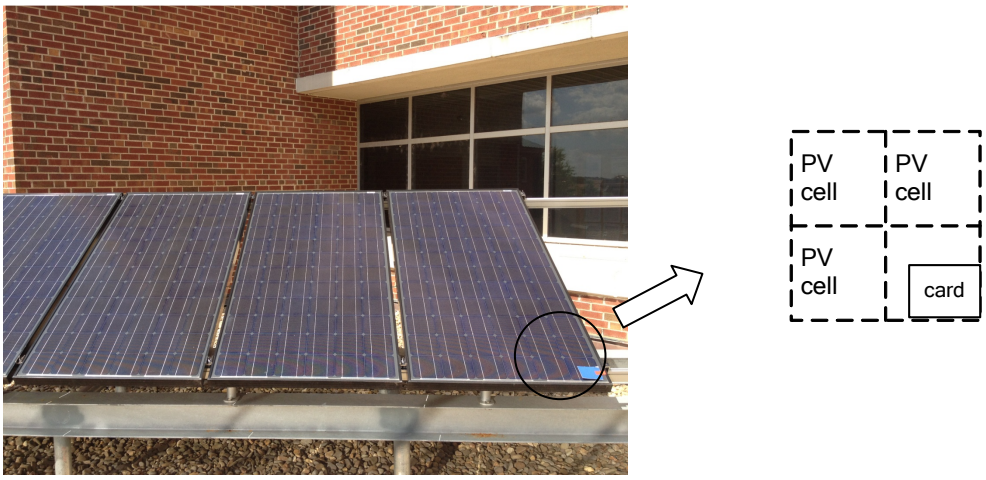


Figure 4.21. PV panels of phase *a*: one cell of the third panel is partly covered.

The experimental results are presented in Figs. 4.22-4.26. Fig. 4.22 shows three dc-link voltages of phase *a*. The output voltage of each PV panel is controlled individually to track its own MPP voltage. Since the third panel is partly covered, its MPP voltage is a little lower. The PV current waveforms of phase *a* are shown in Fig. 4.23. The current of the third panel is much smaller due to the card covering. However, the first and second panels are operated at their own MPP, and their currents will not be influenced. With the individual MPPT control, the efficiency loss caused by PV mismatches can be prevented.

As shown in Fig. 4.22, there is second order harmonic in the output voltage of the PV panels. So the second order harmonic is also seen in the output current of the PV panels. In addition, to have a high utilization ratio of 99%, the voltage ripple is about 1.8 V, which is less than 6% of the MPP voltage.

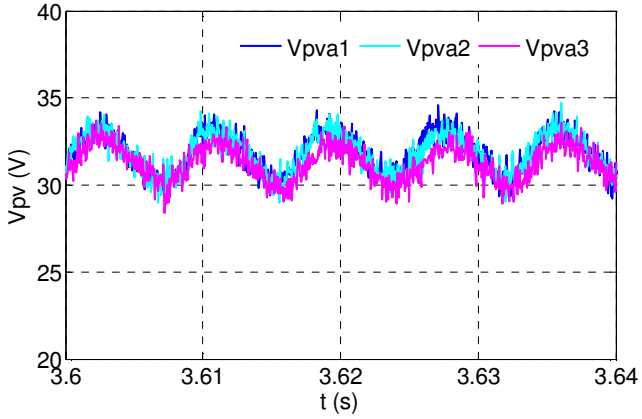


Figure 4.22. Experimental dc-link voltages of phase *a*.

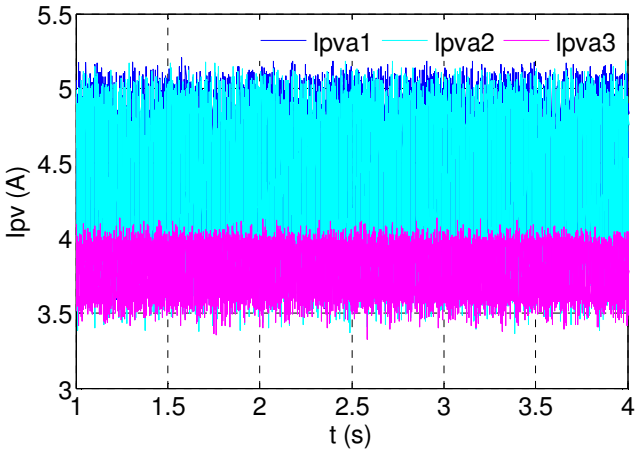


Figure 4.23. Experimental PV currents of phase *a* (test 1.1).

Fig. 4.24 shows the solar power extracted from each phase, which is unbalanced. To balance the injected grid current, the modulation compensation scheme is applied. As presented in Fig.

4.25, a zero sequence voltage is imposed upon the phase legs. The inverter output voltage ($v_{iN}$) is unbalanced proportional to the supplied power of each phase, which helps to balance the grid current. Fig. 4.26 shows the three-phase grid current waveforms. Even if PV mismatch happens and the supplied PV power to the three-phase system is unbalanced, the three-phase grid current is still balanced.

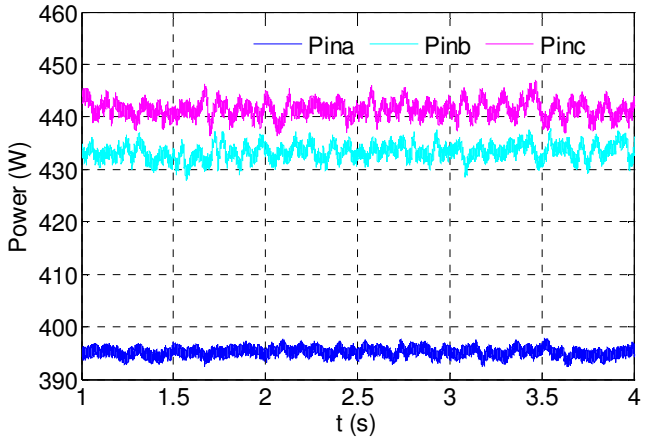


Figure 4.24. Experimental power extracted from PV panels with individual MPPT (test 1.1).

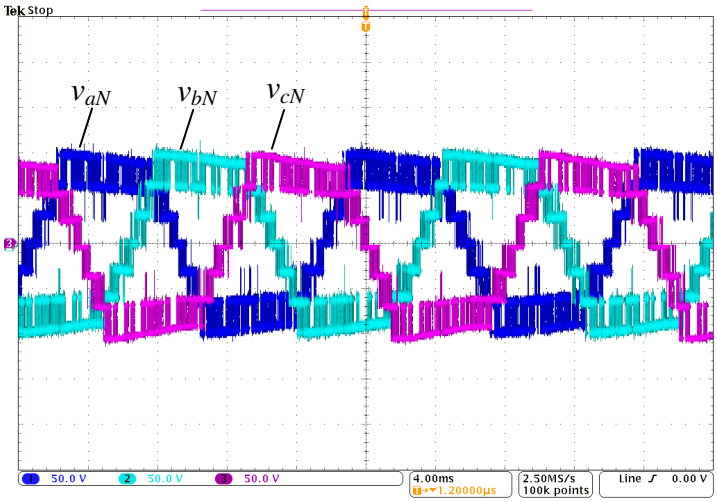


Figure 4.25. Experimental inverter output voltages with modulation compensation (test 1.1).

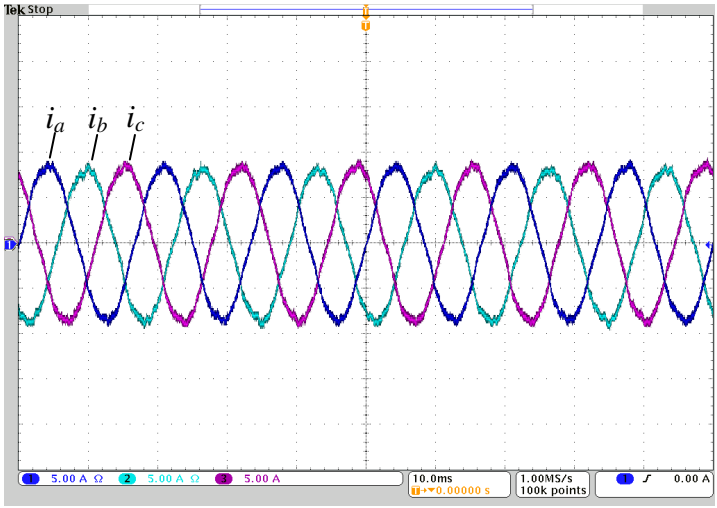


Figure 4.26. Experimental grid currents with unbalanced PV power (test 1.1).

The THD of the grid current is 3.3%, and the rms value is 6.1 A, as shown in Fig. 4.27. The TDD of the grid current is calculated as 2.2%, which is less than 5% and meets power quality standards, like IEEE 1547 in the U.S. and IEC 61727 in Europe.

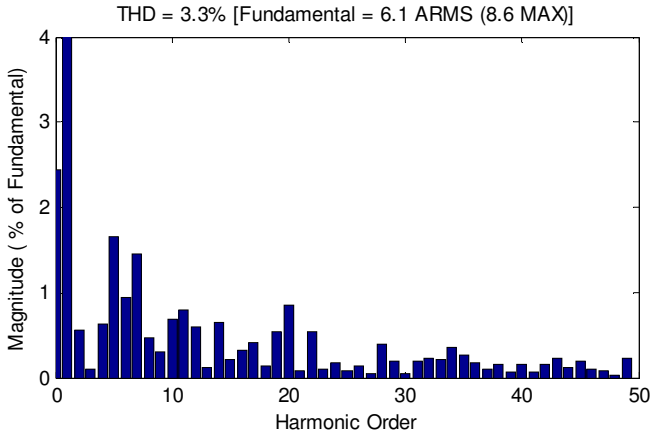


Figure 4.27. THD of the grid current shown in Fig. 4.26 (test 1.1).

Test 1.2: a large blue card (13.5 cm × 9 cm) is placed on the third panel of phase *a*, and one cell of the panel is almost fully covered, as shown in Fig. 4.28.

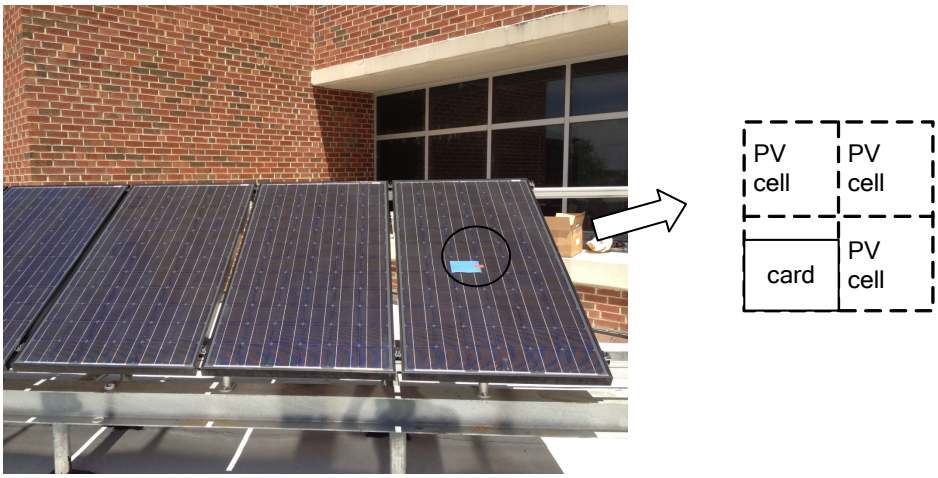


Figure 4.28. PV panels of phase *a*: one cell of the third panel is covered.

Fig. 4.29 shows the PV current waveforms of phase *a*. Since one cell of the third panel is almost fully covered, the current of the panel drops to 2 A, while the currents of the other two panels in the same phase are still 4 A.

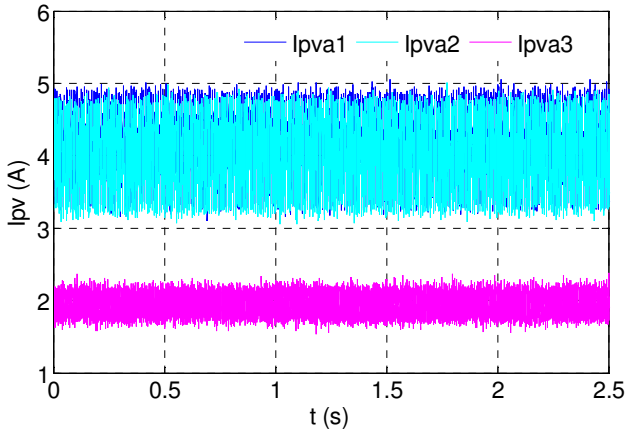


Figure 4.29. Experimental PV currents of phase *a* (test 1.2).

The harvested solar power of each phase is shown in Fig. 4.30. Compared to the test 1.1, the power supplied to the three-phase system is more unbalanced. However, the three-phase grid current can still be balanced by applying the modulation compensation, as presented in Fig. 4. 31.

The THD of the grid current is 4.2%, the TDD is 2.5%, and the rms value is 5.5 A.

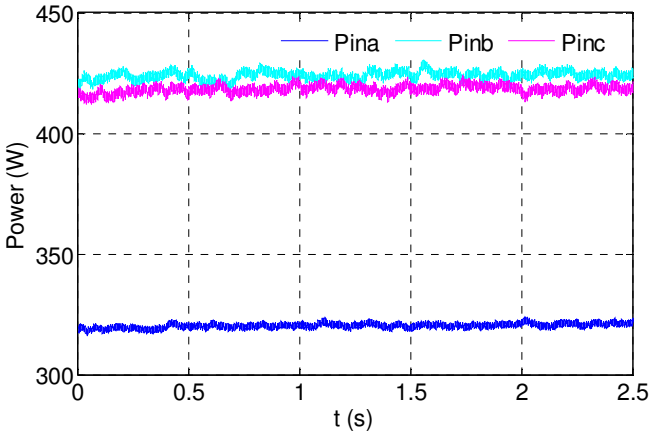


Figure 4.30. Experimental power extracted from PV panels with individual MPPT (test 1.2).

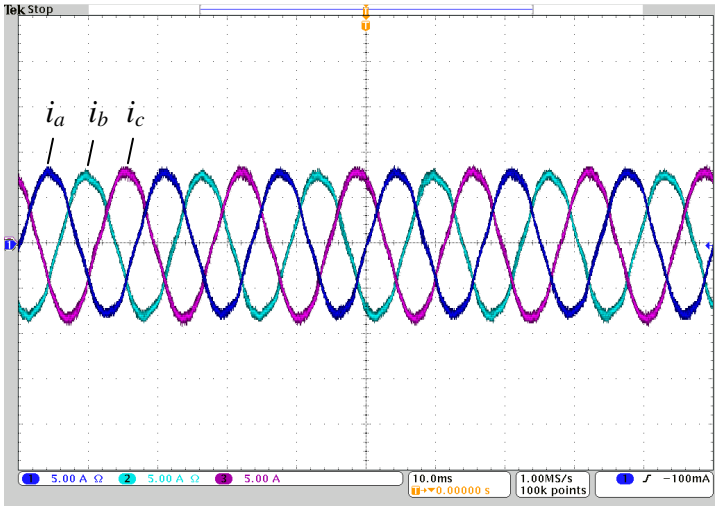


Figure 4.31. Experimental grid currents with unbalanced PV power (test 1.2).

Fig. 4.32 shows the inverter output voltage waveforms. As discussed above, the inverter output voltage ($v_{iN}$) is unbalanced proportional to the supplied power of each phase to help balance the grid current. Thus, the output voltage $v_{bN}$ (76.0 Vrms) and $v_{cN}$ (75.2 Vrms) are higher than $v_{aN}$ (57.9 Vrms).

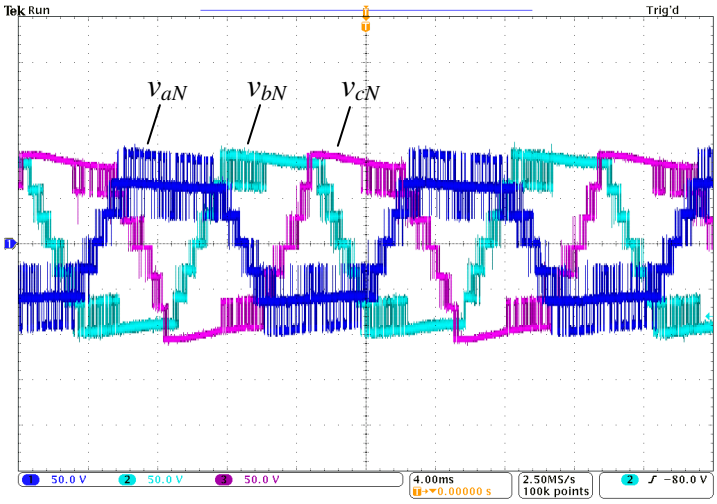


Figure 4.32. Experimental inverter output voltages with modulation compensation (test 1.2).

Test 1.3: a large blue card (13.5 cm × 9 cm) is placed on the third panel of phase *a*, and two cells of the panel are partly covered, as shown in Fig. 4.33.

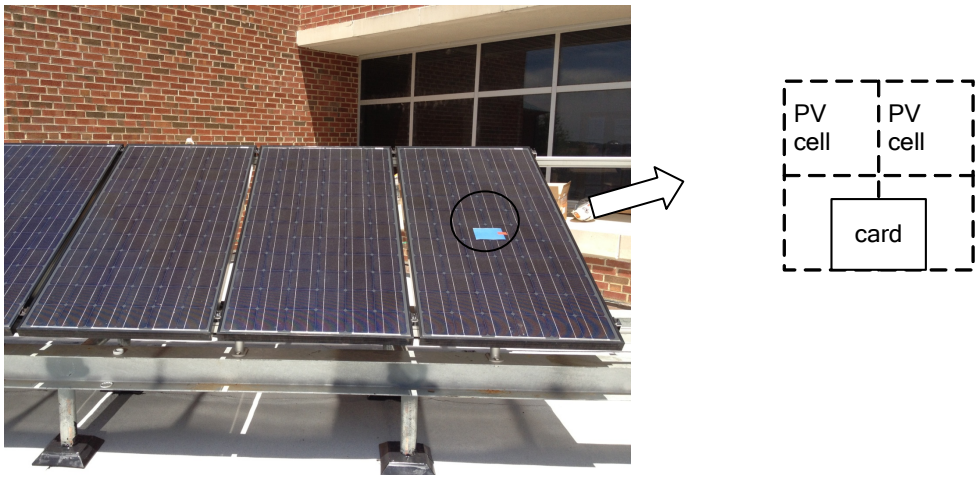


Figure 4.33. PV panels of phase *a*: two cells of the third panel are partly covered.

Fig. 4.34 shows the PV current waveforms of phase *a*. Compared to the test 1.2, though a same size card is put on the third panel, the current of the panel is higher in this case. Meanwhile, the currents of the first and second panels are same as those in the test 1.2, which means the solar

irradiance does not change in these two tests. So compared to two cells are partly covered, only one cell is covered by the same size card would lead to more maximum power decreasing.

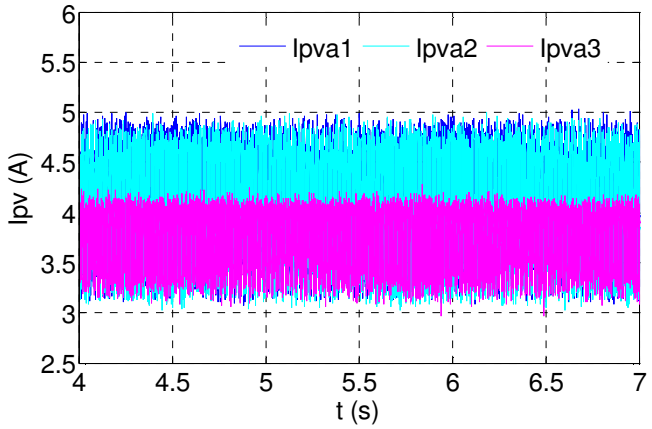


Figure 4.34. Experimental PV currents of phase *a* (test 1.3).

Fig. 4.35 shows the unbalanced extracted solar power, and Fig. 4.36 shows the inverter output voltage, which is proportional to the supplied power of each phase. The balanced grid current waveforms are shown in Fig. 4.37. The THD of the grid current is 4.1%, the TDD is 2.5%, and the rms value is 5.7 A.

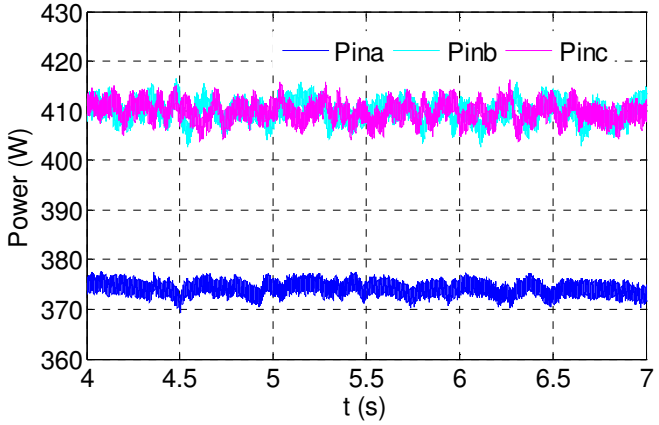


Figure 4.35. Experimental power extracted from PV panels with individual MPPT (test 1.3).

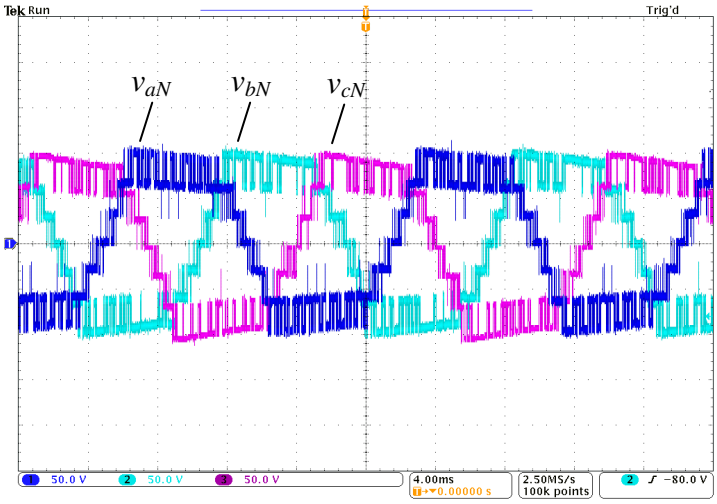


Figure 4.36. Inverter output voltage waveforms with modulation compensation (test 1.3).

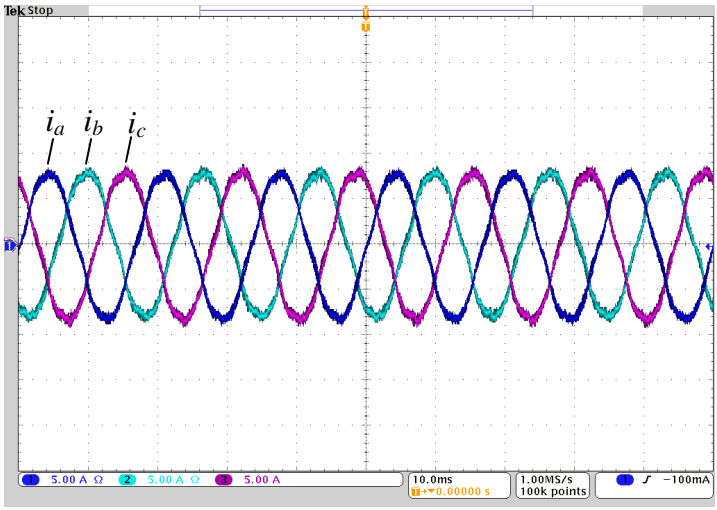


Figure 4.37. Experimental grid currents with unbalanced PV power (test 1.3).

Test 2: two panels of one phase are partly covered.

Test 2.1: two small blue cards (9 cm × 7 cm) are placed on the second and third panels of phase *a*. For each panel, one cell is partly covered, as shown in Fig. 4.38.

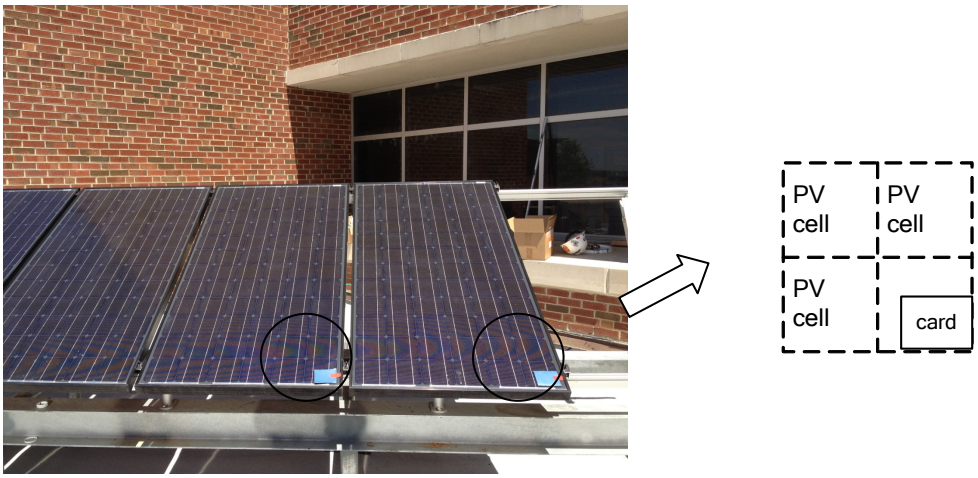


Figure 4.38. PV panels of phase *a*: two panels are partly covered (test 2.1).

Fig. 4.39 shows the PV current waveforms of phase *a*. With the individual MPPT control, each PV panel is operated at its own MPP. Since the second and third panels are both partly covered, the MPP currents of these two panels are lower than that of the first panel.

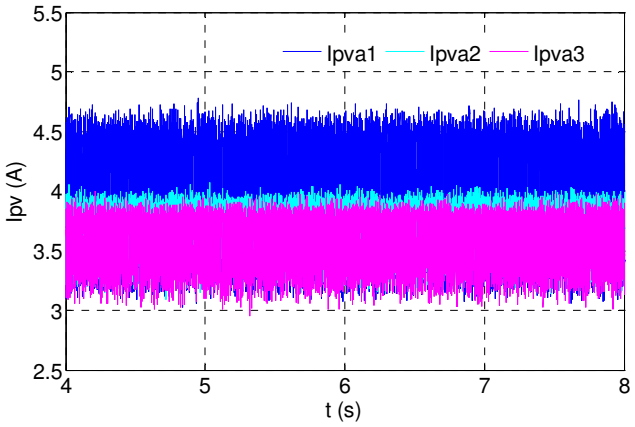


Figure 4.39. Experimental PV currents of phase *a* (test 2.1).

Fig. 4.40 presents the harvested solar power. The power of phase *a* is lower due to the covering. To balance the injected grid current, the inverter output voltage is unbalanced proportional to the extracted solar power of each phase, as shown in Fig. 4.41. Thus, the grid

current is balanced even with the unbalanced supplied power. Fig. 4.42 shows the balanced grid current waveforms. The rms value of the current is 5.6 A, the THD is 4.2%, and the TDD is 2.5%.

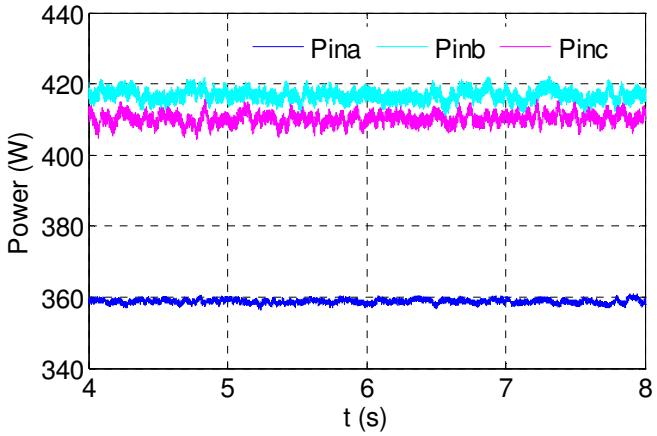


Figure 4.40. Experimental power extracted from PV panels with individual MPPT (test 2.1).

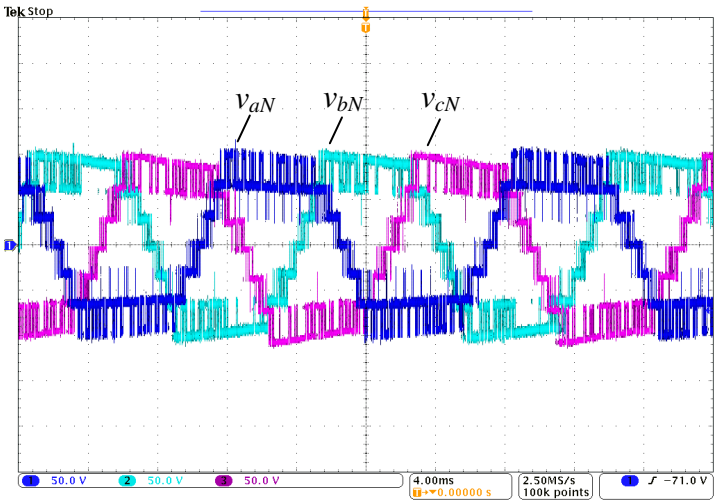


Figure 4.41. Inverter output voltage waveforms with modulation compensation (test 2.1).

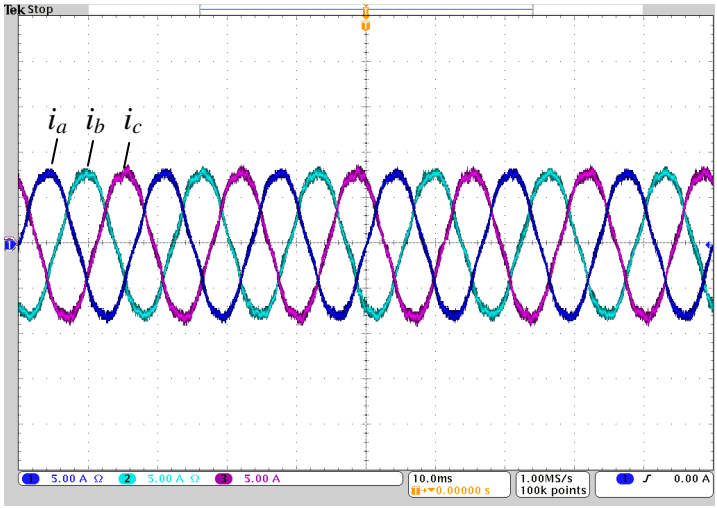


Figure 4.42. Experimental grid currents with unbalanced PV power (test 2.1).

Test 2.2: two large blue cards (13.5 cm × 9 cm) are placed on the second and third panels of phase *a*. For each panel, two cells are partly covered, as shown in Fig. 4.43.

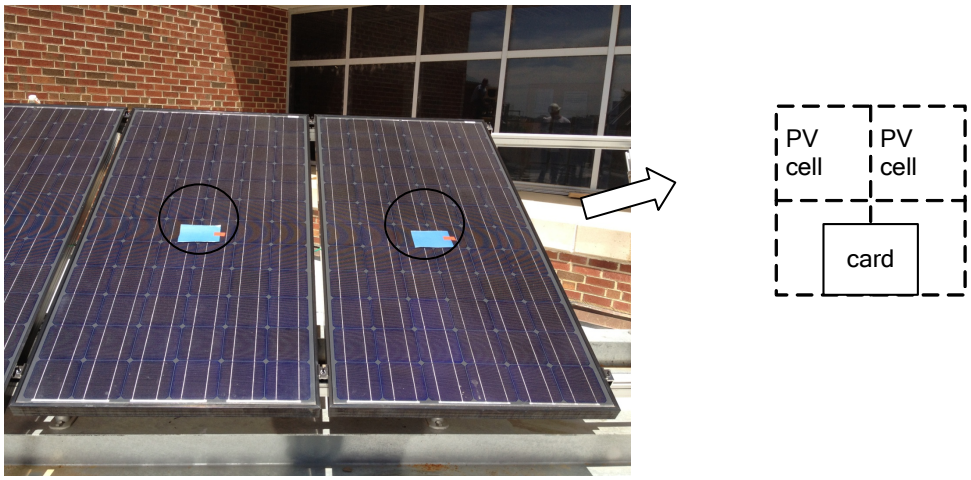


Figure 4.43. PV panels of phase *a*: two panels are partly covered (test 2.2).

The experimental results are presented in Figs. 4.44-4.47. Fig. 4.44 shows the PV current waveforms of phase *a*, and Fig. 4.45 shows the harvested solar power of each phase. As in the test 2.1, due to two panels of phase *a* are partly covered, the extracted solar power of phase *a* is

smaller.

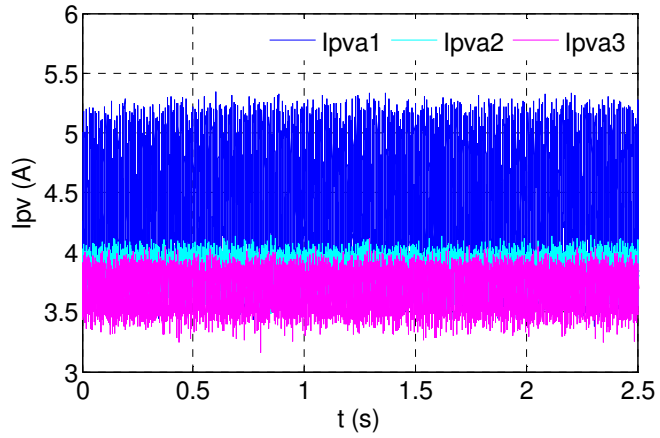


Figure 4.44. Experimental PV currents of phase *a* (test 2.2).

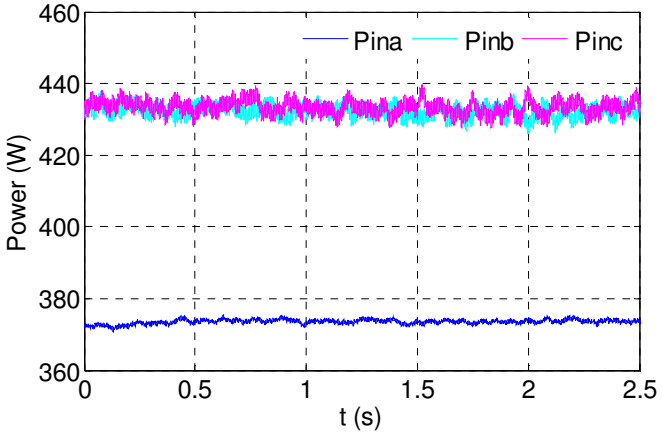


Figure 4.45. Experimental power extracted from PV panels with individual MPPT (test 2.2).

By applying the modulation compensation scheme, the inverter output voltage is unbalanced, as presented in Fig. 4.46. The output voltage $v_{aN}$ is lower as the power of phase *a* is smaller. Fig. 4.47 presents the balanced grid current. The rms value of the current is 6.0 A, and the THD is 4.1%, the TDD is 2.7%.

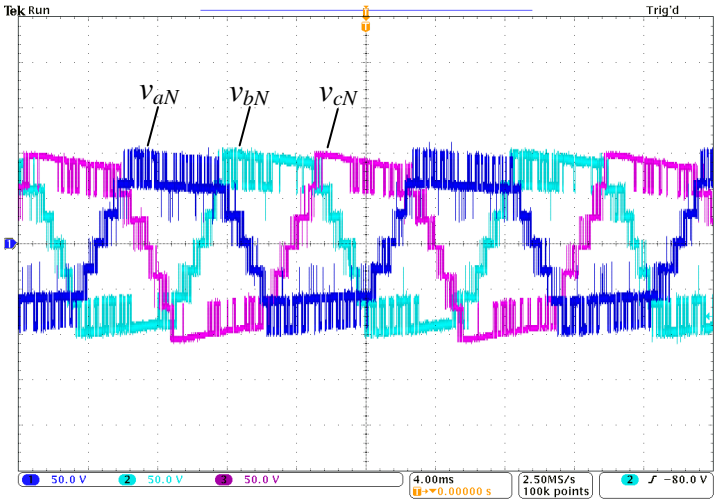


Figure 4.46. Inverter output voltage waveforms with modulation compensation (test 2.2).

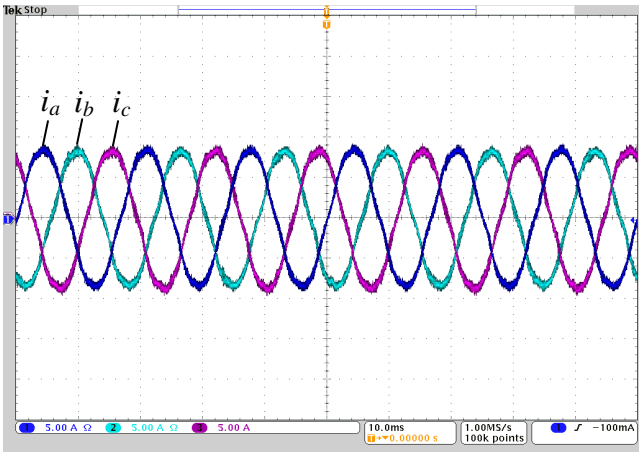


Figure 4.47. Experimental grid currents with unbalanced PV power (test 2.2).

Test 3: one panel in each of two of the phases is partly covered. In this test, one large blue card (13.5 cm × 9 cm) is placed on the third panel of phase *a*, and one is placed on the third panel of phase *b*. For each panel, one cell is almost fully covered.

Fig. 4.48 shows the PV currents of the third panels in each phase. For phase *a* and *b*, since one cell of the third panel is almost fully covered, their PV currents of the third panels are less than 2 A, while the current of the third panel of phase *c* is about 4.5 A. With the individual

MPPT control, each PV panel is operated at its own MPP and not influenced by other panels.

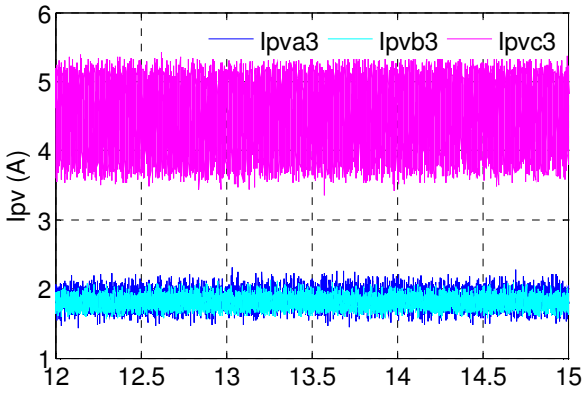


Figure 4.48. Experimental PV currents of the third panels in each phase (test 3).

Fig. 4.49 shows the power extracted from solar panels. Since the third panels of phase *a* and *b* are partly covered, the harvested solar power from these two phases are much smaller. Similarly, the inverter output voltage is unbalanced proportional to the extracted solar power of each phase to balance the grid current. Thus, as shown in Fig. 4.50, the output voltages of phase *a* and *b* are lower than that of phase *c*.

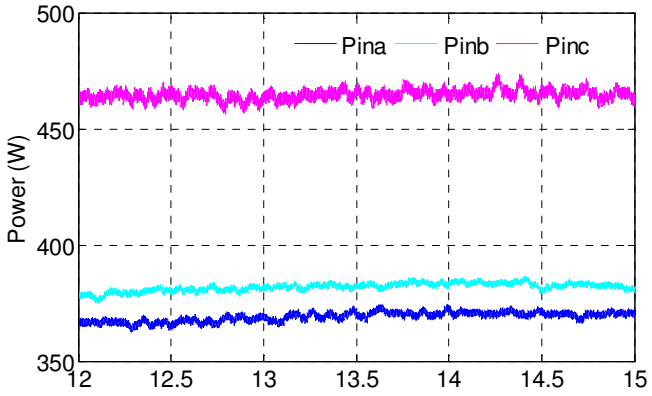


Figure 4.49. Experimental power extracted from PV panels with individual MPPT (test 3).

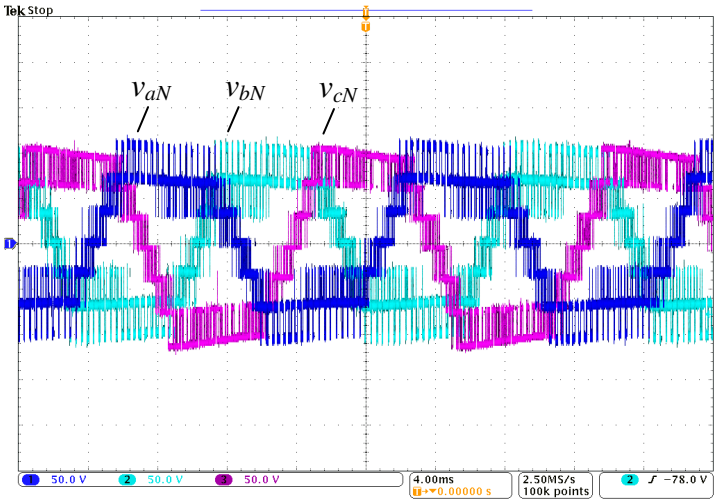


Figure 4.50. Inverter output voltage waveforms with modulation compensation (test 3).

The experimental grid current waveforms are presented in Fig. 4.51. The rms value of the current is 5.7 A, and the THD is 3.6%, the TDD is 2.2%.

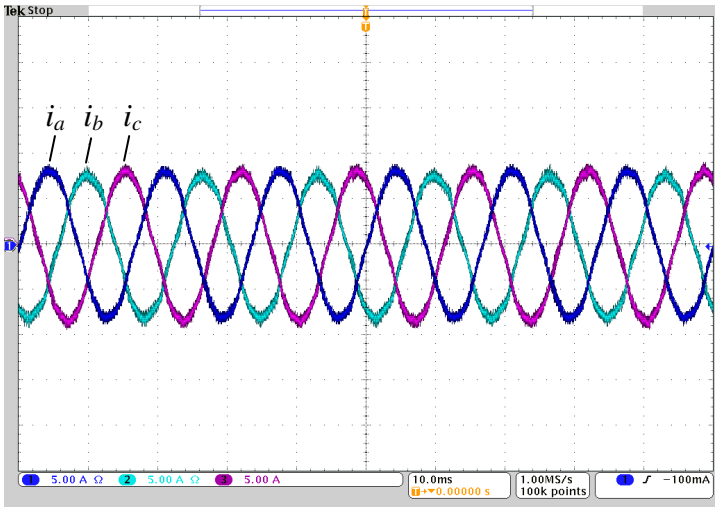


Figure 4.51. Experimental grid currents with unbalanced PV power (test 3).

Test 4: To see the function of the modulation compensation, the system is tested in two conditions: with and without the modulation compensation. In this test, a large blue card (13.5 cm × 9 cm) is placed on the third panel of phase *a*, and one cell of the panel is almost fully

covered.

First, the modulation compensation scheme is applied. Fig. 4.52 shows the extracted solar power. Due to the covering in phase *a*, the solar power of phase *a* is much lower than that of phase *b* and *c*. However, with the modulation compensation, the grid current is still balanced, as shown in Fig. 4.53. The rms value of the current is 5.3 A, and the THD is 3.5%, the TDD is 2.0%.

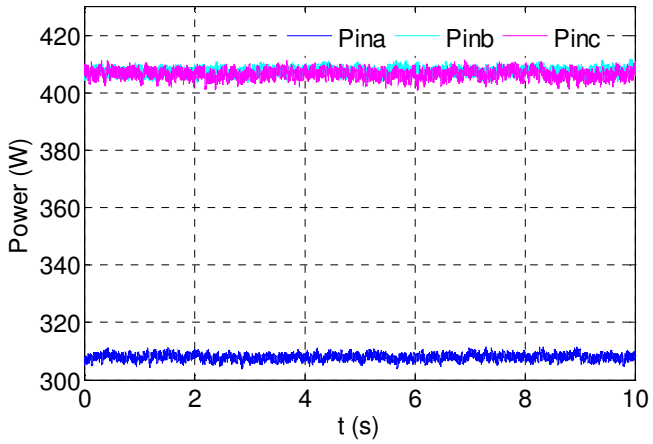


Figure 4.52. Power extracted from PV panels with modulation compensation.

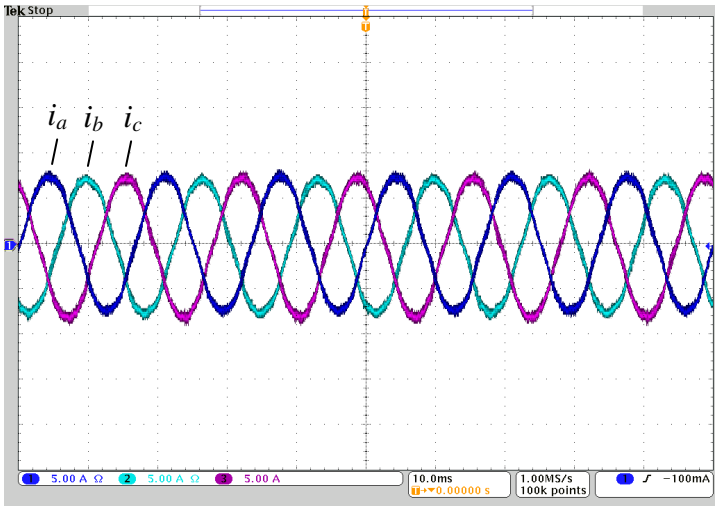


Figure 4.53. Experimental grid currents with modulation compensation.

Fig. 4.54 shows the modulation index of each H-bridge module in phase *a*. Since the connected PV panel of the third module is partly covered and generates less power, the modulation index of this module is smaller.

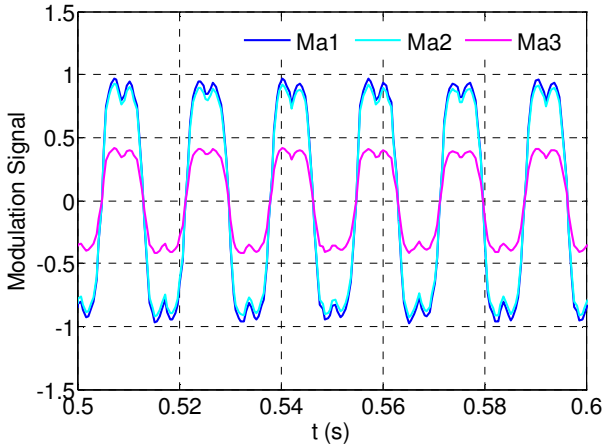


Figure 4.54. Modulation index of each H-bridge module in phase *a* with modulation compensation.

Then, the system is tested again without the modulation compensation scheme. Fig. 4.55 shows the solar power extracted from PV panels. Compared to Fig. 4.52, the harvested solar power has little difference. However, without the modulation compensation, the grid current is not balanced with the unbalanced supplied power, as shown in Fig. 4.56. The rms value of $i_a$ is 5.1 A, while the rms value of $i_b$ or $i_c$ is 5.4 A. The grid current of phase *a* is lower due to the lower supplied power to phase *a*. In addition, the THD of the current is 6.7%, while it is only 3.5% when the modulation compensation scheme is applied.

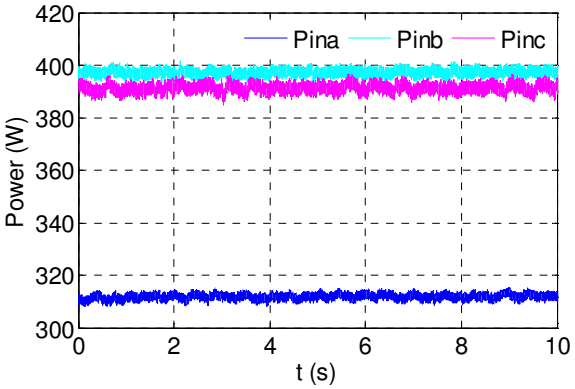


Figure 4.55. Power extracted from PV panels without modulation compensation.

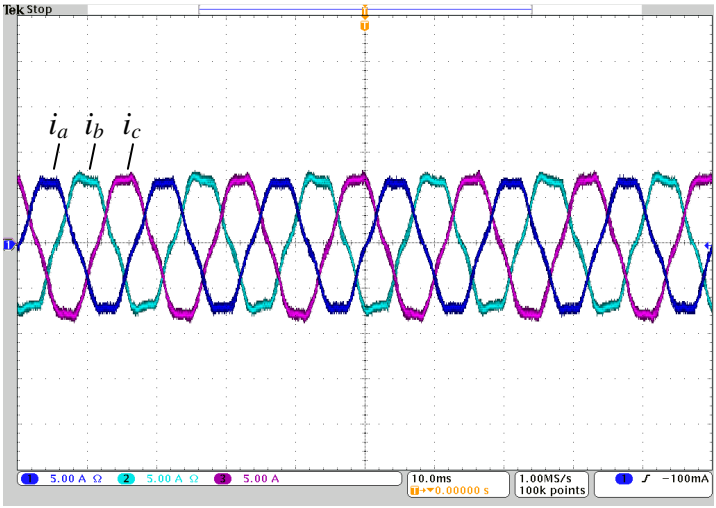


Figure 4.56. Experimental grid currents without modulation compensation.

The modulation index of each H-bridge module in phase *a* is shown in Fig. 4.57. Without the modulation compensation, the first and second modules will be over-modulated. Because the connected PV panel of the third module generates less power, the modulation index proportion of this module is smaller. To maintain the desired output voltage, the first and second modules have much larger modulation index proportion, leading to overmodulation. However, by applying the modulation compensation scheme, the modulation index of each phase will be unbalanced proportional to the power. Thus, the modulation index of phase *a* is reduced and

helps to prevent overmodulation. As presented in Fig. 4.54, the first and second modules are not over-modulated. So the THD of the grid current with the compensation is much better.

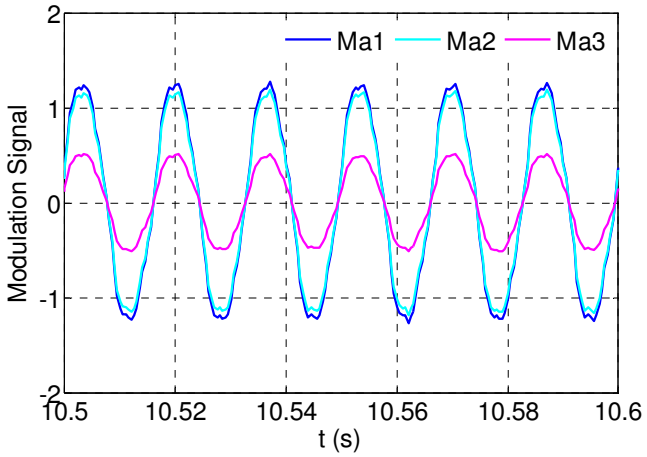


Figure 4.57. Modulation index of each H-bridge module in phase *a* without modulation compensation.

As discussed above, the cascaded H-bridge multilevel inverter topology helps to reduce voltage stresses on the semiconductor switches. Thus, low voltage rating MOSFETs with low cost can be applied. Although more components are employed in this topology, the modular design and mass production will lead to low manufacturing cost. Meanwhile, due to the low switching frequency, the topology itself has higher efficiency when compared to other converter topologies. With the proposed control scheme, individual MPPT in each string can be achieved to harvest more solar energy and increase the efficiency of the PV system further.

## 4.4 Summary

In this chapter, a three-phase modular cascaded H-bridge multilevel inverter for grid-connected PV system has been presented. The modularity and low cost of multilevel converters would position them as a prime candidate for the next generation of efficient, robust, and reliable

grid-connected solar power electronics. As in the single-phase system, the individual MPPT control is achieved to maximize the solar energy extraction of each PV string and improve the overall efficiency. PV mismatches could even introduce unbalanced power supplied to the three-phase grid-connected system. To balance the three-phase grid current, a modulation compensation scheme is added to the control system. Though the ability of balancing the grid current is limited, the compensation scheme still helps to reduce the percentage unbalance of the grid current. The modulation compensation scheme also helps to prevent overmodulation, and will not cause extra power loss. To validate the proposed control scheme, a modular cascaded multilevel inverter prototype has been built and tested under different conditions. Experimental results are presented to show that the individual MPPT can be achieved and the three-phase grid current is balanced even with the unbalanced supplied power.

# 5 Three-Phase Cascaded Voltage Source Inverter for Grid-Connected Photovoltaic Applications

The cascaded H-bridge multilevel inverter topology can be applied in grid-connected PV systems to reduce the inverter cost. However, this topology employs a large number of electrical and mechanical components, especially in three-phase systems, resulting in an increase of systematic volume and labor cost. In addition, the size of the dc-link capacitor is large due to the single-phase pulsating power, and this capacitor is the main limiting factor of the inverter lifetime, which should be kept as small as possible. Thus, a three-phase cascaded VSI composed of three conventional three-phase two-level VSIs can be applied. The topology was first proposed in [81] and applied in medium and high voltage variable speed motor drive systems. The inverter keeps many advantages of the cascaded H-bridge multilevel inverter, and more importantly, it needs fewer switches and reduces the size of the dc-link capacitor [82].

A three-phase cascaded VSI for a grid-connected PV system is proposed in this chapter. To realize the central control, the equivalent model and average model of the three-phase cascaded VSI are established. A control scheme with MPPT control is proposed to harvest more solar energy. Simulation and experimental results are also given to validate the proposed ideas.

## 5.1 System Description

The topology of the proposed three-phase grid-connected PV system is shown in Fig. 5.1. The three-phase cascaded VSI consists of three traditional three-phase two-level VSI units, which are interconnected in a delta to generate higher output voltage. The circulating current in the delta can be limited by placing inductors $L_d$, which are small at the practical switching

frequency. Each VSI unit is connected to a string of PV panels. The three-phase cascaded VSI is connected to the grid through filter *L*.

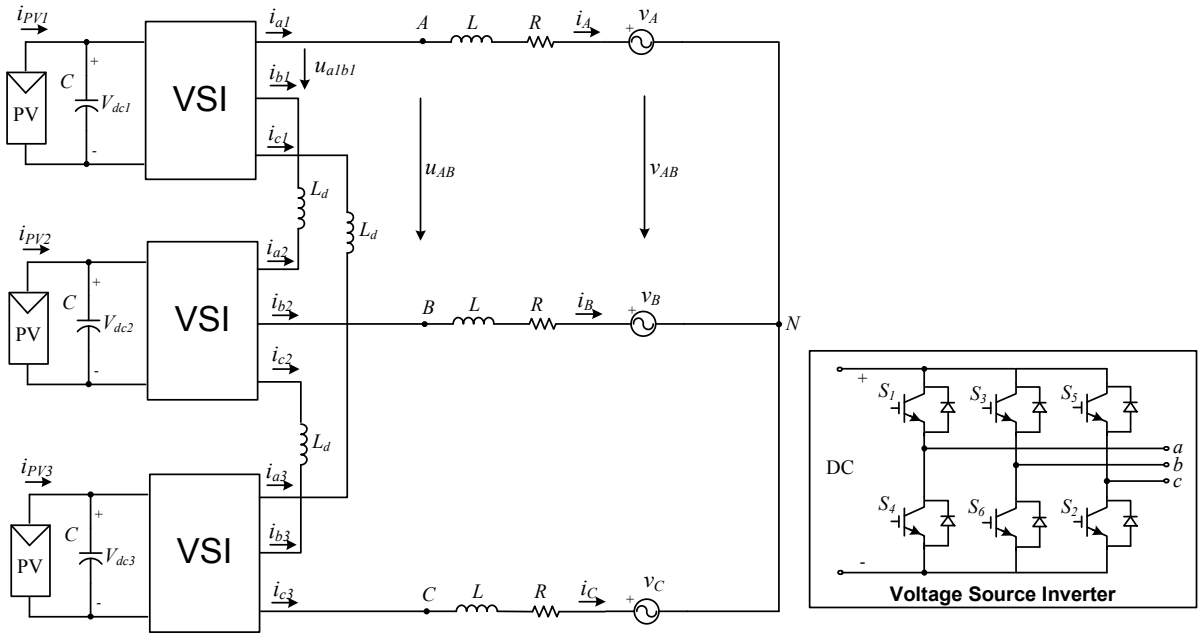


Figure 5.1. Topology of the proposed three-phase cascaded PV system.

As shown in Fig. 5.1, the output line voltage of the three-phase cascaded VSI consists of line voltages of two adjacent VSI units, and the voltage across the current-limiting inductor.

$$\begin{cases} u_{AB} = u_{a1b1} + u_{b1a2} + u_{a2b2} = (j\omega L + R)i_{a1} + v_{AB} - (j\omega L + R)i_{b2} \\ u_{BC} = u_{b2c2} + u_{c2b3} + u_{b3c3} = (j\omega L + R)i_{b2} + v_{BC} - (j\omega L + R)i_{c3} \\ u_{CA} = u_{c3a3} + u_{a3c1} + u_{c1a1} = (j\omega L + R)i_{c3} + v_{CA} - (j\omega L + R)i_{a1} \end{cases} \tag{33}$$

where $u_{AB}$, $u_{BC}$, and $u_{CA}$ are the output line-line voltages of the three-phase cascaded VSI; $u_{aibi}$, $u_{bici}$, and $u_{ciai}$ are the line-line voltages of VSI unit $i$ ($i$=1, 2, 3); $u_{b1a2}$, $u_{c2b3}$, and $u_{a3c1}$ are the current-limiting inductor voltages; $i_{ai}$, $i_{bi}$, and $i_{ci}$ are the output currents of VSI unit $i$; $v_{AB}$, $v_{BC}$, and $v_{CA}$ are the line-line voltages of the grid; $R$ is the internal resistance of filter $L$.

By applying the cascaded topology, the three-phase cascaded VSI provides 7-level output

line voltage, which reduces voltage stresses on the semiconductor switches in each VSI unit, and enables the reduction of harmonics in the synthesized current, reducing the output filters.

The relationship of line currents is analyzed in [81]. Assuming a balanced system, the injected grid current can be expressed as

$$\begin{cases} i_A = i_{a1} = \sqrt{2} I \sin \omega t \\ i_B = i_{b2} = \sqrt{2} I \sin(\omega t - 2\pi / 3) \\ i_C = i_{c3} = \sqrt{2} I \sin(\omega t + 2\pi / 3) \end{cases} \tag{34}$$

where $I$ is the rms value of the grid current.

For each VSI unit $i$, we have

$$\boldsymbol{i}_{ai} + \boldsymbol{i}_{bi} + \boldsymbol{i}_{ci} = 0 \tag{35}$$

Due to the interconnection of three traditional three-phase VSI units, we also have

$$\boldsymbol{i}_{b1} = -\boldsymbol{i}_{a2}, \quad \boldsymbol{i}_{c2} = -\boldsymbol{i}_{b3}, \quad \boldsymbol{i}_{a3} = -\boldsymbol{i}_{c1} \tag{36}$$

The fundamental circulating current within the current-limiting inductors loop is zero. Thus,

$$\boldsymbol{i}_{b1} + \boldsymbol{i}_{c2} + \boldsymbol{i}_{a3} = 0 \tag{37}$$

According to (34)-(37), the output currents of each VSI unit can be solved and expressed as

$$\begin{cases} i_{a1} = \sqrt{2} I \sin \omega t \\ i_{b1} = \dfrac{1}{\sqrt{3}} \cdot \sqrt{2} I \sin(\omega t - 5\pi / 6) \\ i_{c1} = \dfrac{1}{\sqrt{3}} \cdot \sqrt{2} I \sin(\omega t + 5\pi / 6) \end{cases} \tag{38}$$

$$\begin{cases} i_{a2} = \dfrac{1}{\sqrt{3}} \cdot \sqrt{2} I \sin(\omega t + \pi / 6) \\ i_{b2} = \sqrt{2} I \sin(\omega t - 2\pi / 3) \\ i_{c2} = \dfrac{1}{\sqrt{3}} \cdot \sqrt{2} I \sin(\omega t + \pi / 2) \end{cases} \tag{39}$$

$$\begin{cases} i_{a3} = \dfrac{1}{\sqrt{3}} \cdot \sqrt{2} I \sin(\omega t - \pi / 6) \\ i_{b3} = \dfrac{1}{\sqrt{3}} \cdot \sqrt{2} I \sin(\omega t - \pi / 2) \\ i_{c3} = \sqrt{2} I \sin(\omega t + 2\pi / 3) \end{cases} \tag{40}$$

Thus, the current vector diagram of the three-phase cascaded VSI can be obtained, as shown in Fig. 5.2.

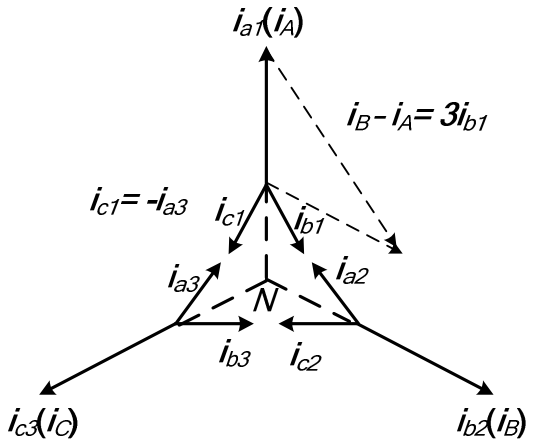


Figure 5.2. Current vector diagram.

It can be seen that the line currents of each VSI unit are unbalanced. Take VSI unit 1 as an example,

$$|\boldsymbol{i}_{b1}| = |\boldsymbol{i}_{c1}| = \frac{1}{\sqrt{3}} |\boldsymbol{i}_{a1}| \tag{41}$$

## 5.2 Comparison

In grid-connected PV applications, the three-phase cascaded VSI topology keeps the advantages of the cascaded multilevel inverter. These two topologies are similar in modular structure and isolated DC buses, and a comparison is conducted between them.

A comparison of the three-phase cascaded VSI and the three-phase 7-level cascaded H-bridge inverter is conducted under the same output power, and the same grid voltage. The comparison results are listed in Table 5.1. $V$ is the rms value of the line-line voltage of the grid, and $I$ is the rms value of the injected grid current.

Table 5.1. Comparison of three-phase cascaded VSI and three-phase cascaded H-bridge inverter

| | Three-phase cascaded VSI | Three-phase 7-level cascaded H-bridge inverter |
|---|---|---|
| Number of switches | 18 | 36 |
| Number of inductors | 3 | 0 |
| Number of capacitors | 3 | 9 |
| Switch voltage stress | $\sqrt{2}V/\sqrt{3}$ | $\sqrt{2}V/3\sqrt{3}$ |
| Switch current stress | 6 switches: $I$<br>12 switches: $I/\sqrt{3}$ | $I$ |

From Table 5.1, it can be seen that the three-phase cascaded VSI topology has a reduced component count of all the components except for the inductors. The switch voltage stress of the three-phase cascaded VSI is three times as much as that of the three-phase 7-level cascaded H-bridge inverter. However, 12 switches out of 18 switches of the three-phase cascaded VSI has much less current stress, while other 6 switches has the same current stress as the switches of the cascaded H-bridge inverter.

In addition, considering these two topologies are applied to PV systems, both of them employ a PV string as the DC source of one inverter module. If the same PV panels are used, the number of panels in one PV string for the three-phase cascaded VSI would be three times more than that for the cascaded H-bridge inverter, which means the three-phase cascaded VSI topology sacrifices the utilization per PV module to reduce the number of required components.

The proposed topology is also compared with the conventional three-phase two-level PV inverter under the same output power, as shown in Table 5.2.

Table 5.2. Comparison of three-phase cascaded VSI and conventional three-phase two-level inverter

| | Three-phase cascaded VSI | Conventional three-phase two-level inverter |
|---|---|---|
| Number of switches | 18 | 6 |
| Number of inductors | 3 | 0 |
| Number of capacitors | 3 | 1 |
| Switch voltage stress | $\sqrt{2}V/\sqrt{3}$ | $2\sqrt{2}V/\sqrt{3}$ |
| Switch current stress | 6 switches: $I$<br>12 switches: $I/\sqrt{3}$ | $I$ |

The number of switches needed by the three-phase cascaded VSI topology is three times more than that of the traditional three-phase VSI. However, the switch voltage stress of the three-phase cascaded VSI is only half of that of the conventional three-phase VSI. In addition, the cascaded topology helps to reduce the size of output filters. Meanwhile, the three-phase two-level PV inverter, where PV strings are connected in parallel through string diodes to reach high power level, includes some severe limitations, such as mismatch losses between the PV strings and losses in the string diodes [81]. The three-phase cascaded VSI PV system will not have these

issues.

## 5.3 Control System

### 5.3.1 Modeling of Three-Phase Cascaded VSI

Due to the structure of the three-phase cascaded VSI, the line currents of each VSI are unbalanced. If each VSI unit is controlled independently, the coordinated operation among three VSIs needs to be considered, and the whole control system is complicated. Therefore, the equivalent model of the system is needed to help design a central controller of the three-phase cascaded VSI, and then phase-shifted PWM technique can be applied to the three VSI units.

To get the equivalent model, a balanced system is considered. The three VSI units will have the same modulation index, and the vector $\boldsymbol{u}_{ab}$ (or $\boldsymbol{u}_{bc}$, $\boldsymbol{u}_{ca}$) in three VSI units will be the same. Thus, we can define

$$\begin{cases} u_{A'B'} = u_{a1b1} + u_{a2b2} \\ u_{B'C'} = u_{b2c2} + u_{b3c3} \\ u_{C'A'} = u_{c3a3} + u_{c1a1} \end{cases} \tag{42}$$

From (33) and (42), we have

$$\begin{cases} u_{A'B'} = (j\omega L + R)i_A + v_{AB} - (j\omega L + R)i_B - j\omega L_d i_{b1} \\ u_{B'C'} = (j\omega L + R)i_B + v_{BC} - (j\omega L + R)i_C - j\omega L_d i_{c2} \\ u_{C'A'} = (j\omega L + R)i_C + v_{CA} - (j\omega L + R)i_A - j\omega L_d i_{a3} \end{cases} \tag{43}$$

According to (38)-(40) and the current vector diagram, the equivalent model of the three-phase cascaded VSI can be obtained

$$\begin{cases} u_{A'B'} = (j\omega L' + R)i_A + v_{AB} - (j\omega L' + R)i_B \\ u_{B'C'} = (j\omega L' + R)i_B + v_{BC} - (j\omega L' + R)i_C \\ u_{C'A'} = (j\omega L' + R)i_C + v_{CA} - (j\omega L' + R)i_A \end{cases} \tag{44}$$

where

$$L' = L + L_d / 3 \tag{45}$$

The equivalent circuit model can be drawn from (42) and (44), as shown in Fig. 5.3. According to (42), the equivalent dc-link voltage $V'_{dc}$ is two times of the average dc-link voltage, while the equivalent capacitance $C'_{dc}$ is half of the dc-link capacitance $C$.

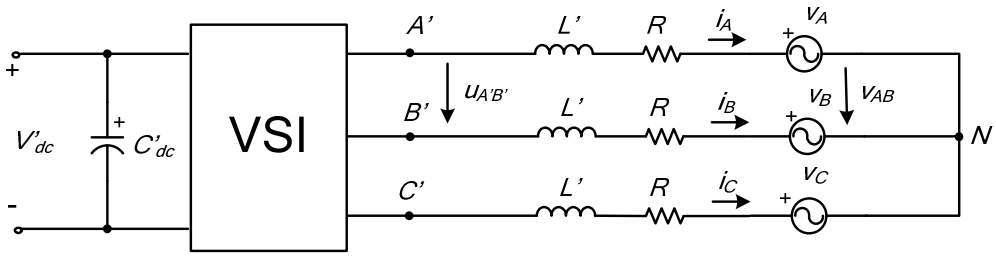


Figure 5.3. Equivalent circuit model of three-phase cascaded VSI.

The average model of the three-phase cascaded VSI in *dq* coordinates is obtained and shown in Fig. 5.4. Thus, the control method used in conventional VSIs can be easily introduced to the three-phase cascaded VSI.

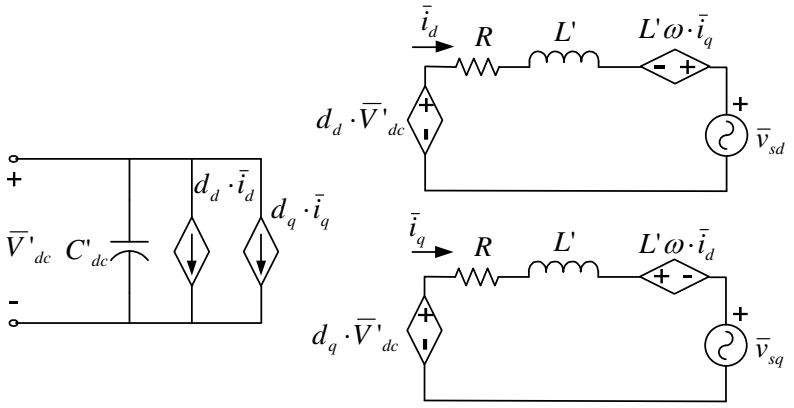


Figure 5.4. Average model of three-phase cascaded VSI in *dq* coordinates.

### 5.3.2 Control Scheme

According to the average model of the three-phase cascaded VSI, the control scheme used in the traditional three-phase system can be easily introduced, and central control of the whole system can be achieved. A control scheme with individual MPPT control for the three-phase cascaded VSI for the grid-connected PV system is proposed, as shown in Fig. 5.5.

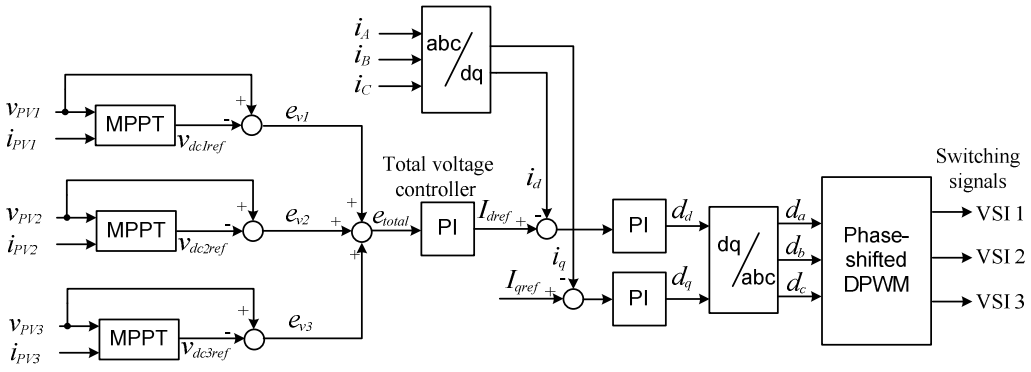


Figure 5.5. Control scheme for three-phase cascaded VSI.

To maximize the solar energy extraction, an MPPT controller is added to generate the dc-link voltage reference of each VSI unit. Each dc-link voltage is compared to the corresponding voltage reference, and the sum of the three voltage errors is controlled through a PI controller

that determines the current reference $I_{dref}$. As the classic control scheme in three-phase systems, the grid currents in *abc* coordinates are converted to *dq* coordinates and regulated through PI controllers to generate the modulation index in *dq* coordinates, which is then converted back to three-phase.

Phase-shifted DPWM is then applied to control the switching devices of the three-phase cascaded VSI. In the cascaded multilevel converter, phase-shifted PWM technique has been widely used. It only needs one carrier to generate all the switching signals, and helps to reduce harmonics in the produced multilevel voltage.

Phase-shifted technique can also be applied in this case. Each VSI unit adopts a DPWM controller, and the carrier corresponding to each unit is shifted by $T_s/3$ in sequence, where $T_s$ is the switching period. Phase-shifted DPWM is easily implemented, and helps to reduce the switching loss of each unit [83].

The proposed control scheme is based on a system with balanced input solar power. If PV mismatch happens, three dc-link voltages may be not equal and the injected grid current may be unbalanced. The control scheme needs to be improved under unbalanced solar power. However, based on the modeling method discussed above, the three-phase cascaded VSI can still be equivalent to a similarly VSI circuit model, which exists a coupled relationship containing $V_{dci}/V_{dcave}$ in the mathematical model. The central control scheme based on the VSI circuit model will not be influenced much.

## 5.4 Results

Simulation and experimental tests are carried out to validate the proposed ideas. A three-phase cascaded VSI prototype has been built in the laboratory. Each VSI unit has a short string

of PV panels connected as the isolated DC source. The solar panels (185 W Astronergy CHSM-5612M) shown in Fig. 4.18 are used in the experiment.

To verify the proposed control scheme, a three-phase cascaded VSI for the grid-connected PV system is first simulated. Each VSI unit is fed by a short string of PV panels, which has four 185 W PV panels connected in series. PV panels are operated under the irradiance S=1000 W/m$^2$ and temperature T=25 ˚C. The three-phase cascaded VSI is connected to the grid, and the phase voltage of the grid is 120 Vrms.

According to (11) and the equivalent circuit model of three-phase cascaded VSI, the inductor *L'* is calculated as

$$L' = \frac{V_{dc}^{'}}{16 f_{sw} \Delta i_{L\max}} \geq \frac{2 \times 4 \times 36.38}{16 \times 4000 \times 1.232} = 3.69mH \tag{46}$$

From (45), the connection inductor is selected as $L$ = 3.5 mH, and the current-limiting inductor is selected as $L_d$ = 1.5 mH. The system parameters are shown in Table 5.3.

Table 5.3. System parameters

| Parameters | Value |
|---|---|
| DC-link capacitor | 3.6 mF |
| Connection inductor $L$ | 3.5 mH |
| Current-limiting inductor $L_d$ | 1.5 mH |
| Grid resistor $R$ | 0.1 ohm |
| Grid phase voltage | 120 Vrms |
| Switching frequency | 4 kHz |

Due to the structure of the three-phase cascaded VSI, the output line currents of each VSI

are unbalanced. For instance, the unbalanced line current of VSI unit 1 is shown in Fig. 5.6, which verifies the relationship given in (38). However, with the proposed control scheme, the grid current is balanced, as shown in Fig. 5.7. The TDD of the grid current is 3.0%, as shown in Fig. 5.8, which is less than 5% and meets the power quality standard.

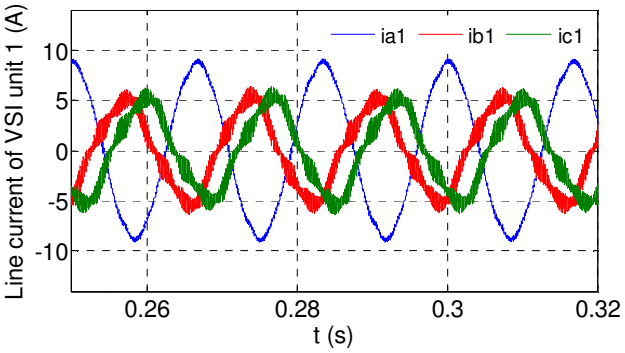


Figure 5.6. Simulated line current of VSI unit 1.

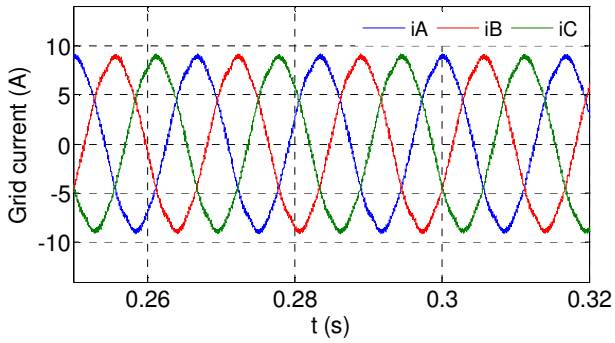


Figure 5.7. Simulated grid current of the proposed PV system.

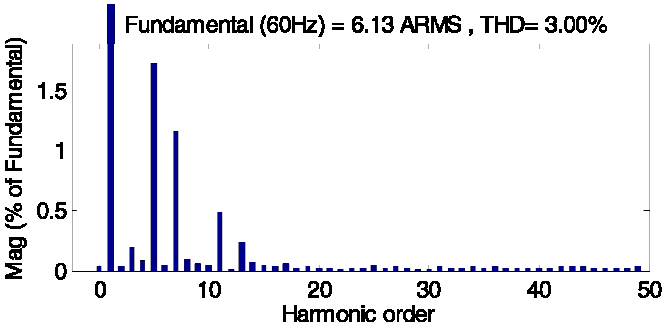


Figure 5.8. THD of the grid current shown in Fig. 5.7.

The output line voltage $u_{AB}$ of the three-phase cascaded VSI is shown in Fig. 5.9. The 7-level voltage enables the reduction of harmonics in the synthesized current, reducing the output filters. The grid voltage and current waveforms of phase $a$ are shown in Fig. 5.10. The grid current has the same phase as the voltage, which means unity displacement power factor has been achieved. Fig. 5.11 shows the dc-link voltage of VSI unit 1. It can be seen that four PV panels in that string are operated at the MPP voltage 36.4 V.

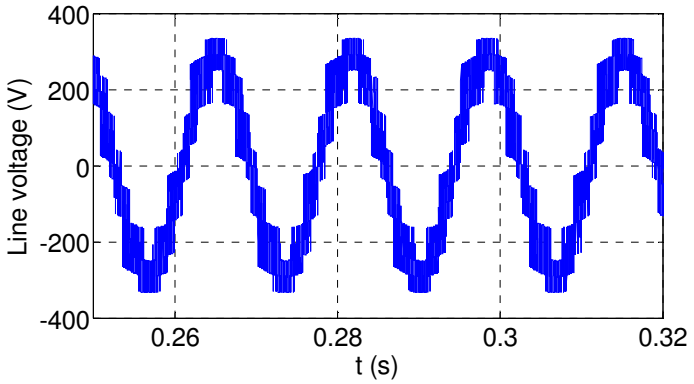


Figure 5.9. Simulated output line voltage $u_{AB}$ of three-phase cascaded VSI.

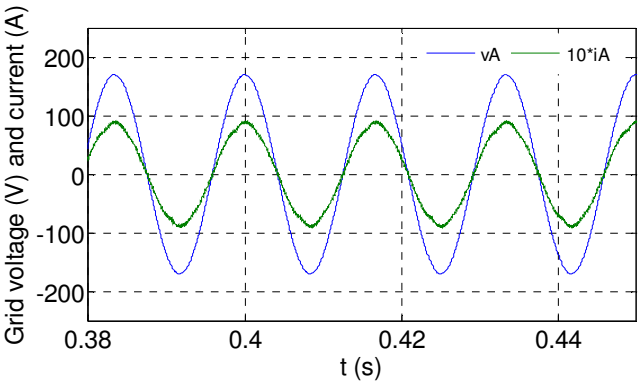


Figure 5.10. Simulated grid voltage and current of phase $a$.

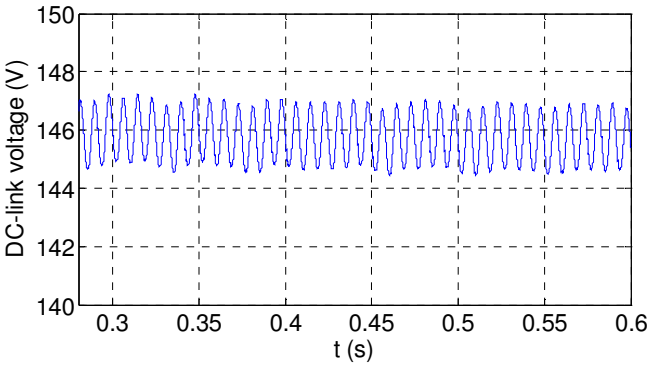


Figure 5.11. Simulated dc-link voltage of VSI unit 1.

To compare the three-phase cascaded VSI topology with the conventional three-phase two-level inverter, a three-phase two-level grid-connected PV inverter is also simulated. The same output filters and switching frequency are chosen. The grid current waveforms are shown in Fig. 5.12. The THD of the grid current is 15.3% for the traditional two-level inverter, which is far more than 5%. However, as shown in Fig. 5.8, the THD of the grid current in the three-phase cascaded VSI PV system is only 3.0%. Thus, the three-phase cascaded VSI topology helps to reduce harmonics in the synthesized current.

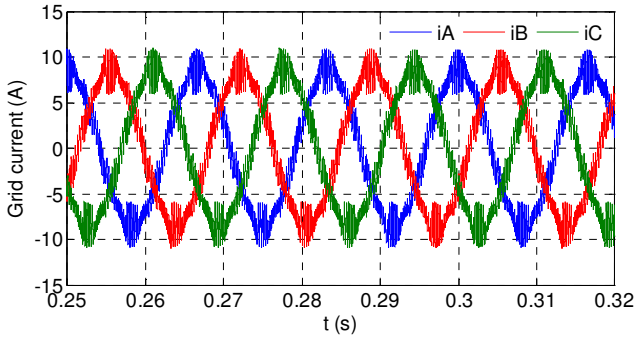


Figure 5.12. Simulated grid currents of three-phase two-level PV inverter.

A three-phase cascaded VSI prototype has been built. The MOSFET IRFSL4127 is selected as inverter switches operating at 4 kHz. The control signals to the inverters are sent by a

dSPACE ds1103 controller. Each VSI unit has two PV panels connected in series as the DC source. The three-phase cascaded VSI is connected to the grid through a transformer, and the phase voltage of the secondary side is 60 Vrms. The connection inductor $L$ is 2.5 mH, and the current-limiting inductor $L_d$ is 1.5 mH.

The experimental results are presented in Figs. 5.13-5.16. Fig. 5.13 shows the three-phase grid current. With the proposed control scheme, the grid current is balanced, and the THD is 4.9%, as shown in Fig. 5.14. The experimental setup was tested in winter, and the solar irradiance on PV panels was not high enough. Thus, the experimental grid current is only 3.8 Arms. Since the rated current is 6.17 A, the TDD is calculated as 3.0%, which also meets power quality standards.

Fig. 5.15 shows the line currents of one VSI unit. As discussed before, they are not balanced. Fig. 5.16 shows the grid voltage and current waveforms of phase $a$. It can be seen that the grid current has the same phase as the grid voltage and has unity displacement power factor.

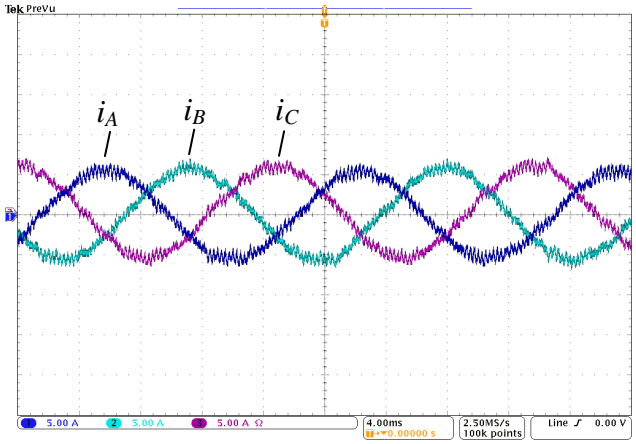


Figure 5.13. Experimental three-phase grid current.

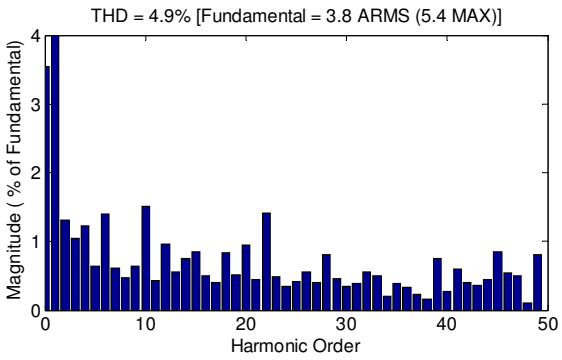


Figure 5.14. THD of the grid current shown in Fig. 5.13.

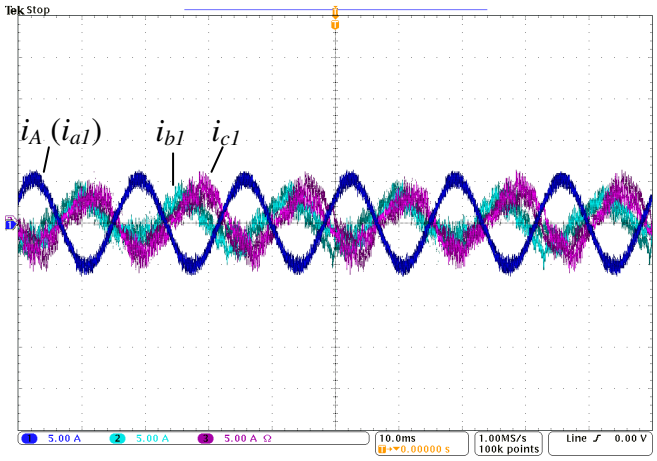


Figure 5.15. Experimental line currents of VSI unit 1.

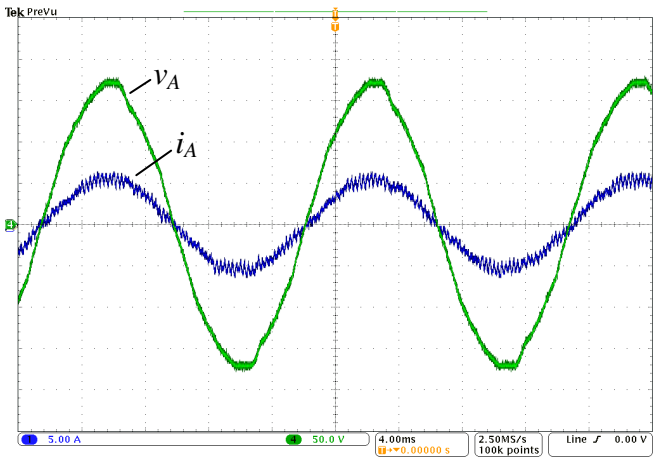


Figure 5.16. Experimental grid voltage and current waveforms of phase *a*.

## 5.5 Summary

In this chapter, a three-phase cascaded voltage source inverter for grid-connected PV applications has been proposed. Compared to the three-phase cascaded H-bridge multilevel inverter, the proposed topology keeps many advantages, and has fewer components. Due to the structure of the three-phase cascaded VSI, the line currents of each VSI are unbalanced. To realize the central control, the equivalent model and average model of the proposed PV system are given. The control scheme used in the traditional three-phase two-level VSI is updated for this topology, and MPPT controllers are also added to harvest more solar energy. Simulation and experimental results are presented to validate the feasibility and effectiveness of the proposed ideas.

# 6 Conclusions and Future Work

## 6.1 Conclusions

### 6.1.1 Summary of the Work

In this dissertation, the cascaded multilevel inverter topologies are chosen to reduce the PV inverter cost and improve the overall efficiency of the grid-connected PV systems.

Five inverter families can be defined according to the different configurations of the PV system. Among these configurations, the DC/AC cascaded inverter can be used in medium- and large scale PV applications without sacrificing the benefits of "converter per panel", and it can employ the single stage inverter, which further increases the overall efficiency and reduces the cost. Many single and dual stage inverter topologies have been reviewed. The cascaded H-bridge multilevel inverter can be used as a single stage inverter for cascaded PV systems.

First, a single-phase cascaded H-bridge multilevel inverter topology for a grid-connected PV system is discussed. The PV mismatch issues are addressed, and simulation results show that the individual MPPT control in each string is required to reduce the adverse effect of the mismatches and increase the efficiency of the PV system. A control scheme with independent MPPT control and reactive power compensation is proposed. Simulation and experimental results show that individual MPPT control is achieved to maximize the solar energy extraction of each PV string, and the reactive power required by the local load can be provided by the proposed system to realize the power factor correction and reduce distribution losses.

The three-phase modular cascaded H-bridge multilevel PV inverter is then discussed. Besides decreasing the overall efficiency, PV mismatches could even introduce unbalanced

power supplied to the three-phase grid-connected system. To solve this issue, a control scheme with individual MPPT control and modulation compensation is proposed. As in the single-phase system, the individual MPPT control is achieved to realize better utilization per PV module, so that the overall efficiency of PV systems can be improved. Modulation compensation is applied to balance the three-phase grid current by injecting a zero sequence voltage. The proposed compensation scheme will not increase the complexity of the control system or cause extra power loss. The ability of balancing the grid current is limited, but the compensation scheme works in reducing the percentage unbalance of the grid current. It also helps to prevent overmodulation. A modular cascaded multilevel inverter prototype has been built and tested under different conditions. Experimental results are presented to show that each PV panel is operated at its own MPP and injected grid current is balanced even with the unbalanced solar power.

By applying the cascaded H-bridge multilevel inverter topology, the target of $0.10 per watt for PV inverters can be reached. However, this topology employs a large number of electrical and mechanical components, especially in three-phase systems, resulting in an increase of systematic volume and labor cost. Thus, a three-phase cascaded voltage source inverter for grid-connected PV applications has been proposed in chapter 5. The proposed topology keeps many advantages of the cascaded H-bridge multilevel inverter, and has fewer components. By establishing the equivalent model and average model of the proposed PV system, the control system design can be simplified. And the control scheme used in the traditional three-phase two-level VSI is updated for the central control of the system. Simulation and experimental results are given to validate the proposed ideas.

### 6.1.2 Contributions of This Dissertation

The contributions of this work are summarized as follows:

- Developed an individual MPPT control scheme in one central controller for both single- and three-phase cascaded H-bridge multilevel PV inverters to realize better utilization of PV modules and increase the overall efficiency of the PV system.
- For the three-phase cascaded H-bridge multilevel PV inverter, balanced the three-phase grid current injection during partial shading or module degradation conditions by applying a modulation compensation scheme. In addition, with the proposed modulation compensation scheme, the overmodulation is less likely to happen. The limitation of the scheme is also pointed out.
- Proposed a three-phase cascaded VSI topology for grid-connected PV applications. Realized the central control of the proposed PV system by establishing the equivalent model and average model of the three-phase cascaded VSI.

## 6.2 Future Work

The following issues can be considered for possible future work:

1. Cascaded inverter topologies are proposed for utility-scale PV systems to improve the efficiency. However, in this dissertation, the cascaded inverter prototypes have been only tested with a low power PV system. It would be interesting to test the cascaded inverters with the proposed control schemes in a high power utility-scale PV system, and verify the advantage of high efficiency. Meanwhile, the leakage current of PV modules is a challenging issue, especially in large-scale PV systems. The leakage current in cascaded PV inverters and its suppression should be studied.

2. For the cascaded PV inverters, an MPPT controller is added to each inverter module to achieve better utilization of PV panels. Thus, one voltage sensor and one current sensor are required for each inverter module. If the MPP voltages in the cascaded PV inverters can be determined by using fewer sensors, the cost of the PV system will be reduced further.
3. The proposed control scheme of the three-phase cascaded VSI is based on balanced input solar power. If PV mismatch happens, the supplied power to the three VSI units would be different. The control scheme needs to be updated to balance the injected grid current.

# REFERENCES

[1] “Renewables 2011: Global status report,” [Online]. Available: http://www.ren21.net/Resources/Publications/REN21Publications.aspx

[2] G. W. Crabtree and N. S. Lewis, “Solar energy conversion,” *Phys. Today*, vol. 60, pp. 37-42, 2007.

[3] “Renewables 2013: Global status report,” [Online]. Available: http://www.ren21.net/portals/0/documents/resources/gsr/2013/gsr2013_lowres.pdf

[4] “Renewables 2012: Global status report,” [Online]. Available: http://www.ren21.net/Resources/Publications/REN21Publications.aspx

[5] J. M. Carrasco, L. G. Franquelo, J. T. Bialasiewicz, E. Galvan, R. C. PortilloGuisado, M. A. M. Prats, J. I. Leon, and N.Moreno-Alfonso, “Power-electronic systems for the grid integration of renewable energy sources: A survey,” *IEEE Trans. Ind. Electron.*, vol. 53, no. 4, pp. 1002–1016, Aug. 2006.

[6] A. R. Jha, *Solar Cell Technology and Applications*. Boca Raton: Taylor & Francis Group, LLC, 2010.

[7] Y. Nakata, “Dynamics of innovation in solar cell industry: Divergence of solar cell techonologies,” *IEEE International Technology Management Conference (ITMC)*, Jun. 2011, pp. 1042-1047.

[8] “2012 SEPA Utility solar rankings,” [Online]. Available: http://www.solarelectricpower.org/media/51302/final-2012-top-10-report-v2.pdf

[9] "Global market outlook for photovoltaics until 2016," [Online]. Available: http://www.epia.org/fileadmin/user_upload/Publications/Global-Market-Outlook-2016.pdf

[10] A. Goodrich, T. James, and M. Woodhouse, "Residential, commercial, and utility-scale

photovoltaic (PV) system prices in the United States: Current drivers and cost-reduction opportunities," NREL report, No. TP-6A20-53347.

[11] M. Meinhardt and G. Cramer, "Past, present and future of grid connected photovoltaic- and hybrid power-systems," in *Proc. IEEE-PES Summer Meeting*, vol. 2, 2000, pp. 1283–1288.

[12] M. Calais, J. Myrzik, T. Spooner, and V. G. Agelidis, "Inverter for single-phase grid connected photovoltaic systems – An overview," in *Proc. IEEE PESC'02*, vol. 2, 2002, pp. 1995-2000.

[13] S. B. Kjaer, J. K. Pedersen, and F. Blaabjerg, "A review of single-phase grid connected inverters for photovoltaic modules," *IEEE Trans. Ind. Appl.*, vol. 41, no. 5, pp. 1292–1306, Sep. 2005.

[14] F. Schimpf, and L. Norum, "Grid connected converters for photovoltaic, state of the art, ideas for improvement of transformerless inverters," in *Proc. of NORPIE 2008*, Finland, Jun. 2008.

[15] B. Liu, S. Duan, and T. Cai, "Photovoltaic DC-building-module-based BIPV system-Concept and design considerations," *IEEE Trans. Power Electron.*, vol. 26, no. 5, pp. 1418-1429, May 2011.

[16] F. Blaabjerg, Z. Chen, and S. B. Kjaer, "Power electronics as efficient interface in dispersed power generation systems," *IEEE Trans. Power Electron.*, vol. 19, no. 5, pp. 1184-1194, Sep. 2004.

[17] M. Meinhardt, G. Cramer, B. Burger, and P. Zacharias, "Multi-string-converter with reduced specific costs and enhanced functionality," *Solar Energy*, vol. 69, no. 1, pp. 217-227, 2000.

[18] J. Schonberger, "A single phase multi-string PV inverter with minimal bus capacitance," in

*Proc. 13th Eur. Conf. Power Electron. Appl.*, 2009, pp. 1-10.

[19] S. Islam, A. Woyte, R. Belmans, P. Heskes, P. M. Rooij, and R. Hogedoorn, "Cost effective second generation AC-modules: Development and testing aspects," *Energy*, vol. 31, no. 12, pp. 1897-1920, 2006.

[20] S. Islam, A. Woyte, R. Belmans, P. Heskes, and P. M. Rooij, "Investigating performance, reliability and safety parameters of photovoltaic module inverter: Test results and compliances with the standards," *Renewable Energy*, vol. 31, no. 8, pp. 1157-1181, 2006.

[21] Q. Li and P. Wolfs, "A review of the single phase photovoltaic module integrated converter topologies with three different dc link configurations," *IEEE Trans. Power Electron.*, vol. 23, no. 3, pp. 1320-1333, May 2008.

[22] C. Rodriguez and G. A. J. Amaratunga, "Long-lifetime power inverter for photovoltaic AC modules," *IEEE Trans. Ind. Electron.*, vol. 55, no. 7, pp. 2593-2601, Jul. 2008.

[23] G. R. Walker and P. C. Sernia, "Cascaded DC-DC converter connection of photovoltaic modules," *IEEE Trans. Power Electron.*, vol. 19, no. 4, pp. 1130-1139, Jul. 2004.

[24] E. Roman, R. Alonso, P. Ibanez, S. Elorduizapatarietxe, and D. Goitia, "Intelligent PV module for grid-connected PV systems," *IEEE Trans. Ind. Electron.*, vol. 53, no. 4, pp. 1066-1073, Jun. 2006.

[25] R. Mechouma, B. Azoui, and M. Chaabane, "Three-phase grid connected inverter for photovoltaic systems, a review," in *Proc. First International Conference on Renewable Energies and Vehicular Technology*, 2012, pp. 37-42.

[26] C. Wang, "A novel single-stage full-bridge buck-boost inverter," *IEEE Trans. Power Electron.*, vol. 19, no. 1, pp. 150-159, Jan. 2004.

[27] N. Kasa, T. Lida, and H. Iwamoto, "An inverter using buck-boost chopper circuits for

popular small-scale photovoltaic power system," in *Proc. IEEE IECON*, pp. 185-190, 1999.

[28] Y. Xue and L. Chang, "Closed-loop SPWM control for grid-connected buck-boost inverters," in *Proc. IEEE PESC*, 2004, vol. 5, pp. 3366-3371.

[29] C. Wang, "A novel single-stage series-resonant buck-boost inverter," *IEEE Trans. Ind. Electron.*, vol. 52, no. 4, pp. 1099-1108, Aug. 2005.

[30] N. Kasa and T. Iida, "Flyback type inverter for small scale photovoltaic power system," in *Proc. IEEE IECON*, 2002, vol. 2, pp. 1089–1094.

[31] N. Kasa, T. Iida, and L. Chen, "Flyback inverter controlled by sensorless current MPPT for photovoltaic power system," *IEEE Trans. Ind. Electron.*, vol. 52, no. 4, pp. 1145-1152, Aug. 2005.

[32] T. Shimizu, K. Wada, and N. Nakamura, "Flyback-type single-phase utility interactive inverter with power pulsation decoupling on the DC input for an AC photovoltaic module system," *IEEE Trans. Power Electron.*, vol. 21, no. 5, pp. 1264-1272, Sep. 2006.

[33] A. C. Kyritsis, E. C. Tatakis, and N. P. Papanikolaou, "Optimum design of the current-source flyback inverter for decentralized grid-connected photovoltaic systems," *IEEE Trans. Energy Convers.*, vol. 23, no. 1, pp. 281-293, Mar. 2008.

[34] S. Araujo, P. Zacharias, and R. Mallwitz, "Highly efficient single-phase transformerless inverters for grid-connected photovoltaic systems," *IEEE Trans. Ind. Electron.*, vol. 57, no. 9, pp. 3118-3128, Sep. 2010.

[35] German Patent HERIC-Topology: DE 10221592 A1, issued Dec. 4. 2003.

[36] German Patent H5-Topology: DE 102004030912 B3, issued Jan. 19. 2006.

[37] German Patent Karschny-Topology: DE 19642522 C1, issued Apr. 1998.

[38] H. Patel and V. Agarwal, "A single-stage single-phase transformer-less doubly grounded

grid-connected PV interface," *IEEE Trans. Energy Convers.*, vol. 24, no. 1, pp. 93-101, Mar. 2009.

[39] D. Cao, S. Jiang, X. Yu, and F. Z. Peng, "Low-cost semi-Z-source inverter for single-phase photovoltaic systems," *IEEE Trans. Power Electron.*, vol. 26, no. 12, pp. 3514-3523, Dec. 2011.

[40] J. Rodriguez, J. S. Lai, and F. Z. Peng, "Multilevel inverters: A survey of topologies, controls, and applications," *IEEE Trans. Ind. Electron.*, vol. 49, no. 4, pp. 724-738, Aug. 2002.

[41] M. Mohr and F. Fuchs, "Comparison of three phase current source inverters and voltage source inverters linked with DC to DC boost converters for fuel cell generation systems," in *Proc. Eur. Conf. EPE*, Dresden, Germany, Sep. 2005.

[42] B. Sahan, A. N. Vergara, N. Henze, A. Engler, and P. Zacharias, "A single-stage PV module integrated converter based on a low-power current-source inverter," *IEEE Trans. Ind. Electron.*, vol. 55, no. 7, pp. 2602-2609, Jul. 2008.

[43] F. Z. Peng, "Z-source inverter," *IEEE Trans. Ind. Appl.*, vol. 39, no. 2, pp. 504-510, Mar. /Apr. 2003.

[44] Y. Huang, M. Shen, F. Z. Peng, and J. Wang, "Z-source inverter for residential photovoltaic systems," *IEEE Trans. Power Electron.*, vol. 21, no. 6, pp. 1776-1782, Nov. 2006.

[45] R. Badin, Y. Huang, F. Z. Peng, and H. Kim, "Grid interconnected Z-source PV system," in *Proc. IEEE Power Electronics Specialists Conference*, Jun. 2007, pp. 2328–2333.

[46] T. Kerekes, M. Liserre, C. Klumpner, and M. Sumner, "Evaluation of three-phase transformerless photovoltaic inverter topologies," *IEEE Trans. Power Electron.*, vol. 24, no. 9, pp. 2202-2211, Aug. 2009.

[47] K. C. Oliveira, M. C. Cavalcanti, J. L. Afonso, A. M. Farias, and F. A. S. Neves, "Transformerless photovoltaic systems using neutral point clamped multilevel inverters," in *Proc. IEEE International Symposium on Industrial Electronics*, Jul. 2010, pp. 1131-1136.

[48] W. Li and X. He, "ZVT interleaved boost converters for high-efficiency, high step-up DC/DC conversion," *IET Electr. Power Appl.*, vol. 1, no. 2, pp. 284-290, Mar. 2007.

[49] Y. Kanthaphayao and C. Boonmee, "Dual-output DC-DC power supply without transformer," *TENCON 2004 - IEEE Region 10 Conference*, vol. 4, pp. 41-44, Nov. 2004.

[50] D. Kim, "Transformerless dc/dc converter produces bipolar outputs," *Design Ideas*, EDN, Apr. 2004.

[51] S. V. Araujo, P. Zacharias, and B. Sahan, "Novel grid-connected non-isolated converters for photovoltaic systems with grounded generator," in *Proc. IEEE Power Electron. Spec. Conf.*, Jun. 2008, pp. 58-65.

[52] Sunny Boy 5000TL Multi-String - Operating Instructions, SMA. [Online]. Available: www.sma.de

[53] A. Pandey, N. Dasgupta, and A. K. Mukerjee, "A simple single-sensor MPPT solution," *IEEE Trans. Power Electron.*, vol. 22, no. 6, pp. 698-700, Mar. 2007.

[54] V. V. R. Scarpa, S. Buzo, and G. Spiazzi, "Low complexity MPPT technique exploiting the effect of the PV module MPP locus characterization," *IEEE Trans. Ind. Electron.*, vol. 56, no. 5, pp. 1531-1538, May 2009.

[55] A. K. Abdelsalam, A. M. Massoud, S. Ahmed, and P. N. Enjeti, "High-performance adaptive perturb and observe MPPT technique for photovoltaic-based microgrids," *IEEE Trans. Power Electron.*, vol. 26, no. 4, pp. 1010-1021, Apr. 2011.

[56] F. Liu, S. Duan, F. Liu, B. Liu, and Y. Kang, "A variable step size INC MPPT method for

PV systems," *IEEE Trans. Ind. Electron.*, vol. 55, no. 7, pp. 2622-2628, Jul. 2008.

[57] T. Esram, J. W. Kimball, P. T. Krein, P. L. Chapman, and P. Midya, "Dynamic maximum power point tracking of photovoltaic arrays using ripple correlation control," *IEEE Trans. Power Electron.*, vol. 21, no. 5, pp. 1282-1291, Sep. 2006.

[58] R. Faranda, S. Leva, and V. Maugeri, "MPPT techniques for PV systems: Energetic and cost comparison," in *Proc. PESGM*, 2008, vol. 9, pp. 1-6.

[59] T. Esram and P. L. Chapman, "Comparison of photovoltaic array maximum power point tracking techniques," *IEEE Trans. Energy Convers.*, vol. 22, no. 2, pp. 439-449, Jun. 2007.

[60] M. A. G. Brito, L. G. Junior, L. P. Sampaio, and C. A. Canesin, "Evaluation of MPPT techniques for photovoltaic applications," in *Proc. ISIE*, 2011, vol. 20, pp. 1039-1044.

[61] D. Sera, T. Kerekes, R. Teodorescu, and F. Blaabjerg, "Improved MPPT algorithms for rapidly changing environmental conditions," in *Proc. Power Electron. Motion Control Conf. (EPE-PEMC)*, 2006, pp. 1614-1619.

[62] G. Carannante, C. Fraddanno, M. Pagano, and L. Piegari, "Experimental performance of MPPT algorithm for photovoltaic sources subject to inhomogeneous insolation," *IEEE Trans. Ind. Electron.*, vol. 56, no. 11, pp. 4374-4380, Nov. 2009.

[63] G. Velasco-Quesada, F. Guinjoan-Gispert, R. Pique-Lopez, M. Roman-Lumbreras, and A. Conesa-Roca, "Electrical PV array reconfiguration strategy for energy extraction improvement in grid-connected PV systems," *IEEE Trans. Ind. Electron.*, vol. 56, no. 11, pp. 4319-4331, Nov. 2009.

[64] A. I. Bartcu, I. Munteanu, S. Bacha, D. Picault, and B. Raison, "Cascaded dc-dc converter photovoltaic system: Power optimizing issues," *IEEE Trans. Ind. Electron.*, vol. 58, no. 2, pp. 403-411, Feb. 2011.

[65] L. M. Tolbert, F. Z. Peng, "Multilevel converters as a utility interface for renewable energy systems," *IEEE Power Engineering Society Summer Meeting*, Seattle, Washington, Jul. 2000, pp. 1271-1274.

[66] H. Ertl, J. Kolar, and F. Zach, "A novel multicell DC-AC converter for applications in renewable energy systems," *IEEE Trans. Ind. Electron.*, vol. 49, no. 5, pp. 1048-1057, Oct. 2002.

[67] F. Filho, Y. Cao, and L. M. Tolbert, "11-level cascaded H-bridge grid-tied inverter interface with solar panels," in *Proc. IEEE Applied Power Electronics Conference and Exposition (APEC)*, Feb. 2010, pp. 968-972.

[68] S. B. Kjaer, "Design and control of an inverter for photovoltaic applications," Ph.D. dissertation, Inst. Energy Technol., Aalborg University, Aalborg East, Denmark, 2004/2005.

[69] J. A. Gow, C. D. Manning, "Development of a photovoltaic array model for use in power electronics simulation studies," in *Proc. IEE Electr. Power Appl.*, vol. 146, no. 2, pp. 193-200, Mar. 1999.

[70] K. Nishioka, N. Sakitani, Y. Uraoka, and T. Fuyuki, "Analysis of multi crystalline silicon solar cells by modified 3-diode equivalent circuit model taking leakage current through periphery into consideration," *Solar Energy Materials and Solar Cells*, vol. 91, Aug. 2007, pp. 1222-1227.

[71] M. G. Villalva, J. R. Gazoli, and E. R. Filho, "Comprehensive approach to modeling and simulation of photovoltaic arrays," *IEEE Trans. Power Electron.*, vol. 24, no. 5, pp. 1198-1208, May 2009.

[72] A. Dell'Aquila, M. Liserre, V. Monopoli, and P. Rotondo, "Overview of pi-based solutions for the control of DC buses of a single-phase H-bridge multilevel active rectifier," *IEEE*

*Trans. Ind. Appl.*, vol. 44, no. 3, pp. 857-866, May/Jun. 2008.

[73] Y. Liu, J. Bebic, B. Kroposki, J. de Bedout, and W. Ren, "Distribution system voltage performance analysis for high-penetration PV," in *Proc. Energy 2030 Conference*, Nov. 2008, pp. 1-8.

[74] K. Turitsyn, P. Sulc, S. Backhaus, and M. Chertkov, "Use of reactive power flow for voltage stability control in radial circuit with photovoltaic generation," in *Proc. IEEE Power Engineering Society General Meeting*, Jul. 2010.

[75] K. Turitsyn, P. Sulc, S. Backhaus, and M. Chertkov, "Options for control of reactive power by distributed photovoltaic generators," in *Proc. IEEE*, vol. 99, no. 6, pp. 1063-1073, Jun. 2011.

[76] Y. Xu, L. M. Tolbert, J. N. Chiasson, F. Z. Peng, and J. B. Campbell, "Generalized instantaneous nonactive power theory for STATCOM," *IET Electric Power Applications*, vol. 1, no. 6, Nov. 2007, pp. 853-861.

[77] "IEEE Std 1547™ – 2003, IEEE Standard for interconnecting distributed resources with electric power systems," [Online]. Available: http://ieeexplore.ieee.org

[78] "Standard for electric installation and use," [Online]. Available: https://www.xcelenergy.com/

[79] S. Rivera, S. Kouro, B. Wu, J. I. Leon, J. Rodriguez, and L. G. Franquelo, "Cascaded H-bridge multilevel converter multistring topology for large scale photovoltaic systems," in *IEEE International Symposium on Industrial Electronics (ISIE),* Jun. 2011, pp. 1837 – 1844.

[80] T. J. Summers, R. E. Betz, and G. Mirzaeva, "Phase leg voltage balancing of a cascaded H-bridge converter based STATCOM using zero sequence injection," *European Conference on Power Electronics and Applications*, Sept. 2009, pp. 1-10.

[81] E. Cengelci, P. Enjeti, C. Singh, F. Blaabjerg, and J. K. Pederson, "New medium voltage PWM inverter topologies for adjustable speed AC motor drive systems," in *Proc. IEEE Applied Power Electronics Conference and Exposition (APEC)*, Feb. 1998, pp. 565-571.

[82] E. Cengelci, S. U. Sulistijo, B. O. Woo, P. Enjeti, R. Teodorescu, and F. Blaabjerg, "A new medium-voltage PWM inverter topology for adjustable-speed drives," *IEEE Trans. Ind. Appl.*, vol. 35, no. 3, pp. 628-637, May/Jun. 1999.

[83] O. Ojo, "The generalized discontinuous PWM scheme for three-phase voltage source inverters," *IEEE Trans. Ind. Electron.*, vol. 51, no. 6, pp. 1280-1289, Dec. 2004.

# VITA

Bailu Xiao was born on September 7, 1984 in Wuhan, Hubei, China. She received her B.S. and M.S. degrees in Electrical Engineering from Huazhong University of Science and Technology, Wuhan, China, in 2006 and 2008, respectively. To pursue a Ph. D., she enrolled the graduate program in the department of Electrical Engineering and Computer Science at the University of Tennessee, Knoxville in fall, 2009. She worked at the Power Electronics and Engineering Laboratory, which is now CURENT. During her Ph. D. study, her research focused on multilevel converters and grid-connected inverters for distributed energy resources. She completed her Doctor of Philosophy degree in Electrical Engineering in spring, 2014.